# Aix-Marseille Université

## FACULTE DES SCIENCES

UMR7345 - Physique des Interactions Ioniques et Moléculaires


Thèse présentée pour obtenir le grade universitaire de docteur

Discipline : Energie, Rayonnement, Plasma


Florin GHIORGHIU


---

# Interaction gaz/surface pour les matériaux des composants face au plasma d'ITER

# Gas/surface interaction for plasma facing components relevant for ITER

---

Soutenue le 15/11/2017 devant le jury :

| | | |
|---|---|---|
| Wolfgang JACOB | IPP Garching | Rapporteur |
| Pascal LARREGARAY | ISM Bordeaux | Rapporteur |
| Cécile ARNAS | PIIM Marseille | Examinateur |
| Marie-France BARTHE | CEHMTI Orléans | Examinateur |
| Christian GRISOLIA | IRFM CEA | Examinateur |
| Guillaume LOMBARDI | LSPM Villetaneuse | Examinateur |
| Thierry ANGOT | Aix-Marseille Univ | Directeur de thèse |
| Régis BISSON | Aix-Marseille Univ | Co-directeur de thèse |

# Acknowledgements

I would like to gratefully thank to my two supervisors, Régis Bisson and Thierry Angot, who guided me throughout the work of this thesis. I was lucky to have their advices and their support from the first day of my arrival to Marseille and until I defended my thesis and became a doctor. They were always there for me and they made me feel like a part of the team. I give a huge thank you to you.

I would like to thank to all the people from the Plasma – Surface team that made these three years feel like they were very well spent in terms of human interactions. In no particular order, I would like to thank to Daniel-Beato Medina, Marco Minissale, Yang Xin, Dmitry Kogut, Rouba Moussawi, Kostiantyn Achkasov, Eric Salomon, Gilles Cartry, Jean-Marc Layet, Guy Le Lay, Jean-Bernard Faure, Remy Rigard-Cerison.

I would like to specially thank to Jean-Bernard Faure for all the times I had problems with my device and he helped me to fix them in no-time. I would have gotten way less measurements without his help.

I would like to thank to the administration team (everybody in Service 322) for being the best administration team ever.

Finally, I would like to thank to the members of the jury, Wolfgang Jacob, Pascal Larregaray, Christian Grisolia,Cécile Arnas, Marie-France Barthe and Guillaume Lombardi, for being there for the defense of my thesis and for the great discussion that followed my presentation. I felt honored to defend my thesis in front of this impressive jury.

# Table of Contents

# Chapter 1
# Introduction

## 1.1 Motivation

The world population grew from 2 billion people in 1927 to around 7.5 billion in 2017 [1] and this increase will go up to around 9.5 billion until 2050 according to United Nations Department of Economic and Social Affairs/Population Division [2]. At the same time, due to the technological progress, the energy consumption will also increase by almost 50% until 2050, as it is predicted by the U.S. Energy Information Administration [3]. The main source of energy that is used today and which was used thoroughly in the decades following the Industrial Revolution is the burning of fossil fuels. This has led to an increase of the $CO_2$ level above the 300 ppm level, a level which has never been crossed for the past centuries [4]. This level was surpassed around the year 1950 and has risen since then up to the 400 ppm level. Due to the greenhouse effect of $CO_2$ this resulted in the increase of the average temperature at the Earth surface with 0.6 to 0.7 ºC. The rate of this increase reached roughly 0.15 – 0.2 ºC per decade since 1975 [5]. According to The Intergovernmental Panel on Climate Change (IPCC) [6] an increase of 1ºC will already put 30% of the world's fresh water supply at risk, and an increase of 4ºC and above will make the survival of human population uncertain.

In this context, the European Commission is looking to make the economy more climate-friendly and has designed a roadmap that should lead to a reduction of greenhouse gases emissions of around 80% until 2050 [7]. The way to achieve this should be the use of renewable energy sources and of low carbon energy sources such as nuclear fusion and nuclear fission. The change of energy sources should also be accompanied by improvements in energy efficiency use in general.

The work presented in this thesis is a part of this context and it is related to the use of nuclear fusion as a source of clean energy.

## 1.2 Nuclear fusion

Nuclear fusion was first explained by Hans Bethe who proved that the energy of the stars comes from the interaction of lighter nuclei which leads to the creation of heavier nuclei [8].

At first the research on nuclear fusion was kept secret in US, UK and USSR. As soon as it was realized that there were no military applications for nuclear fusion, like thermonuclear weapons, research was declassified and US and USSR began to cooperate for the development of nuclear fusion.

Around 1970, the US decided to focus mainly on fusion devices based on magnetic confinement. The research was performed using the fusion reaction between the two isotopes of hydrogen (H): deuterium (D) and tritium (T); the reaction is described by equation 1:

***Equation 1***

$$ {}_{1}^{2}D + {}_{1}^{3}T \rightarrow {}_{2}^{4}He(3.5MeV) + \mathrm{n}^{0}(14.1MeV) $$

The disadvantage of this reaction lies mostly in the high energy of the resulted neutron [9], but it was considered to be the most achievable one, and it will also be the reaction used in the first international project which aims to prove the possibility of using fusion as a source energy, namely ITER [10].

### 1.3 Nuclear reactors: ITER and DEMO

Research on nuclear fusion is being performed in many different tokamaks around the world. The focus of many of these reactors is to provide results which will contribute to the construction of ITER, currently under construction in the south of France.

ITER is a scientific project that involves the collaboration between 35 nations, and that aims to test the feasibility of nuclear fusion as a clean source of energy. The aim is to build the first nuclear fusion device that will produce net energy from fusion.

The goals of ITER, as presented on the official website [11], are:

a. to produce 500 MW of power from a 50 MW input, resulting in a return of energy Q = 10;
b. to provide a passing from the technologies which are now used in smaller fusion devices to those expected in future power plants based on fusion; the plasma conditions in ITER will be similar to those in future power plants;
c. to achieve a sustained plasma reaction of deuterium and tritium by the help of internal heating;
d. to test the breeding of tritium inside a real fusion environment; breeding should be used as a source of tritium for future power plants;
e. to demonstrate that fusion devices are a safe way to produce energy.

ITER has essentially a purpose of scientific research and does not aim to provide electricity in a commercial way. The next step after ITER would be the construction of DEMO (Demonstration Power Station), which should have its conceptual design completed by 2020. As a baseline for the design of DEMO, it is foreseen that it should provide at least 2 GW of fusion power continuously and that it should produce 25 times more power than the input one. The purpose of DEMO is to make the transition from ITER as a scientific project to future commercial power plants.

### 1.3.1 Issues related to fuel retention in the divertor and pumping systems

From the multiple challenges encountered for the design and construction of ITER, in the present work the issue that is addressed is represented by the interaction of plasma with the materials of the vacuum vessel of the reactor. In the final design of ITER, the plasma facing materials will be made of beryllium for the first wall (blanket) and the divertor area will be made of tungsten. In figure 1 a graphic image representing the design of ITER is shown. The source of this image is the official website www.ITER.org [11].

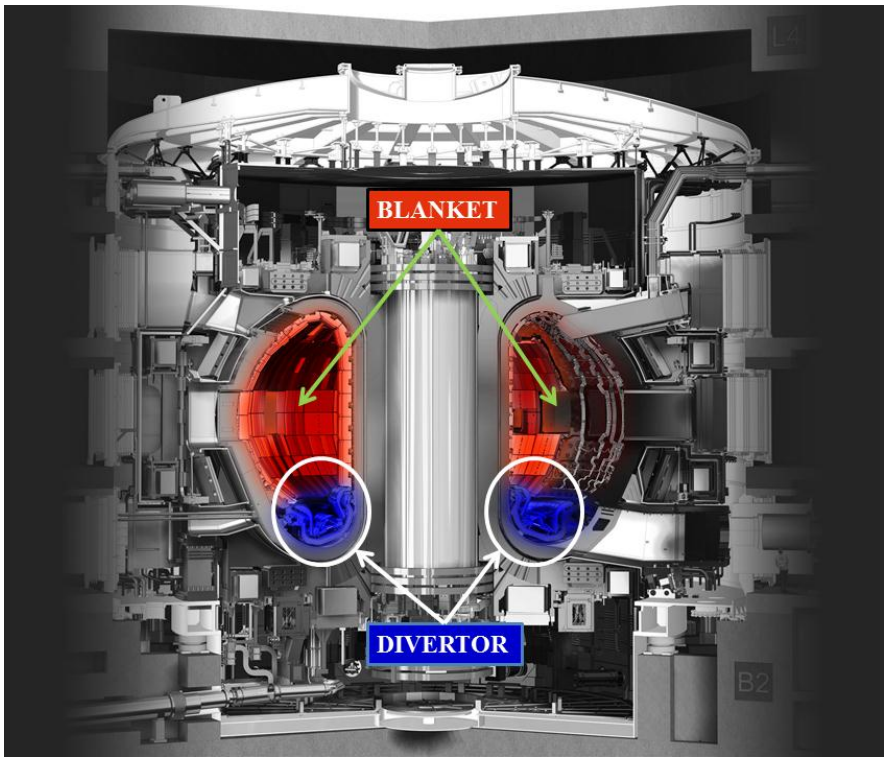


***Figure 1 – The current design of ITER [11]***

The divertor represents the exhaust of the reactor and will therefore be constantly bombarded with high fluxes of particles. Due to the edge-localized modes (ELM), it will also be exposed to high heat fluxes which could lead to the melting or the sputtering of the

tungsten surface. This issue would be critical for the well-functioning of the fusion reaction since the melted tungsten could reach the core of the plasma, and drive the shut-off of the reaction. A solution for this issue was proposed as the puffing of nitrogen gas in the divertor area with two purposes in mind. First, the plasma confinement will be improved by enhancing the detachment of the core fusion plasma from the walls. Second, the edge plasma radiation will be enhanced in order to tame the high heat fluxes directed towards the divertor. This leads to a plasma/surface system composed of tungsten, as surface, deuterium and tritium as fusion fuel, nitrogen as a seeded species, helium and energetic neutrons as direct reaction products of fusion.

In this configuration, several concerns have been raised related to the well-functioning of the reactor. Firstly, the plasma particles can get trapped inside the plasma facing material. This means that deuterium and tritium atoms will go from the plasma state to being trapped inside the tungsten material. In the fusion community the trapping of the fusion fuel inside the plasma facing materials of the reactor is defined as the fuel retention. The retention of deuterium and tritium can lead to their unbalanced proportion as fusion fuel, which can have as a result the failing of the fusion reaction. Following the retention issue there are also the concerns related to the use of tritium. Since it is a radioactive isotope its use needs to abide to the nuclear safety regulation. At this moment, the law in France sets the limit to 700 g of tritium inside the machine at any time. Also, from the practical point of view, tritium is not abundant on earth and is therefore expensive. Any retained tritium needs to be retrieved in order to be reused.

A second major concern is represented by the eventual production of ammonia due to the presence of nitrogen and hydrogen isotopes, which could be released from the surface as deuterated or/and tritiated ammonia. Since the ammonia molecule incorporates three hydrogen isotopes, the formation of ammonia could also affect the gas balance inside the reactor. Furthermore, the formation of tritiated ammonia would be another way for the tritium to be lost. What can happen with the formed ammonia is that it is pumped out from the main vacuum vessel and reaches the cryo-pumps stage where it will condense to the walls. Not only there is a need to find a way of removing this condensed ammonia in order to retrieve the incorporated tritium but ammonia is corrosive and hazardous in itself. The corrosiveness can lead to the deterioration of the pumping system while the hazardousness leads to the need of ammonia amounts to be well known and controlled.

These concerns are addressed in this thesis, by performing measurements in a laboratory environment using an ultra-high vacuum device in order to simulate conditions

relevant for fusion reactors. Since the use of tritium is not possible inside the laboratory where these measurements are being performed, the tungsten is exposed only to its isotope deuterium, as well as to nitrogen.

### 1.4 State of the art

In this work, gas/surface interactions are studied for tungsten samples characterized by natural defects that can be of the following types: single vacancies, grain boundaries, dislocations and a thin layer of tungsten oxide with a thickness of a few nanometers. In order to study the interaction of the tungsten surface with nitrogen and deuterium, the plasma surface interaction is simplified experimentally by exposing samples to molecular ion beams ($N_2^+$ and $D_2^+$), and to the residual pressure of neutral species ($N_2$ and $D_2$). In the next two sections a general description of gas/surface interactions will be presented followed by a summary of the literature on the subject of tungsten interaction with nitrogen and deuterium.

#### 1.4.1 Gas/tungsten interactions: generalities and introduction to energetics and kinetics

In order to give an overview of the different type of interactions that will be considered during this thesis, let's have a look at the fate of one of the ions that are present in the ion beams used during this thesis. In a typical experiment, the molecular ion hits the tungsten surface with an energy of 500 eV (~ 48240 kJ/mol). In terms of velocity, this energy corresponds to $1.55 \times 10^5$ m/s for a $D_2^+$ molecular ion, and to $5.87 \times 10^4$ m/s for a $N_2^+$ molecular ion. Because of their impact energy, the molecules, with their bond energies in the range of a few eV (<10 eV), are dissociated into $D^{(+)}$ fragments and further neutralized into D atoms. The interaction of the atoms with the tungsten target results in a mix of physical and chemical phenomena.

Depending on their kinetic energy, the incident ions can cause the erosion of target atoms (tungsten), meaning the sputtering of the surface material. When tungsten is bombarded with deuterium the sputtering becomes significant above impact energies of 300 eV/$D^+$ (at 500 eV/$D_2^+$ the sputtering yield is around $1.3 \times 10^{-4}$ at/ion [12]) while for nitrogen, at 500 eV/$N_2^+$ the sputtering yield is around 0.1 – 0.2 at/ion [13]. In this thesis, the sputtering of the surface material is not studied.

The retention concerns are related mostly to the hydrogen isotopes and less to nitrogen which is, at this point, the main candidate as the gas to be puffed in the divertor area. Therefore, for the study of deuterium retention with and without the presence of nitrogen, an

introduction on the energetics and kinetics for the interaction of deuterium with tungsten is provided in the following paragraphs.

First, a simplified schematic for the interaction of deuterium with tungsten is presented in figure 2:

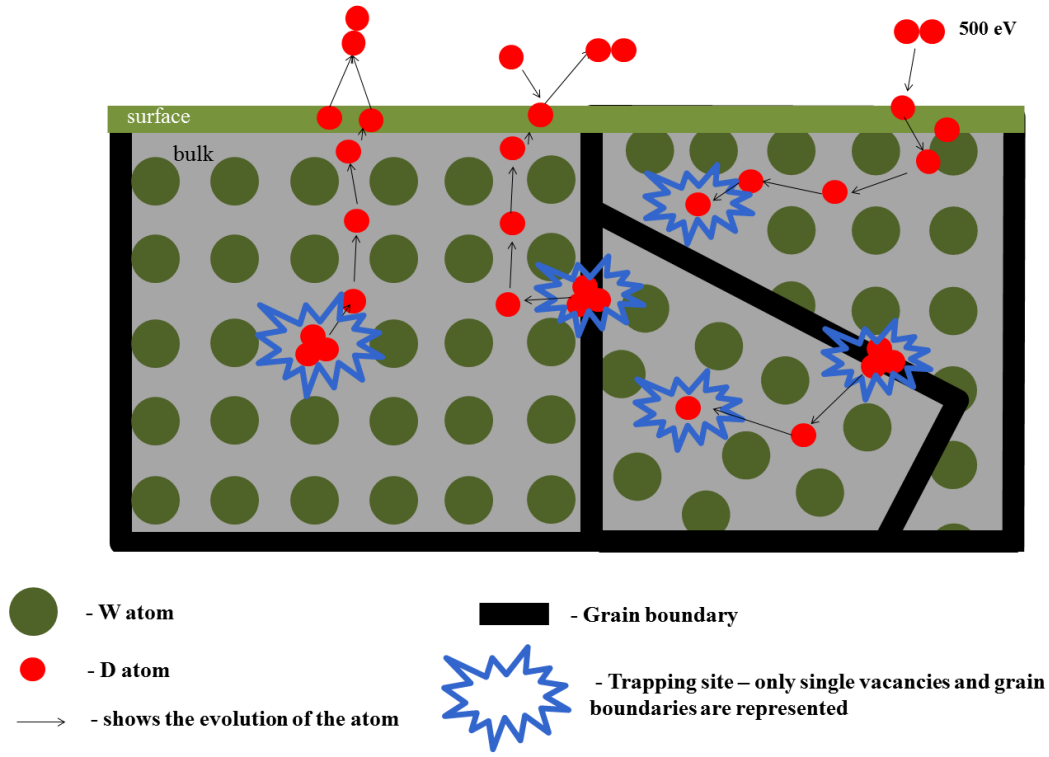


***Figure 2 – Simplified schematic representation of interaction between D and W***

When molecular ions hit the surface, they can be either reflected or dissociated. The ions formed upon molecules dissociation again can be reflected, or be neutralized and penetrate into the sample. The species that get reflected will deposit a small part of their kinetic energy, due to the high difference of mass between a molecular ion (less than 30 atomic mass unit) and the mass of the surface atoms (around 183.84 atomic mass units for tungsten atoms), and will recoil away from the sample.

The atoms that penetrate into the sample will be stopped on a range of a few nanometers, being neutralized and reaching thermal equilibrium at the target sample temperature. These atoms will be referred to as implanted atoms. The depth of implantation will depend on the kinetic energy at the moment of impact and on the species of the incident atoms. The stopping range (which is another term used for the depth of implantation and which is defined as the depth on which the implanted atom loses its initial kinetic energy) is

higher for deuterium than for nitrogen, for the same kinetic energy due to the smaller mass of deuterium.

Apart from that, the two species of atoms have different evolutions after their implantation, as it will be discussed in the next sections. In the following paragraph, the evolution of a typical implanted atom will be discussed for the case of deuterium, and most of the discussion could apply to nitrogen.

Several situations can occur regarding a deuterium (D) implanted atom:

- it can be found as a solute inside the bulk at an interstitial site, which is the tetrahedral site of the tungsten bcc lattice for D (e.g. Fernandez et al [14]); diffusion can happen between tetrahedral site, in any direction, towards the surface or deeper into the bulk; for the diffusion process to be activated, the atom needs to possess an energy high enough so that it overcome the diffusion barrier $E_{Diff}$ ;
- it can be trapped by (or bound to) a defect site typical of the bulk (vacancies, grain boundaries, dislocation loop); the atom will be able to de-trap from (or break the bond from) the defect if it possesses an amount of energy equal to the de-trapping activation energy $E_a$ of the considered bulk defect;
- it can go from the bulk (being absorbed) to the surface (being adsorbed) overcoming the so-called resurfacing energy $E_R$; from the surface, the atom can form a $D_2$ molecule as soon as it will meet another D atom and the molecule will desorb with an activation energy $E_{DES}$. ;
- if the near surface region of the sample contains a thin layer of oxide, the atom will need to diffuse through this oxide layer before to reach the surface, with a diffusion barrier $E_{diff\text{-}oxide}$;

A convenient way to represent these mechanistic steps is to represent them on an idealized energy diagram for the interaction of a D atom with the tungsten sample:

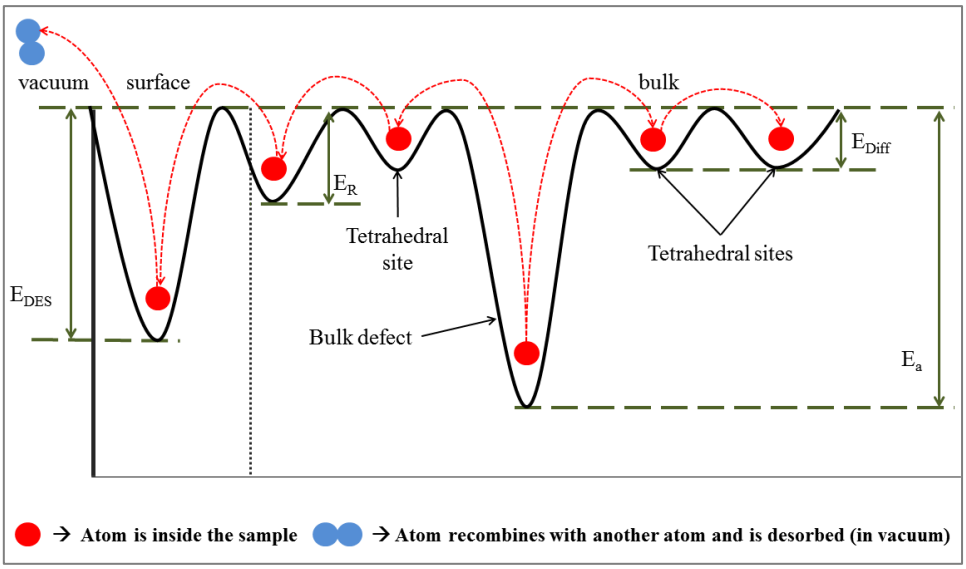


***Figure 3 – Energy diagram for the processes that can take place following the implantation of a D atom***

In figure 3, the arrows show the way an atom could move, starting from a trapping site from the bulk, and then diffusing from one interstitial to another until it gets resurfaced, recombined into a molecule and then desorbed. Similarly, it shows how it may diffuse deeper in the bulk and get re-trapped.

The rate at which the different mechanistic steps presented above can occur are usually described using the Arrhenius equation which relates the rate of occurrence of the step with the temperature:

***Equation 2***

$$k = A \times e^{-\frac{E_{activation}}{k_B \times T}}$$ , where:

- $k$ is the rate constant, which gives the number of occurrence of the considered mechanistic step per second;
- $A$ is the pre-exponential factor (also called frequency factor or attempt frequency of the reaction) and it is usually interpreted as the number of attempts the atom does with the right orientation for the mechanistic step to happen; it does not take into account if the reaction happens or not;
- $E_{activation}$ is the activation energy and it represents the minimum amount of energy necessary for the reaction to occur;
- $k_B$ is the Boltzmann constant;
- $T$ is the temperature.

From equation 2, it can be seen that the rate constant is higher for lower activation energy at a given temperature, and that an increase of the temperature will lead to an exponential increase of the rate constant.

When the rate constant is described by the Arrhenius equation, the expression for the reaction rate at a surface is referred to as the Polanyi-Wigner equation. For the desorption of deuterium molecules from tungsten, the desorption rate ($r_{des}$) is given by:

***Equation 3***

$$r_{des} = -\frac{d\theta}{dT} = A \times \theta^{n} \times e^{-\frac{E_{DES}}{k_B T}}$$

where $E_{DES}$ is the activation energy for desorption, $\theta$ is the deuterium surface coverage, and $n$ is the kinetic order for the desorption process.

As observed in the energy diagram from figure 3, for an atom to reach the surface and be desorbed it first needs to overcome the barriers for bulk defect de-trapping, bulk diffusion and resurfacing. For the kinetic rates of each of these homo-molecular processes ($r_{process}$), the Arrhenius formulation is used in the general form below:

***Equation 4***

$$r_{process} = k_{process} \times [atom]$$

where:

***Equation 5***

$$k_{process} = A^{0}_{process} \times e^{-\frac{E_{barrier}}{k_B \times T}}$$

$A^{0}_{process}$ is the pre-exponential factor of the process, $E_{process}$ is the activation energy for the respective process and [atom] is the concentration of atoms in position to perform this process.

Recently, it has been shown with Density Functional Theory (DFT) that it is possible for a bulk tungsten defect to accommodate several deuterium atoms at once [14], [15] and the activation energy required for the release of a single atom is not a fixed value. It is instead a function of the number of atoms found inside the trap [14]–[16]. There is, in this case, an extra factor that needs to be considered, namely the filling level *l* of a defect i.e. the number of atoms accommodated by the defect. To represent this behavior on an energy diagram, one needs to modify the schematic of bulk defects from figure 3. Figure 4 shows how a bulk defect potential well is changed upon accommodation of additional D atoms:

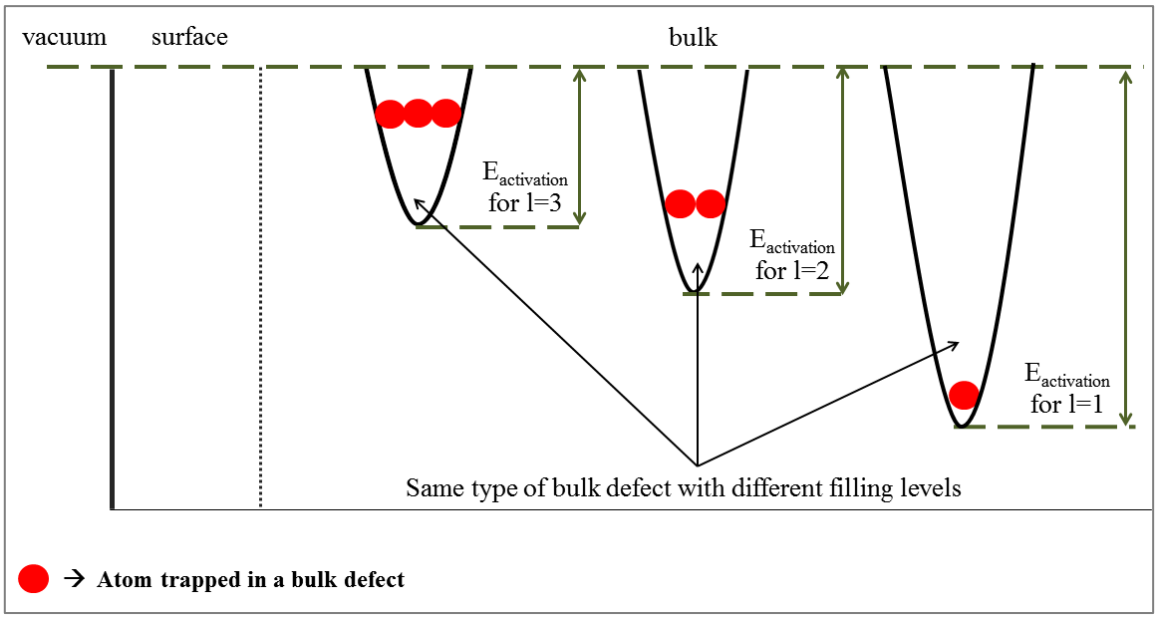


***Figure 4 – Energy diagram for a bulk defect with various filling levels***

The three types of defects represented inside the bulk are considered to be identical. When more atoms are trapped by the defect, the activation energy decreases. At ambient temperature, the number of deuterium atoms trapped inside a vacancy bulk defect can go as high as six atoms.

In the fusion community, the atoms that penetrate into the sample and remain there are referred to as retained atoms, independently of their binding state (trapped in a defect, soluted as an interstitial or adsorbed on the surface). The total number of retained atoms of a certain species is referred to as the species retention. However, retained species can be more or less mobile inside the sample (depending on the diffusion activation barrier and the temperature) and thus the value of the total retention is being referred in relation with the time as to the dynamic retention. Thus, the unit for the total retention is defined as the number of atoms that are still retained per surface area unit (atoms/$m^2$) at a specific moment in time.

Before presenting the results obtained in the present work, an overview on the research already available on the topic of tungsten interaction with nitrogen and deuterium will be presented in the next sections.

### 1.4.2 Deuterium interactions with tungsten

When deuterium atoms get implanted in tungsten, as soon as their kinetic energy dissipates, they start to diffuse from a tetrahedral interstitial site to another, against a diffusion barrier $E_{Diff}^{D}$. If we consider the activation energy for the diffusion of deuterium to be similar to the one of hydrogen, the values found in literature fall between 0.2 eV, calculated by

Fernandez et. al [14], up to 0.39 ± 0.08 eV measured by R. Frauenfelder [17]. At room temperature, the diffusion range of deuterium was determined using Nuclear Reaction Analysis (NRA) [18] and it was found to spread for a depth of around 1 μm, for the parameters used in this thesis (molecular ion energy, flux, incident fluence and sample temperature). As deuterium diffuses deeper in the bulk, it will encounter bulk defects like single vacancies, dislocations and grain boundaries and could get trapped by them. When the temperature of tungsten is increased, the atoms will be de-trapped from these bulk defects if enough thermal energy is provided. The activation energy values for de-trapping need to be given as a function of the filing level of the traps (number of atoms inside the trap). The values, calculated using DFT are:

- for grain boundaries: l = 1: 1.50 eV; l = 2: 1.30 eV; l = 3: 1.10 eV; l = 4: 0.52 eV; l = 5: 0.62 eV; l = 6: 0.90 eV; l = 7: 0.86 eV; values are calculated by Xiao and Geng [15]
- for vacancies:
    - Fernandez et al. calculated: l = 1: 1.43 eV; l = 2: 1.42 eV; l = 3: 1.25 eV; l = 4: 1.17 eV; l = 5: 1.11 eV; l = 6: 0.86 [14];
    - Heinola et al. calculated: l = 1: 1.60 eV; l = 2: 1.57 eV; l = 3: 1.39 eV; l = 4: 1.28 eV; l = 5: 1.17 eV; l = 6: 0.64 [19]
    - You et al. calculated: l = 1: 1.36 eV; l = 2: 1.36 eV; l = 3: 1.03 eV; l = 4: 1.03 eV; l = 5: 0.95 eV; l = 6: 0.74 [20]
- for dislocations:
    - Xiao and Geng [15] calculated: l = 1: 2.06 eV; l = 2: 1.96 eV; l = 3: 1.00 eV; l = 4: 0.90 eV; l = 5: 0.55 eV; l = 6: 0.50 eV (the diffusion barrier is added – 0.2 eV found by Fernandez et al. [14]);
- for oxide layer:
    - Kong X.-S. et al. [21] calculated: l = 1: 1.40 eV; l = 2: 1.12 eV; l = 3: 1.10 eV; l = 4: 1.09 eV; l = 5: 0.60 eV; l = 6: 0.41 eV.

After the implantation is stopped, the atoms that diffuse towards the surface and get resurfaced will need to overcome the diffusion through the native oxide layer in order to be desorbed. To our knowledge, this oxide diffusion activation energy has not been calculated nor measured in the literature.

In the nuclear fusion community the interaction of deuterium with tungsten is studied experimentally using various deuterium sources: ion sources, cold plasma and tokamak plasmas. In parallel with experiments, modeling codes are being built. These models have as main purposes, firstly to interpret the vast and varying range of experimental results but also

to help determining the values of some key parameters involved in the interaction of deuterium with tungsten, like the activation energies for different types of barriers, or the values of different pre-exponential factors. The measurements performed during this thesis were in part used to develop and validate a Macroscopic Rate Equations (MRE) model that describes the retention and the release of the implanted D atoms in W. The interested reader is invited to read the corresponding thesis of Dr. Etienne Hodille [22]. In the present thesis, the analysis of the experimental results will be performed assuming that a rate-limiting step dominates the release of implanted species and the kinetic equations detailed in section 1.4.1 will be used.

The W specimens used for the present thesis consist in tungsten samples containing natural defects like single vacancies, dislocations, a surface oxide layer, and grain boundaries for polycrystalline specimens. The experimental method applied for the quantification of retention consisted in Temperature-Programmed Desorption (TPD). The method consists in linearly heating a W sample that was previously implanted with D and to record the number of desorbed atoms as a function of temperature. On the one hand, the rate-limiting trapping mechanism and its corresponding activation energy(ies) will have a strong word to say for the shape and the position of the desorption peak (this position is defined as the position of the peak maximum). For example, a single vacancy defect is described in DFT by a set of filling level-dependent activation energies between 0.8 and 1.4 eV [14], [19], [20]. It should result in a broad desorption peak situated between 400 and 600 K [23], [24]. On the other hand, the diffusion barrier for D in W will have a non-negligible influence on the desorption peak position. The diffusion activation energy is situated somewhere between 0.2 eV (DFT value [14]) and 0.39 eV (experimental measurement [17]), which is smaller than the ones of a vacancy defect. Nevertheless, the diffusion barrier will have an effect on desorption peak when D atoms will diffuse towards the surface from high depth: diffusion barriers will create a time lag for D to resurfacing and therefore the result will be to broaden and to shift to higher temperature the desorption peak of a few tens of Kelvins. Finally, the surface and near-surface processes could have a certain influence on the desorption kinetics. On the one hand, if the near-surface region is composed of a thick layer of tungsten oxide $WO_3$, it could act as a diffusion barrier [24], i.e. a layer in which the effective diffusion activation energy is higher than in bulk tungsten. On the other hand, a surface oxide layer seems to reduce deuterium surface re-trapping and should ease the observation of bulk trapping mechanism [25].

In practice, the interaction of deuterium with tungsten is studied experimentally in relation with a large set of interesting parameters: the incident fluence (defined as the total

number of particles that bombards the surface during plasma or ion exposure); the particle flux density; the temperature of the sample during exposure; the quality of the sample and the state of the surface from the point of view of the density of damage; the kinetic energy of the incident particles; and finally the time interval between exposure and any desired action that is performed on the exposed surface. Only a few experiments are performed *in-situ*, avoiding exposure to air of an implanted surface before analysis, while in most other experiments it is technically necessary to expose the sample to air in order to apply diagnosis methods.

In the literature, deuterium fluences reaching the tungsten samples usually start around $10^{20}$ D/m$^2$ [24] and go as high as $10^{27}$ D/m$^2$ [26], [27]. The latest range of incident fluence is considered to be relevant for fluences that will be reached during a plasma discharge on the divertor of ITER. The fluence accessible in a certain experiment will depend on the available particle flux density, since the incident fluence is given by the integration of the particle flux for the entire duration of the exposure. If only a low flux is available like in an ion beam apparatus, the duration of the implantation to reach a given fluence will be longer than the duration needed for an experiment with high flux like a plasma source. In the literature, fluxes range starts around $10^{18}$ D/m$^2$s and can reach $10^{23}$ D/m$^2$s [28] in one of the most intense linear plasma device like Magnum-PSI [29], which is capable of providing a flux density only 10 times smaller than the one expected in the ITER divertor [29].

The incident fluence and the flux density used for the experiments presented in this thesis were both smaller than the ones described above. The flux density was kept constant at around $1.6 \times 10^{16}$ D/m$^2$s and the incident fluence was varied between $10^{17}$ and $10^{21}$ D/m$^2$. Implantation was performed by using an ion source, which limited the flux density. This allowed completing the range of incident fluence available in literature towards fluences typical of the monolayer and sub-monolayer range (a monolayer is here defined as the typical surface density of metals around $1. 10^{19}$ atom/m$^2$). Additionally, this low flux was a good fit for two purposes: first, the little quantity of energy contained in a low flux ion beam allows the surface temperature to be defined unambiguously, avoiding significant temperature gradient; second, extracting the values of trapping barriers for D in W with low filling levels could necessitate low flux.

The temperature of the samples during exposure is usually varied from ambient temperature up to temperatures relevant for ITER divertor of around 600 – 900 K. The effect of temperature is followed in relation with the retention and also in relation with the surface modifications induced by high fluxes, high fluences or high energies of the incident D atoms. In the chapter dedicated to D retention in W, implantations at various temperatures will be

presented. From the point of view of the kinetic energy of the incident D atoms and the defect density found in the exposed samples, for the measurements presented in this thesis, a fixed energy of 250 eV per D atom was used to remain below the displacement threshold. An additional annealing step was performed at the end of each TPD (10 minutes at around 1300 K) to avoid the evolution of the W samples.

An important concern for the plasma operations in ITER comes from the evolution of the trapped atoms with time, meaning that it is necessary to assess the atoms inventory for both short and long term. In [30] it is shown that, for implantation at higher temperature (450 K) more atoms get released in less than 20 minutes after exposure, compared to the implantation at lower temperature (350 K) where release happens on the hour time scale

The evolution of trapped atoms with time was studied extensively in this thesis and the term "storage time" is often used. The term will be explained here and in future chapters where it will be used. The "storage time" is defined as the time interval between the end of the implantation and the start of the analysis of the sample, e.g. through a controlled desorption. The retention of D atoms was studied for storage times as long as around 13 days.

In this thesis, due to the way that the storage time evolution of the retained D atoms was studied, it was possible to directly determine the activation energy for the release-from-the-sample process. The known value of this barrier was further used in order to perform an extensive analysis of the data obtained for the retention of D in W, in the case of low flux and low fluences.

### 1.4.3 Nitrogen interactions with tungsten

The diffusion barrier is of course different for different species of atoms. For nitrogen, the diffusion barrier is relatively high, with a value of $E_{Diff}^{N} = 2.3\,\mathrm{eV}$ found by Keinonen et al. [31]. Therefore, due to the low diffusivity of N, once implanted, the N atoms will remain trapped in the initial stopping range for temperature below 600 K [32]. This usually means a short implantation depth of a few nanometers. The formation of tungsten nitride ($WN_x$) from long N implantation has been discussed in [16]–[18]. The low diffusivity of the implanted N atoms leads to a quick saturation of the implanted zone where a 50% ratio W/N ratio is reached [32]. This 1-to-1 stoichiometry for N and W atoms is found for temperatures below 600 K. Above this temperature, nitride decomposition has been predicted [32].

Thus after implantation, if the temperature is sufficiently increased enough, the provided heat will lead to the decomposition of these nitrides. This may be considered as a

diffusion process of N atoms in the W bulk as described by equation 3. Lastly, N atoms that reach the surface will need to overcome the barrier from the surface recombination process for the desorption, as it is described by equation 2. Surface dissociated molecular nitrogen desorbs in the 1200 – 1300 K range [35] with a corresponding activation energy around $E_{DES}$ = 3.2 eV [35]. However, one needs to note that this experimental measurement and interpretation was obtained on clean tungsten (i.e. without the natural surface oxide inherently present on our samples, see Chapter 3).

The interaction of nitrogen with tungsten has become of interest for the fusion community since nitrogen was proposed to be the gas puffed in the divertor area of ITER. The concerns related to the implantation of nitrogen came originally from the possibility of having an increased erosion of the tungsten atoms [33]. Contrarily, the formation of WN leads to a reduced erosion as found by Schmid et al. [32] and it also improves plasma performance due to a better detachment of the plasma from the first wall [36]. Most of the research performed in this context is now targeting the synergistic effects of N and D on W [37]: the influence of the pre-implantation of N on D retention [38] and the formation of deuterated ammonia and its quantification [39], [40]. Evidencing of ammonia formation in a reactor environment came from the experiments performed in ASDEX Upgrade, where ammonia was detected as a result of N seeded discharges [39].

The interaction of N with W was studied in this thesis for implantation at ambient temperature, for low flux density (around $10^{16}$ N/m$^2$s) and for a range of fluence between $10^{19}$ and $10^{21}$ D/m$^2$. The energy of the impinging N species was set to a constant value of 500 eV/$N_2^+$. These values have been chosen similarly to the ones used for the D species implantation in this thesis. A literature overview on the synergistic effects of N and D atoms implanted in W is detailed in section 1.4.4.

### 1.4.4 Synergetic Deuterium and Nitrogen interactions with Tungsten

The study of nitrogen interaction with tungsten and the interaction of both nitrogen and deuterium with tungsten in fusion related environment was tackled only in the last years by a few groups. There are so far two different ways that the interaction of nitrogen and deuterium in tungsten is approached. One method consists in the exposure of tungsten samples to plasmas with various ratios of nitrogen and deuterium mixtures. A second method uses the magnetron-sputtering deposition in order to obtain tungsten nitride films which should act as a model for a tungsten surface exposed to nitrogen plasma. Then these nitrides film are exposed to deuterium plasmas.

The phenomena that are usually followed are:

a) changes in retention as compared to individual exposures
b) changes in depth distribution as compared to individual exposure
c) changes of the surface composition and morphology
d) the production of ammonia and its dependencies on the above mentioned phenomena
e) the step by step formation of ammonia
f) the effect of sample surface temperature on the above mentioned phenomena
g) the effect of the N to D ratio inside the plasma on the above mentioned phenomena
h) the effect of pre-implanted nitrogen on deuterium retention
i) the influence of the wall material on the ammonia formation and on the amounts of formed ammonia

In order to place the results obtained in the present thesis in the framework presented above, literature results will be presented for each point (from a. to i.) and then, the contribution of the present work will be mentioned:

a) Ogorodnikova et al. have shown in [37] that, for N seeded D plasma it is noticed an increase of D retention, as compared to pure D plasma, that becomes more significant when fluence is increased. The same work shows that deuterium is found deeper in the bulk when N is seeded in plasma. Similar results are obtained by L. Gao et al. in [38] for D implantation at 500 K, in N pre-implanted tungsten. The extra D amount is shown to be related to the formation of blisters. However, at 300 K implantation, in [38] there is no obvious change for the D retention and neither for the depth profile of D.

In contrast to these observations obtained for tungsten specimens, in [41] L. Gao shows that the D implanted in tungsten nitride ($WN_x$) obtained by magnetron sputtering does not diffuse at ambient temperature. It is found that D remains trapped in the topmost surface. Similar results are presented by V. Tiron et al. in [42] where D is also implanted in $WN_x$ films obtained by reactive multi-pulse HiPIMS. It is observed that D retention is diminished when the amount of nitrogen in the coatings is increased.

A consistent set of results is provided by G. Meisl et al. in [34] where it is shown that the concentration of nitrogen in tungsten can reach a ratio between 33% and 66%. This result is in agreement with [32] where it is shown that the nitride that is formed due to exposure of tungsten to nitrogen plasma is WN. The maximum concentration for nitrogen in tungsten becomes, in this case 50%. For higher fluences, G. Meisl et al. show in [34] that D also has an

effect on N by firstly leading to a physical erosion of N and secondly pushing it deeper into the bulk. It is shown that these two effects depend on the D energy and also on the N ratio in the N+D plasma, with the N amount increasing for lower D energies and with the implantation depth of N increasing when N content in the plasma decreases.

In this thesis, N is implanted first in tungsten and it is followed by D bombardment. The implantation is achieved by using an ion gun which corresponds more to plasma implantation than to film deposition. Retention wise, we expect to see therefore the effect of D on pre-implanted N and also the effect of pre-implanted N on D retention as compared to their individual implantations. The thermo-programmed desorption (TPD) spectra will be used to detect any changes in trapping mechanisms while the evolution of retention with parameters like fluence, temperature and storage time will allow the testing of phenomena like nitrogen saturation, nitrides acting as diffusion barrier and nitrogen sputtering by incident deuterium.

b) The changes of depth distribution were already mentioned at point a) for the results of Ogorodnikova et al. [37] where more N in the plasma leads to higher densities of D deeper in the bulk. No changes are noticed by L. Gao et al. in [38] for implantation at 300 K but at 500 K the formation of blisters due to N implantation leads to changes of D depth profile. Implantation of D in nitride films was shown to lead to no D diffusion deeper in the bulk [41], [42].

In this thesis, information about diffusion is obtained by performing the TPD step after different intervals of storage and analyzing firstly the change in position and width of the desorption peaks, and secondly the evolution of retained amounts when the storage time is increased, with the sample being stored at room temperature. These analyses give, in the end, an idea about how atoms diffuse inside the bulk but also in the surface region.

c) The most notable changes on the tungsten surface, upon ion bombardment are related to the sputtering of W atoms and to the reduction of the native tungsten oxide ($WO_3$) found on the surface. The sputtering yield depends on the energy of the impinging particles onto the tungsten sample. This dependency can be found in [12],[43] for deuterium, and in [13] for nitrogen.

R.D. Bringans et al. [44] have shown that even though the oxide state can be reduced by the formation of hydrogen tungsten bronze, therefore by attaching a hydrogen (discussed by E. Salje et al. in [45]), the loss of oxygen (O) atoms from the surface has a more significant role for the reduction of the oxide. E. Salje et al. [45] have also shown that $Ar^+$ bombardment can remove some oxygen atoms from the surface. It can be expected then, that N

implantation will also remove some of the oxygen found in the oxide layer leading to the generation of active sites.

For the surface and the sub-surface zone, N bombardment leads to the formation of tungsten nitrides $WN_x$ [34]. The depth distribution of implanted N depends on the energy of the incident atoms. This means that for higher energies the maximum N density will shift to slightly higher depths [17],[20],[43]. From the point of view of blister formation or the suppression of blister on the surface, both [37] and [38] show no effect related to the use of N. The implantation of N and the formation of $WN_x$ lead to the hardening of the surface [46]. When ions are implanted in tungsten it is found that, for an energy of 300 eV the areal N density is equal to around $8 \times 10^{15}$ N/m$^2$ [46]. The exposure to molecular $N_2$ does not lead to the formation of nitrides [46].

In this thesis, the surface changes determined by the N bombardment were evidenced by showing their effects on D retention and on $D_2$ (dissociative chemisorption), when sequential exposures were performed. This means that the changes were not followed quantitatively but only qualitatively.

d) & f) Ammonia production was observed in a tokamak environment inside ASDEX Upgrade following nitrogen seeded discharges [39]. D. Neuwirth et al. reported that from the total amount of nitrogen being seeded, 8% was released in the form of ammonia. From other experiments it was noticed that the amount of produced ammonia is not correlated to the plasma duration [40] (which is the same as saying that it is not correlated to the fluence) and it was shown that the formation of ammonia takes place at the wall [47], [48]. The dependency of ammonia formed amount with the surface temperature is studied in [49] where it is shown that the increase of the temperature of the surface leads to a slow increase of the produced ammonia.

In the present work the amount of formed ammonia is investigated at ambient temperature for various fluences of N and D and for various durations of storage between the implantation and the TPD step.

e) In [50] H. Kiyooka and O. Matsumoto have established the step by step process leading to the formation of ammonia on stainless steel walls for a N-H plasma. The process consists in the dissociative adsorption of the $N_2$ molecules and the $N_2^+$ molecular ions together with the adsorption of $NH_x$ products on the walls. The formation of $NH_x$ takes place also between adsorbed N and H from the plasma. Ammonia is formed and desorbed when enough H atoms have been attached to the adsorbed N, meaning that they desorb in the form of $NH_3$.

In this thesis, the production of deuterated ammonia is first evidenced and then, an hypothesis of the way it is formed is given, in consistency with the model found in literature.

g) & h) In some of the above points it was shown that ammonia is formed at the walls and that the produced amount does not increase significantly when more N is available. On the other hand, N is found to quickly reach saturation when the fluence is increased, which be equivalent to the saturation of the surface coverage. In Gmelin Handbook of Inorganic and Organometallic Chemistry [46] the saturation concentration for W implanted with N ions is shown to be equal to $8 \times 10^{17}$ N/m$^2$ for an N energy of 300 eV and equal to $9 \times 10^{17}$ N/m$^2$ for an N energy of 400 eV. Since different N/D ratio will not necessarily lead to different amounts of ammonia, it becomes useful to know how these different ratios influence the retention of each species. The increase of D retention due to the presence of N was already mentioned at point a) for the results presented in [37]. Similarly, the erosion of N by incident D was mentioned at point a) for the results presented in [38].

In this thesis the sequential implantation of N and D is performed for two regimes of incident fluence chosen in relation with the nitrogen fluence that leads to saturation. The incident fluences chosen for deuterium are similar to the ones used for the implantation of deuterium alone. Since in plasma devices the saturation of N in the implanted zone will be achieved quickly due to high fluxes, the regime of low incident fluences used in the present work aims at the configuration where saturation is not yet reached. A comparison between the two regimes should bring valuable new information related to the influence of N saturation on D retention, related to the barrier effect of the implanted N, and related to the amounts of ammonia that are produced in the two cases.

i) An investigation of ammonia formation for different materials exposed to plasmas is presented in [49] for the metals found in fusion devices (tungsten, stainless steel and aluminium as a substitute for beryllium). The use of catalysts for ammonia formation is well known [46], [48], [51]. The steel is one of these catalysts, resulting therefore in a real necessity in knowing the amounts of ammonia generated inside a fusion reactor as a result of the presence of the three types of metal. A. de Castro et al. show in [49] that, from the three metals, W corresponds to the lowest amount of produced ammonia, followed by the stainless steel and with aluminium having the highest amount of produced ammonia.

In this thesis the formation of ammonia is quantified only for the tungsten surface.

## 1.5 Summary

The construction of ITER and the starting of its operation will not be without challenges. The interactions between plasma and plasma facing materials represent one source of these challenges. In order to tackle issues like fuel retention, material damage, and to have control over the hazardous substances (tritium, beryllium, ammonia), they are usually divided in function of their localization inside the machine: the first wall and the divertor area. These concerns, related to the divertor area, for a plasma/surface system composed by N, D and W have been described in the previous sections. The descriptions of these interactions have been further divided in three situations: the interaction of D with W, the interaction of N with W, and the synergistic interaction of N and D with W. It was shown that, the interaction of the two species of gas with W are somehow different, as a result of different values of the energies describing their interactions. The trapping mechanisms are different (bulk defects for D vs. nitride formation for N), and the diffusivity is different for the two species. The possibility of deuterated ammonia production was addressed for the case of W exposed to both N and D, together with other changes related to the presence of both species of gas in this configuration. The experiments presented in this thesis are aiming at completing the research already available for the aforementioned issues, by studying fundamental interactions between gas and surface using low fluxes and low fluences, but by still remaining relevant for the phenomena encountered on the divertor area of ITER.

In the following chapter the experimental method (Chapter 2) will be presented and will be then followed by chapters dedicated to the steps discussed earlier: the interaction of deuterium with tungsten (Chapter 3), the interaction of nitrogen with tungsten (Chapter 4) and the synergistic effects of implanting both nitrogen and deuterium in tungsten (Chapter 5).

In Chapter 3, the interaction of D with W will be studied on both polycrystalline tungsten samples (PW) and on single crystal W (SW) samples, for various values of the incident fluence, for various implantation temperatures, and for various storage times.

In Chapter 4, the interaction of N with W will be studied only for PW samples and by performing implantations at ambient temperature only. Various values of the incident fluence will be tested and the evolution of N retention with the storage time will also be studied.

The results obtained from the studies on D interaction with W, and on N interaction with W will then be used for Chapter 5 focused on the synergistic effects of both N and D implanted in W.

Finally, Chapter 6 will consist in a summary for the work performed during this thesis, for the results that were obtained and for the perspective that they will provide.

# Chapter 2

# Experimental setup

## 2.1 Overview

The synergetic effects of nitrogen and deuterium bombardment on tungsten were investigated in a laboratory environment, in an *all in-situ* apparatus that provides ultra-high vacuum (UHV) conditions. The exposure of tungsten specimens to the aforementioned gas species were performed in the form of molecular ion beams. The diagnostic techniques consisted in the use of a mass spectrometer that detected the particles desorbed from a specimen, when the specimen was heated up. Other diagnostic techniques were applied, consisting in quantifying the number of particles found inside the sample and in the imaging of the samples.

## 2.2 Experimental methods

The main technique used in order to characterize the samples following their exposure to molecular ion implantation is "Temperature-Programmed Desorption" (TPD). Additionally, the samples were characterized by AFM, SEM, NRA and AES. Descriptions of these techniques are provided in the next two sections.

### 2.2.1 Temperature-Programmed Desorption (TPD) – Principle and theory

The temperature-programmed desorption (TPD) technique is a characterization method used to determine kinetic and thermodynamic parameters for desorption processes. It consists in heating a sample according to a pre-defined heating programmed temperature ramp. Usually, the heating is performed in a linear manner, in which case the heating rate $\beta$ is defined as:

***Equation 6***

$$\beta = {dT}/{dt}$$

where $T$ is the temperature of the sample, and $t$ represents the time. As the temperature of the sample increases, desorption of absorbed particles is enabled. Depending on their type, the desorbed particles will leave the surface of the sample as atoms or as molecules. They will

further be counted by recording them directly with the help of a mass spectrometer, i.e. by measuring their partial pressures.

For the case when a mass spectrometer (MS) is used, the TPD technique provides the desorption rate traces for all the desorbed species counted by the MS [52]. These curves of desorption provide straight away important information: firstly, the total number of particles (atoms or molecules) desorbed from the sample can be determined by integrating the peaks of desorption; this implies the subtraction of the baseline representing the noise signal followed by the conversion of the integrated raw signal into number of particles; secondly, the peaks of desorption are showing the range of temperature at which the desorption takes place; the peak maximum's position in temperature is correlated with the energy of activation for the release process [52]. This correlation is explained by looking at the three steps that an atom needs to overcome in order to get from being trapped in the sample to being desorbed into the vacuum:

a) the release of atoms from their respective trapping sites;
b) the diffusion through the bulk which can make the atom diffuse to another trap or to reach the surface where it switches from the absorbed state into the adsorbed one;
c) the desorption from the surface towards vacuum which may involve a recombination with other species;

The release from a trapping mechanism is a process described by the energy needed for the atom to escape the trap (activation energy $E_a$). As soon as enough heat (thermal energy) is provided to the sample during the temperature ramp, so that atoms can overcome the activation energy, the atoms pass from the trapped state to the solute state and start to diffuse. The release step being activated by the increase of the sample temperature, it is generally described by an Arrhenius equation [2],[3] (Eq. 2 in Chapter 1). In the solute state, the atoms will move against a diffusion barrier $E_{diff}$ until they get re-trapped or they reach the surface and get desorbed. This third step, meaning desorption from the surface, is described by the Polanyi-Wigner equation (Eq. 3 in Chapter 1) [54].

Another method of applying the TPD technique for the deuterium experiments presented in this thesis is by performing the heating ramp after different intervals of storage. The sample is stored, in this case, at constant temperature after ion implantation and it suffers therefore an isothermal desorption. By knowing the amount of trapped atoms at different times after implantation, with the temperature being kept constant and with the rate-limiting

step being a first order kinetic process (trap release or surface desorption with n = 1), the activation energy of the rate-limiting step can be extracted from eq. 3 (from Chapter 1):

***Equation 7***

$$E_{DES} = k_B \times T_{storage} \times \ln(\mathrm{A} \times \tau)$$

where $\tau$ is the time constant of the exponential decay (deduced by fitting the curve of retention as a function of the storage time).

This method of extracting an activation energy is presented in our 2015 publication [16] for deuterium desorption from tungsten and will be used in Chapter 3 and Chapter 5.

### 2.2.2 Other techniques: NRA, AFM, SEM and AES

The number of atoms found inside the sample, following an implantation, was also determined for a small number of samples using the Nuclear Reaction Analysis (NRA) technique. The purpose of using NRA was to validate the results obtained with TPD. The NRA technique consists in irradiating a target sample with certain nuclei that possess a well-known kinetic energy. The elements found in the target will undergo a nuclear reaction when resonance conditions are met. The result consists in excited nuclei of the probed element, which decay and emit radiation. The value of the kinetic energy for the incident nuclei allows probing different depths. In order to reach higher depths, higher kinetic energy is used. Since NRA could create local lattice damage, it was not used repeatedly in order to avoid irreversible changes of our samples. The NRA measurements were performed at the Jozef Stefan Institute in Ljubljana, Slovenia, with a description of the device being available in the paper published by A. Zaloznik et al. [55]. For deuterium depth profiling, the $D(^3He, p)\alpha$ nuclear reaction is used. The impact energies of the incident $^3$He are 780, 1550, 2580, 3400 and 4300 keV [55]. The deuterium depth profiles measured by NRA for an incident fluence of $9.8 \times 10^{20}$ D/m$^2$ are shown in figure 5 for two different samples, each of them being probed after two different durations after implantation (31 hours and 147 hours).

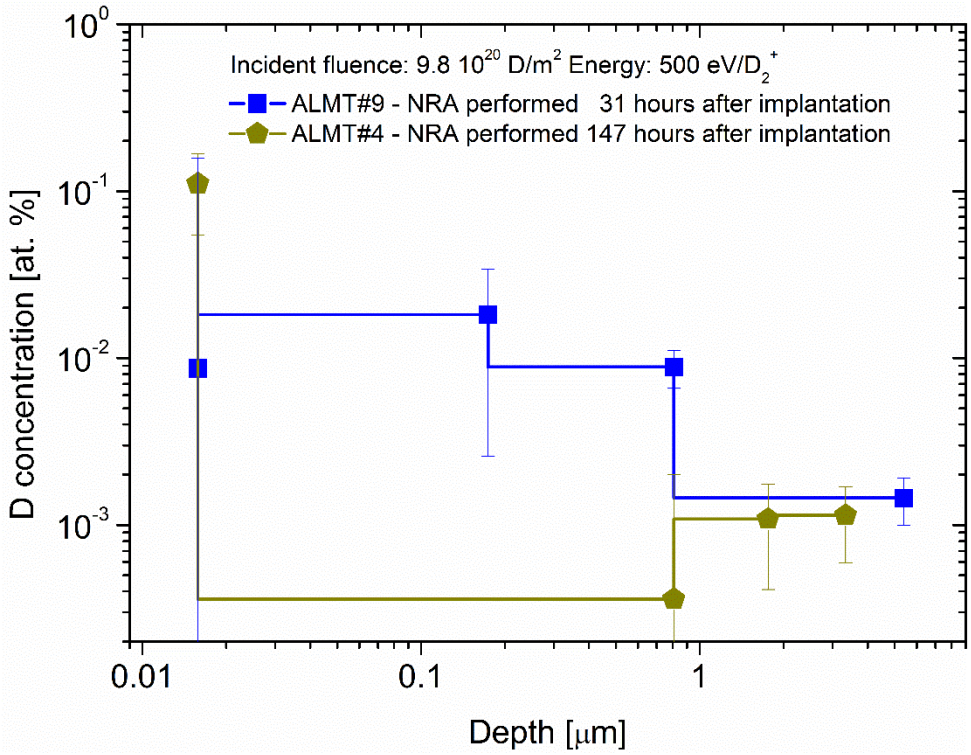


***Figure 5 - Deuterium depth profiles obtained for two different durations after implantation; Incident fluence: 9.8 × 10^20 D/m^2; Samples: ALMT#4 and ALMT#9***

From figure 5 it can be seen that the diffusion depth of deuterium atoms implanted in tungsten at 500 eV/$D_2^+$ is on the order of several hundreds of nanometers. The difference between the two profiles should be related with the dynamic release of deuterium from tungsten (see Chapter 3 for the discussion of this phenomenon), meaning that some deuterium is still being released after the 31 hour time mark. The amounts of deuterium measured by NRA were consistent with the values quantified by TPD, but showed slightly higher values as compared to the TPD results (within a factor of 2). These slightly higher values may be explained by the fact that the sample is exposed to air in order to be transported for NRA. This exposure could increase the amount of oxide found on the surface, affecting therefore the dynamic release of the implanted atoms as it will be discussed later in this thesis, and leading to these differences of measured retention values.

The surface evolution of our samples was also probed using the following surface sensitive techniques: Atomic Force Microscopy (AFM), Scanning Electron Microscopy (SEM), and Auger Electron Spectroscopy (AES).

The AFM technique is a scanning probe microscopy with a very high spatial resolution (up to fractions of nanometers) based on the contact between the sample and a mechanical probe (the cantilever). It is capable of performing imaging, but also many other features (force measurements, capacitance, etc…). For imaging purposes, which were targeted

for our samples, the probe scans the surface of the sample in the x-y plane, in the so-called tapping mode. While the probe is scanning the surface, the topography is obtained by lightly tapping the surface with the (oscillating) probe, and by monitoring the changes in oscillation amplitude with the use of a laser pointing on the cantilever.

The SEM technique is based on the use of a focused beam of high-energy electrons that interact with the sample. The electrons get decelerated inside the solid sample and their energy gets dissipated resulting in a variety of signals. Examples of these signals include secondary electrons, backscattered electrons (BSE), diffracted backscattered electrons (EBSD) which helps determining the crystal structures and orientations, X-rays, visible light and heat. Some of these signals are used to obtain information about the morphology, the chemical composition, and the crystalline structure of the samples bulk together with the crystalline orientation inside the sample. For our samples imaging, mostly secondary electrons and backscattered electrons signals were used.

Whenever possible, AFM and SEM images of the samples were obtained in between set of measurements, when the samples were put out to air. This insured that the evolution of the surface is observed regularly. In some cases, the imaging was considered necessary; therefore the samples were put out to air specially for the imaging. One example of this is the case of a high cumulated fluence on a single sample due to the numerous cycles of implantation/desorption performed on the sample. Another example is the case of the implantations that are suspected to lead to changes of the surface, like the bombardment with nitrogen molecular ions. For this case, nevertheless, the sample that was exposed to nitrogen implantations was cracked before being put out to air. This happened by unintentionally hitting the QMS entrance orifice with the sample; however, AFM and SEM images after the nitrogen bombardment are not available, and a comparison of the surface before and after is not possible.

The AES is a technique with a restricted use for the surface analysis due to its very small range of depth sensitivity, typically about a few atomic layers. The technique relies on probing the electronic energy levels of elements undergoing auto ionization. The secondary electrons that get created when a surface is bombarded with an electron beam are analyzed and their energy distribution is obtained. AES has the capability of identifying every element found on the surface, located within the first few atom layers.

The imaging techniques that were used (AFM, SEM) and the elemental and chemical state investigation of the surface (AES) are non-destructive, so the techniques could be used repeatedly in order to follow the evolution of the surface of the samples.

## 2.3 Experimental apparatus: the CAMITER setup

The interaction of tungsten with nitrogen and deuterium is studied using an ensemble of interconnected vacuum chambers, named CAMITER (Carbone et Autres Matériaux pour ITER), located in the PIIM (Physics of Ionic and Molecular Interactions) laboratory of Aix Marseille University.

### 2.3.1 General description

The experimental apparatus consists in three different ultra-high vacuum (UHV) chambers connected to a forth chamber used for plasma exposures:

a) A load-lock chamber (base pressure lower than $1\times10^{-9}$ mbar) also used for sample storage;
b) An implantation/thermo-desorption (impl/TPD) chamber, with a base pressure lower than $4\times10^{-10}$ mbar;
c) A chemical analysis chamber;
d) A plasma exposure chamber.

The impl/TPD chamber is connected with all the other three vacuum chambers thanks to a transfer rod. Due to the design of the load-lock chamber, a given sample can be transferred from air to UHV in less than five minutes. The sample is first introduced from air, through a doubly differentially pumped quick sample introduction system, inside the load-lock chamber. Then it can be further moved to any of the other chambers. From the ensemble of vacuum chambers, the impl/TPD and the load-lock chambers have been used extensively for the measurements presented in this thesis. Schematics of the load-lock and the impl/TPD chambers are presented in figure 6 and 7. For simplicity, schematics of the other chambers are not included.

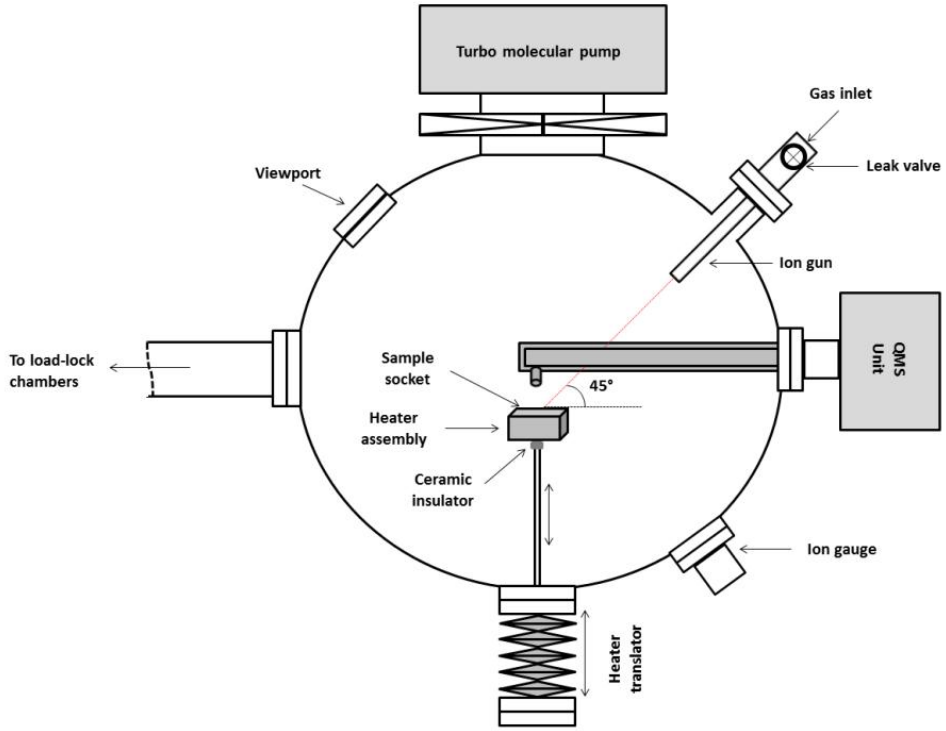


***Figure 6 – Schematic of the impl/TPD vacuum chamber***

For implantation, a low flux, low energy ion gun is used. For quantifying the retention, a Temperature-Programmed Desorption (TPD) technique is applied thanks to a UHV-compatible heater. Since the implantation and the desorption are performed inside the same impl/TPD chamber, a degasing of the heater assembly is necessary after implantation in order to record only the signal coming from the sample and keeping the signal from the heater assembly within the noise level. For this, the sample is moved to the load lock chamber (and kept under UHV) and a temperature ramp is applied to the heater. The sample is moved back in the impl/TPD chamber when the heater has cooled down to room temperature. This procedure takes usually around 90 minutes since no external cooling is applied. The experimental apparatus has the capability to do implantations and to perform sample analysis without exposing the sample to air (*in situ* experiment).

The impl/TPD chamber has a spherical shape with a diameter of roughly 40 cm and it has its own pumping system. The UHV pressure in the impl/TPD chamber is obtained with a rotary vane pump backing a turbo pump (Agilent TV 1001 Navigator) and an adequate baking of the chamber after any air exposure. The base pressure obtained this way is better than $4 \times 10^{-10}$ mbar. In addition to several viewports, the impl/TPD chamber has flanged connections for two ion guns, for a movable UHV heater assembly (Section 2.3.3), and for the differentially pumped Quadrupole Mass Spectrometer (QMS) (Section 2.3.4).

The load-lock chamber (storage chamber) has two main uses: it serves for introducing a sample from air to UHV and for the storage of a sample which needs to be moved away from the impl/TPD chamber. This need arises because the heater assembly needs to be degassed, between ion implantation and the TPD ramp. The degassing of the heater assembly insures a low background signal for the step of temperature-programmed desorption measurement. The sample is moved between the impl/TPD and the load-lock chambers with the help of a metallic rod located in the load-lock and driven by an exterior magnetic handle. By the use of different suspension rings, the rod can be moved horizontally and vertically in order to facilitate the sample transfer in respect to both the load-lock sample-introduction assembly and the UHV heater assembly. The UHV pressure in the load-lock chamber is obtained by a separate set of pumps than the impl/TPD chamber. The three stages mechanism used for pumping and sample transfer is presented in figure 7:

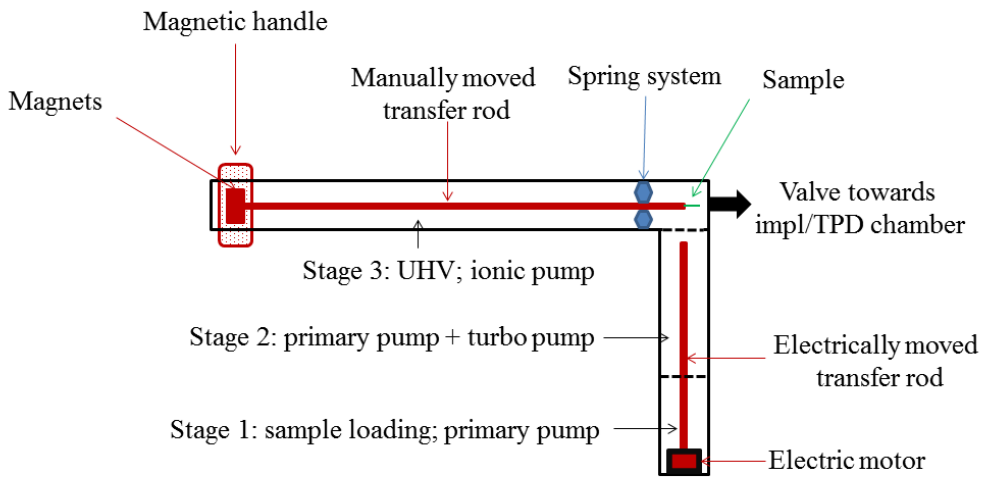


***Figure 7 – Schematic of the load-lock system (UHV storage chamber)***

In order to reach UHV pressure inside Stage 3, the entire load-lock is firstly pumped with the primary pumps and a turbo pump, and it is adequately baked. Then, a valve is used to separate Stage 3 and Stage 2, and an ionic pump is used to bring the Stage 3 pressure in the UHV range. The base pressure obtained this way is below $1 \times 10^{-9}$ mbar.

Upon sample loading, the transfer is achieved by using two transfer rods. The first rod is electrically controlled and it is used to transfer the sample from air to Stage 3. The manually controlled transfer rod is used to grab and remove the sample from the first rod. The first transfer rod is then retracted all the way to Stage 1, and the sample remains attached to the transfer rod inside Stage 3. From this point on, the sample can be moved back and forth

between the load-lock chamber and the impl/TPD chamber without the loss of UHV quality. The gate valve separating these two chambers insures that the sample can be safely stored in the load-lock while degassing operations are performed inside the impl/TPD chamber.

### 2.3.2 Ion implantation

The implantation of molecular ions is performed by using an OMICRON ISE 10 ion source connected to a KREMER PS 10 control unit. This type of ion source was originally designed for cleaning samples used in surface science analysis. The gas flow is controlled by an all-metal leak valve whose gas inlet is connected directly to the ionization cage. Here, thermal electrons are emitted by a cathode constituted of an Yttrium oxide coated ribbon filament and are accelerated towards an anode grid which has a potential of +120 V with respect to the filament. On their way to the anode the accelerated electrons ionize by impact the leaked gas.

The ions are extracted from the source volume and can be accelerated to a set kinetic energy between 0.2 keV and 5 keV. The beam can also be focused with the help of an ion-optic lens that is positioned behind the extractor electrode. The alignment of the ion beam on the sample is provided by the use of a port aligner composed of three threaded shafts installed between the ion gun flange and the Impl/TPD chamber flange. In our case the beam has an incident angle of 45° leading to an ellipse shaped beam spot. A "Degas" function on the control unit allows for the ion gun to be degassed before every implantation.

The size and position of the ion beam spot was checked by mounting a quartz sample on a similar type of platen and with the same type of mask used for a real sample.

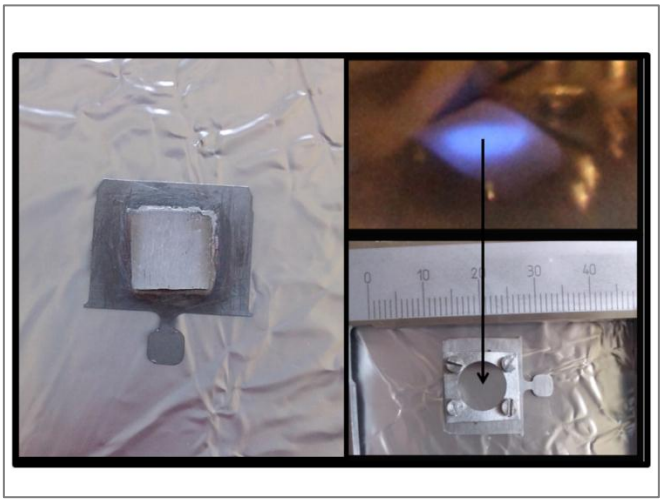

***Figure 8 – a quartz sample mounted on a molybdenum platen (left); the quartz sample emits light when bombarded with ions (up-right); the position of the ion beam spot is positioned in such a way that it falls only on the sample and the implantation of the molybdenum mask is avoided (right-bottom)***

The incident ions hit the quartz sample and they induce the emission of light (luminescence). A CMOS photo-camera with an adequate exposure time setting was used to record the emitted light. By moving vertically the entire heater assembly, the exact vertical position for which the beam falls on the sample without touching the molybdenum mask was determined. This position is different from the position at which the heater assembly is placed for the TPD step. These two positions are marked on the outside of the chamber, on the translation stage of the heater assembly.

In order to avoid electrical charging of the implanted sample and for measuring the ion current through the sample during ion implantation, a Keithley picoammeter (410A) is connected between the heater assembly and the ground. A schematic of the system formed by the ion gun, sample, heater assembly and picoammeter is shown below:

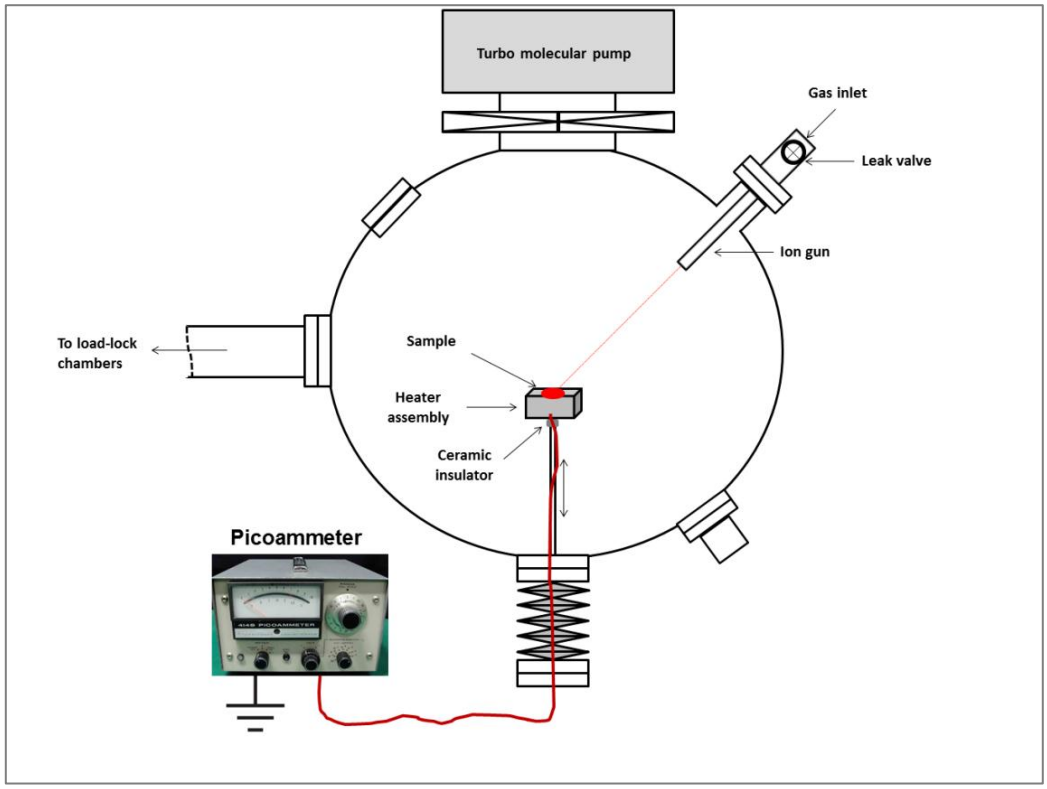


***Figure 9 – Schematic of the configuration that allows the electrical charge to flow between the sample, which is bombarded by molecular ions, through the picoammeter and to the ground***

The entire heater assembly is isolated from the UHV chamber by ceramic parts but it is in direct contact with the sample. A feed-through connector allows reading the current on a picoammeter. This allows the sample current to be drained and measured during implantation. The total incident fluence is calculated by converting the sample current into particle flux and by integrating the particle flux for the duration of the implantation. A practical relation for this is:

***Equation 8***

$$fluence = \frac{I_s \times t}{e \times A_s}$$

where $I_s$ is the current drained through the sample, $t$ is the total time of implantation, $e$ is the elementary charge and $A_s$ is the area of the sample that falls under the incidence of the ion beam. Equation 8 gives the incident fluence as the total number of molecules that have hit the sample during implantation.

### 2.3.3 Temperature calibration

The temperature of the sample is controlled by a heater assembly constructed as a molybdenum box with approximate dimensions of 5.5×3.5×2.5 $cm^3$. Pictures of the heater assembly are presented in the figure below:

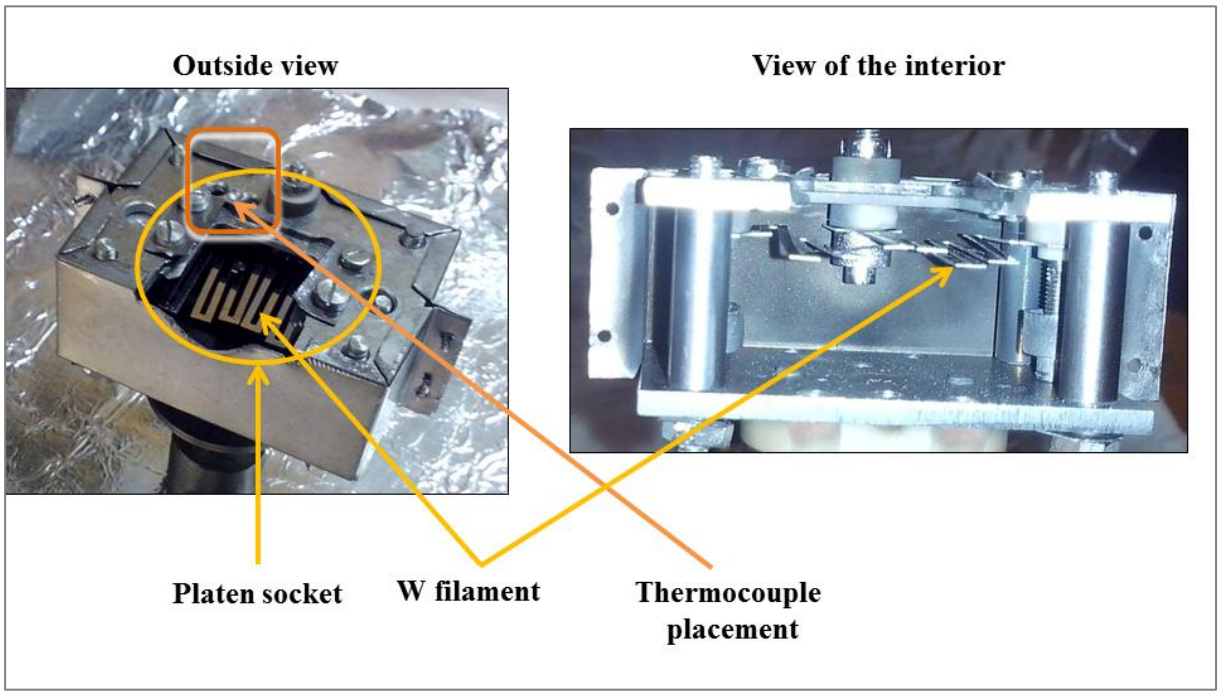


***Figure 10 - Pictures of the heater assembly: outside view – left; inside view (heater is dismounted for reparations) – right***

The upper face of the box is cut in such a way that it serves as a socket for the transfer platen. Inside the box, a tungsten filament is held in place by three molybdenum screws isolated from the filament by ceramic parts. Using molybdenum ribbons and copper feed-through connectors, the filament is connected to the power supply, both of them being kept floating in respect to the UHV chamber.

The heat transfer between the filament and the sample is achieved mostly by radiation, the contact surface between the transfer platen and the heater assembly being very small. A K-type thermocouple is mounted on the upper face of the heater assembly and is held in place by a molybdenum clip and two molybdenum screws at a distance of 2 mm from the platen's socket. In order to control the temperature of the heater assembly, the thermocouple is connected to an EUROTHERM 2604 high accuracy and high stability temperature and process controller. It is an advanced ramp/dwell programmer with storage for up to 50 programs and with several inputs and outputs. In our case the thermocouple attached to the heater assembly is connected to one of the inputs. This input serves on one hand to feed the process controller (run in a PID mode) and, on the other hand to record the temperature evolution thanks to a transmission output connected to the HIDEN Analytical control unit of the Quadrupole Mass Spectrometer (Section 2.3.4). Therefore, the temperature trace is saved synchronously with the desorption rates for the different species followed by the mass spectrometer during a typical TPD measurement. A second output of the EUROTHERM device is used to control the current delivered by the power supply that feeds the filament of the heater.

Both the ion implantation and the TPD are performed in the impl/TPD chamber. However, in order to record only the signal from the sample, the heater assembly needs to be degassed prior to the TPD step and the sample is stored in the load-lock chamber during degassing. Because of this necessity to move the sample between chambers, it is not possible to attach a thermocouple to neither the platen nor the sample. As a consequence, since the temperature of the sample cannot be measured directly, information about the sample temperature is obtained by using the thermocouple mounted on the heater assembly. For this purpose, a calibration procedure is performed to define correspondence between the sample temperature and the heater assembly's temperature.

Two types of calibrations were needed. The first type of calibration concerns the implantation at a certain sample temperature. The second type of calibration is related to the linear ramp used to heat the sample during the TPD step.

In order to perform these calibrations, a typical tungsten sample was used as a dummy sample. A second K-type thermocouple was spot-welded on its ion gun facing side (implantation side), and was connected to a second PID controller (MICROMEGA CN77352-PV).

The first type of calibration, for the implantation temperature, was performed as follows:

- the dummy sample was mounted on the heater assembly, in the same position as for a real implantation and both temperature traces, the sample and the heater assembly, were monitored;
- power was applied gradually to the heating filament until the temperature of the dummy sample is stabilized at the desired implantation temperature;
- the stability of the two temperature traces were verified for at least 30 minutes;
- an average temperature was determined, on each temperature trace, giving this way the temperature of the heater assembly at which the sample is stable at the desired implantation temperature;
- the four steps presented above were repeated at all implantation temperatures used in this thesis.

For the second type of calibration, the linear ramp of temperature applied to the sample during the TPD step, it is necessary to calibrate the entire program used by the EUROTHERM controller. The goal is to control the temperature of the (dummy) sample using only the readings from the heater assembly's thermocouple. The heater-sample temperature calibration is achieved in two steps:

Step 1 consists in obtaining the nonlinear profile of the heater temperature trace which corresponds to the linear increase of the sample's temperature:

- the dummy sample is mounted on the heater assembly in a position suitable for the TPD measurement (i.e. the sample surface is located ~2 mm from the entrance tip of the mass spectrometer stage);
- the sample thermocouple is connected to the EUROTHERM controller and the heating assembly thermocouple to the MICROMEGA controller (this step is just a technicality and it is performed due to the better performance of the EUROTHERM controller against the MICROMEGA);
- a linear ramp of temperature is imposed on the sample with a heating rate $\beta = 1$ K/s, from ambient temperature up to 1300 K; at the same time, the temperature trace of both thermocouples, the heater assembly and the sample, are recorded;

Step 2 consists in applying the nonlinear profile for the heater, obtained in Step 1, and obtaining (verifying) the linear increase of the temperature of the sample:

- the two PID controllers are switched so that, this time, the temperature can be imposed (controlled) on the heater assembly;
- the heater temperature trace obtained in Step 1 is divided in linear segments;
- the slopes of the obtained segments are entered in the EUROTHERM controller in order to recreate the heater temperature trace observed in Step 1. This is the so-called nonlinear profile of the heater temperature;
- when the heater temperature is regulated with the EUROTHERM nonlinear profile, the temperature of the sample is recorded using the MICROMEGA controller. The sample temperature deviation to the ideal 1 K/s ramp is analyzed;
- the calibration obtained this way is verified and modified multiple times until all deviations and oscillations from the ideal 1 K/s ramp on the sample are removed. This is basically a trial and error process. In particular, it was found that a pre-heating step is needed to help eliminating eventual oscillations at the beginning of the ramp.

Calibrations were performed between sets of measurements, in order to check for any evolution of the thermal contacts with time, and also for every situation when the heater assembly was modified in any physical way (change of thermocouple or heater ceramics for example). It was noticed that a small modification of the heater assembly can alter its behavior in such a way that a new calibration is necessary.

Finally, for the representation of TPD measurements, the TPD curves need to be plotted as a function of the sample temperature. The heater assembly temperature trace, which is recorded during TPD needs therefore to be converted into sample's temperature trace. To achieve this, a reverse procedure is applied to the calibration of the temperature ramp, in the following manner:

- the recorded sample temperature trace ($T_s$) is plotted as a function of the recorded heater temperature trace ($T_h$); these two real traces are available from the calibration procedure;
- a polynomial fit is applied and the dependency between the two real temperature traces is obtained; a $9^{th}$ order polynomial was used;
- for the case of a typical TPD measurement, when only $T_h$ is recorded, the polynomial fit obtained at the previous step is used to convert $T_h$ trace into $T_s$; this procedure was tested and it was found to give a reliable $T_s$ trace.

### 2.3.4 TPD - QMS detection

During the TPD step, the particles getting desorbed from the sample, as the sample is linearly heated, are detected by a Quadrupole Mass Spectrometer (QMS). The QMS is differentially pumped and it is mounted above the heater assembly. The distance between the sample's surface and the entrance tip of the QMS stage is set to 2 mm for the TPD step, as depicted in the schematic presented in the figure below:

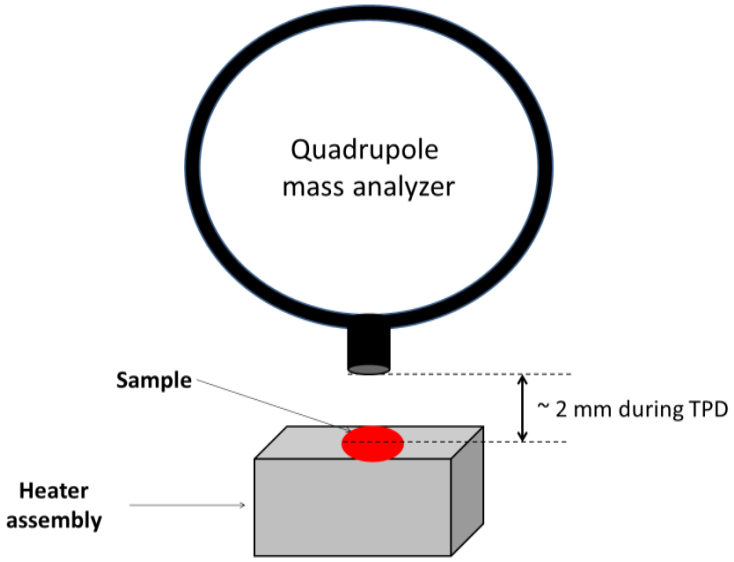


***Figure 11 – Distance between the sample and the QMS entrance orifice is 2 mm for TPD***

The base pressure inside the QMS stage is $2 \times 10^{-11}$ mbar, and it is provided by a separate set of pumps (primary pump plus turbo pump) and an adequate baking after any exposure to air.

The QMS is used to determine the rate of desorption for the molecules that get desorbed from the sample. The raw data consists in the number of counts per second recorded when particles with a certain value of mass to charge ratio (m/z) are detected. Since the same value of m/z can correspond to different type of molecules or to molecular fragments, calibrations are needed in order to convert the raw signal into the rate of desorption expressed as molecules per second. The method consists in a leak calibration experiment that gives a direct correspondence (applied as a conversion coefficient) between the number of detected counts per second and the number of desorbed molecules per second. This method is described in detail in the next section.

Since deuterated ammonia ($ND_3$) was not available for a similar leak calibration experiment, the coefficient of conversion from counts to molecules was calculated by using

the coefficients measured for $D_2$ and $N_2$ molecules. The method used for this calculation will also have a dedicated section (2.3.4.2).

### 2.3.4.1 Conversion of QMS signal into numbers of molecules: calibration method for $D_2$ and $N_2$ signals

The principle of the leak calibration experiment consists in leaking the gas of interest inside the impl/TPD chamber to various fixed pressures and recording the raw QMS signal for the gas for which the calibration is being performed. For each setting of the pressure, an average of the detected signal is calculated. This way the correspondence between the pressure inside impl/TPD ($p$) and the number of recorded counts per second ($RawS$) is determined.

By using the kinetic theory of gas and considering the geometry of the experimental configuration, the pressure inside impl/TPD ($p$) is converted into a flux of molecules ($j$) reaching the entrance surface of the QMS stage. For a Maxwell-Boltzmann distribution of the gas particles, the relation for the flux density is:

***Equation 9***

$$j = \frac{1}{4} n v = \frac{1}{4} \frac{p}{k_B T} \sqrt{\frac{8 k_B T}{\pi m}} = \frac{p}{\sqrt{2 \pi m k_B T}}$$

where $n$ is the volume particle density, $v$ is the average velocity, $p$ is the pressure in the vacuum chamber, $k_B$ is the Boltzmann constant, $T$ is the temperature of the gas and $m$ is the mass of the particles expressed in atomic mass units. The flux density can be further used to determine the flux of particles ($\Gamma$) going inside the QMS by considering the surface area of the QMS entrance orifice ($A_{QMS}$):

***Equation 10***

$$\Gamma = j \times A_{QMS}$$

At this point, $RawS$ can be plotted as a function of the flux of molecules reaching the QMS ($\Gamma$). The slope obtained for the linear fit of this data set represents the sensitivity coefficient ($S_{coeff}$), defined as the number of counts recorded for a certain number of molecules that have passed through the surface of the QMS entrance orifice. The unit of this coefficient if [$S_{coeff}$] = counts/molecules.

An analytical model was used to determine the percentage of the total number of molecules which, after getting desorbed from a certain area of the sample, reach the entrance

of the QMS and get counted. This percentage is related to the geometry of the system, and will therefore be described as the geometrical factor (*G)*. Its value depends on the area of ion implantation on the sample ($A_s$), the area of the QMS entrance ($A_{QMS}$) and the distance between the two. The unit of the geometrical factor is [G] = % and it expresses the percentage of molecules that reaches the QMS, from the total amount of molecules that were initially desorbed from the entire surface area of the sample. In order to estimate the value of *G*, the spatial distribution of the desorbed molecules was considered to follow a cosine distribution law, and a Monte Carlo simulation was used. For all the measurements presented in this thesis the value of *G* was set to 4% corresponding to distance of 2 mm between the sample and the QMS orifice.

If the desorption rate is needed in the form of the desorption rate of individual atoms, an extra term can be considered, namely the number of the respective atoms in a molecule, $N_{at.}$

In order to calculate the total number of atoms that have been desorbed, per second, from the entire surface of the sample ($A_s$) (i.e. the desorption rate in atoms per meter squared per second), the following expression is used:

***Equation 11***

$$r = \frac{RawS}{S_{coeff} \times A_s \times G} \times N_{at}\,.$$

Equation 11 is valid for the types of molecules for which the sensitivity coefficient $S_{coeff}$ was directly determined (i.e. that was obtained following the QMS calibration procedure). If the sensitivity coefficient of another molecule (not available for direct calibration) is needed (e.g. HD or $ND_3$), its sensitivity coefficient can be derived from the experimentally measured coefficients of our reference molecules ($D_2$ and $N_2$). The method used for the derivation of these coefficients ( $S_{coeff}^{calc}$ ) is described in the next section.

For the detection of deuterium molecules ($D_2$), the following mass to charge ratio was followed: m/z = 4, naturally. However, for the detection of nitrogen molecules ($N_2$), the signal of m/z = 14 was used instead of m/z = 28. Indeed, the m/z = 28 signal, which corresponds to the main ionization product $N_2^+$, is not suitable for the quantification of the desorbed nitrogen due to its overlap with the signal from $CO^+$. In practice, the signal of an unexposed sample was compared to the signal obtained after nitrogen implantation and it was observed that the peak of nitrogen overlaps with a peak for m/z = 28 that is always present on an unexposed sample due to the presence of residual CO molecules in the chamber that stick to the metal

surfaces. Therefore, we chose to record the signal at m/z = 14, which corresponds mostly to $N^+$ with some additional signal from $N_2^{++}$ at high electron energy inside the QMS ionizing stage [56]. Statistically, the numbers of $N^+$ and of $N_2^{++}$ responsible for the measured signal at m/z=14 have a fixed ratio for a given electron energy. Thus it is possible to use this signal to calibrate the number of $N_2$ molecules entering the QMS stage.

### 2.3.4.2 Extrapolation of $N_2$ and $D_2$ calibrations for the quantification of HD and $ND_3$ molecules

Throughout the experiments performed using deuterium and/or nitrogen, the sensitivity of detection was calculated (and not measured) for the quantification of two molecules of interest: HD and $ND_3$. The starting point consists in using a known sensitivity, measured for a somehow similar molecule. For the case of HD, it is at hand to use the sensitivity measured for the detection of $D_2$. For the case of $ND_3$, the sensitivity of detection was determined by using the calibrations for both $D_2$ and $N_2$ and by calculating an averaged final value. In this case the signal of m/z = 28 was used for nitrogen.

The sensitivity of detection is calculated by applying a correction factor to the measured sensitivity for the calibrated molecule ($S_{coeff}$). This correction factor accounts firstly for the difference in ionization cross section for the two molecules which is implemented as the ratio between the two ionization cross sections), and secondly, it accounts for the difference in transmission through the QMS entrance orifice, of the two molecules. This second correction is obtained as the ratio of the flux densities, for equal pressures. With $\sigma$ being the ionization cross section following electron-impact with known electron energy, the sensitivity for the two molecules mentioned above is determined as follows:

a) for HD:

***Equation 12***

$$S_{coeff}^{calc} = S_{coeff}(\mathrm{D}_2) \times \frac{\sigma_{HD}}{\sigma_{D_2}} \times \frac{\sqrt{m_{D_2}}}{\sqrt{m_{HD}}}$$

b) for $ND_3$:

- the sensitivity was calculated using both $D_2$ and $N_2$ calibrations:

***Equation 13***

$$S_{coeff}^{calc} = S_{coeff}(\mathrm{D}_2) \times \frac{\sigma_{ND_3}}{\sigma_{D_2}} \times \frac{\sqrt{m_{D_2}}}{\sqrt{m_{\mathrm{ND}_3}}}$$

***Equation 14***

$$S_{coeff}^{calc} = S_{coeff}(\mathrm{N}_2) \times \frac{\sigma_{ND_3}}{\sigma_{N_2}} \times \frac{\sqrt{m_{\mathrm{N}_2}}}{\sqrt{m_{\mathrm{ND}_3}}}$$

- an average of the two sensitivities calculated above was obtained as the final value for the sensitivity coefficient for the detection of $ND_3$.

The values used for the ionization cross sections were taken from the literature (Straub et al. [56] for $H_2$, and $N_2$, Itikawa et al. [57] for $H_2O$, and Rejoub et al. [58] for $NH_3$ and $ND_3$) and the fragmentation patterns were taken from the NIST database.

## 2.4 Retention quantification using TPD analysis

The main result given by the TPD technique and used for the experiments presented in the next chapters, is the total number of atoms desorbed from the sample, which is assumed to be equivalent to the notion of total retention. The method of determining the retention, starting from a raw desorption curve obtained during TPD is presented in this section. The retention results obtained with TPD were validated using the Nuclear Reaction Analysis technique.

During TPD, the desorption rate of various molecules is recorded as a function of the heater's temperature and as a function of time. The heater temperature trace is then converted into sample temperature trace using the method described in section 2.3.3. The desorption curve is at this point available as a function of both the temperature of the sample and as a function of time. In order to determine the retention of a certain species, the plot of desorption rate vs. time is used. An example of the retention quantification procedure is shown in the figure 12 for the signal of m/z =4, meaning for $D_2$ molecules. The x-axis represents the time in seconds and the y-axis represents the desorption rate in counts per second. The total number of detected counts ($RawS_{total}$) is obtained by integrating the peak of desorption. To achieve this, firstly, a baseline of the background signal is constructed, and then, it is subtracted from the signal. A center for the peak of desorption is chosen in such a way that it approximates the maximum of the peak. The limits of integrations are chosen in such a way that they contain the peak of desorption but they leave out unnecessary parts of the curve. This approach limits the errors induced by the quality of the baseline construction since the integration is not performed on the entire curve of desorption. In figure 12, these limits are represented by the blue vertical markers. On the example below, a small bump can be noticed just before the first blue marker. This bump is the result of the first power impulse applied to

the heating filament of the heater assembly and it is considered to come from a flash desorption of the heating filament. It is therefore not included in the integration.

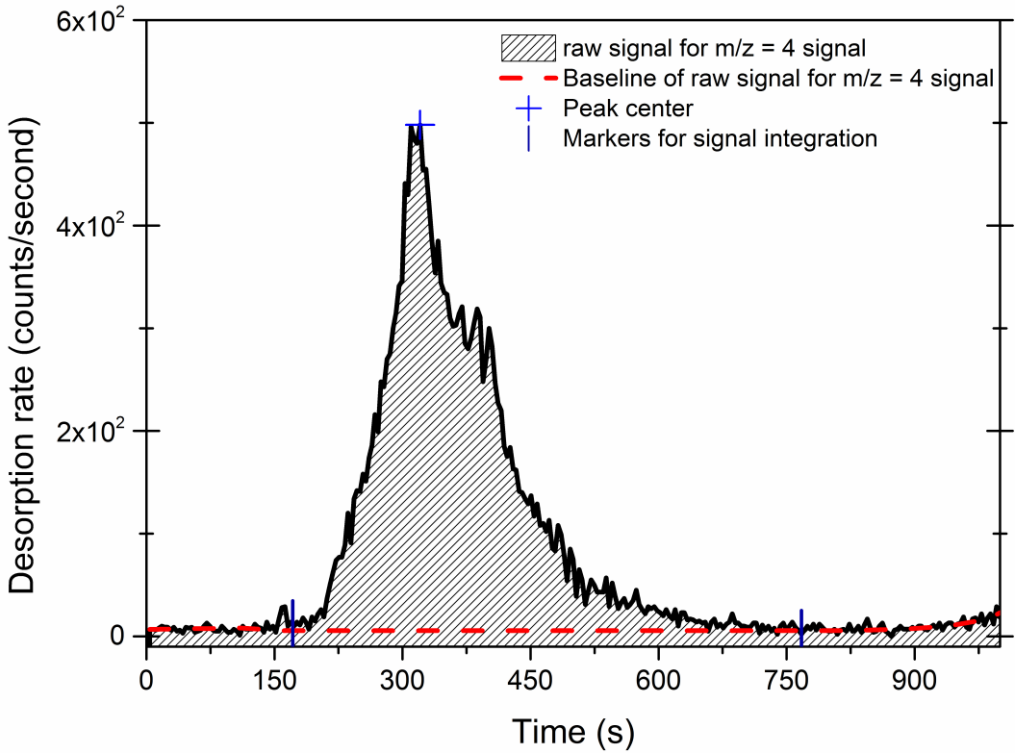


***Figure 12 – Method of integration of a desorption peak used for the quantification of desorbed molecules***

The integration of the desorption peak gives the total number of recorded counts ($RawS_{total}$). By integrating equation 11, the expression for the total retention ($R$) is obtained:

***Equation 15***

$$R = \frac{RawS_{total}}{S_{coeff} \times A_s \times G} \times N_{at}$$

For the example used above, the real values corresponding to the measurement in figure 12 will be used in order to determine the number of D atoms that desorbed in the form of $D_2$:

***Equation 16***

$$R = \frac{RawS_{total}}{S_{coeff} \times A_s \times G} \times N_{at} = \frac{68797.70}{(2.8006 \times 10^{-8}) \times (0.04 \times 5.03 \times 10^{-5})} \times 2 = 2.44 \times 10^{18}\, D/m^2$$

In this calculation $A_s$ represents the area of the sample surface that is not covered by the molybdenum mask (particle emitting surface). Since deuterium is desorbed also in the form of HD molecules, the same procedure is applied for the HD spectrum (m/z = 3). In this case $N_{at}$ = 1 since the molecule incorporates only 1 D atom. The total number of D atoms desorbed

from the sample will therefore consist in the sum of the two values of *R* calculated for the two desorption spectra. Similar procedures are applied for quantifying the release of nitrogen in the form of $N_2$, calibrated for the signal m/z = 14, and for quantifying the amount of deuterated ammonia released as $ND_3$, measured as the signal of m/z = 20. When deuterated ammonia is present, the number of deuterated ammonia molecules is also taken into account to determine the total retention of deuterium and nitrogen.

Throughout this thesis, TPD spectra are usually presented as an average of replicate measurements spectra. In order to obtain the average spectrum, the spectra from each individual measurement are binned-averaged in 5 K temperature intervals.

### 2.5 Samples

Two types of samples were used for the experiments presented in this thesis: polycrystalline tungsten (PW) and single crystal tungsten (SW). In both cases, the samples were mounted on a molybdenum transfer platen.

#### 2.5.1 Source and preparation

The polycrystalline tungsten samples used in this thesis were provided by A.L.M.T. Corp with a specified purity of 99.99 wt.%, and were cut into specimens with the following dimensions: 10.0×10.0×0.4 $mm^3$. They were delivered mechanically polished to a mirror finish and recrystallized with a typical grain size of ~ 30 μm. The preparation process performed before introducing the samples inside the UHV chamber consists in an electro-polishing procedure with a 2.5 wt. % NaOH solution followed by rinsing with distilled water. Dry nitrogen was blown in order to remove eventual dust from the sample.

One single crystal tungsten sample was available for this thesis. It was provided by Surface Preparation Laboratory (The Netherlands). The specimen was mechanically polished such that the (111) surface orientation was exposed to ion beams. The single crystal has the following dimensions: 14×12×2 $mm^3$. No extra preparation procedure was applied before the sample was introduced to UHV, except for the use of dry nitrogen to remove any dust.

Since the samples need to be moved between several chambers during experiments, they are mounted on a molybdenum transfer platen. The platen has a surface area of 16×14 $mm^2$, which makes it slightly larger than the sample, and it has a circular hole (9 mm diameter) located under the sample's usual position on the platen. Since the heating of the sample is achieved by radiation from the tungsten filament of the heater assembly, this hole allows an easier heat transfer from the heater's filament to the sample.

The platen is also machined with a grabbing key (a flat nipple) on which a transfer rod tool can be screwed. When the platen is locked by the transfer rod it can be removed or introduced from/into the heater assembly and it can also be moved to the load-lock if it needs to be put to air. The same locking system is used when the sample is introduced inside UHV or when it needs to be transferred to one of the other vacuum chambers. Photograph images of the sample and the sample mounted on the platen are shown in figure 8. On the left side, a PW sample is placed on a broken platen used in this case for the sole purpose of illustrating the occasional occurrence of the breaking of a sample platen due to a problematic sample transfer. On the right side, the PW sample is mounted on a ready-for-UHV platen.

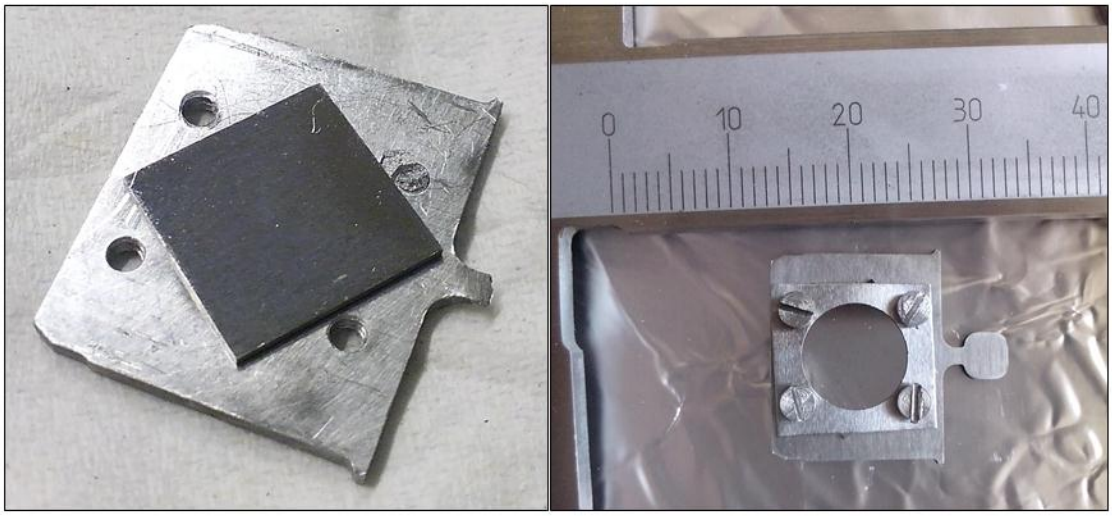


***Figure 13 – A PW sample with a broken grabbing key (left); A PW sample mounted on the transfer platen (right)***

The PW samples are fixed onto the platen by a mask and by 4 screws. All the components of the sample holder (platen, mask and screws) are made from molybdenum (>99.9 wt.%). Due to the slightly higher dimensions of the SW sample, only two molybdenum screws were used to fix the sample, and no mask was applied. Indeed, bore holed where machined (by Surface Preparation Laboratory) in the single crystal to allow directly attachment of the SW sample onto the platen. If all four screws would be used to fix the SW sample on the platen, it would become impossible to load the sample-platen assembly into the first transfer rod (see section 2.3.1 for load-lock description).

After a sample is introduced in the UHV chamber and before implantation/desorption measurements are performed, at least two linear heating ramps of 1 K/s are performed, with a temperature excursion going from room temperature up to 1300 K. Each of these degassing procedures is followed by a 10 minutes annealing at 1300 K.

### 2.5.2 Characterization with AFM and SEM

Examples of sample characterization, obtained with AFM and SEM are presented in this section.

AFM images for polycrystalline tungsten samples and for the single crystal are shown in the figure below.

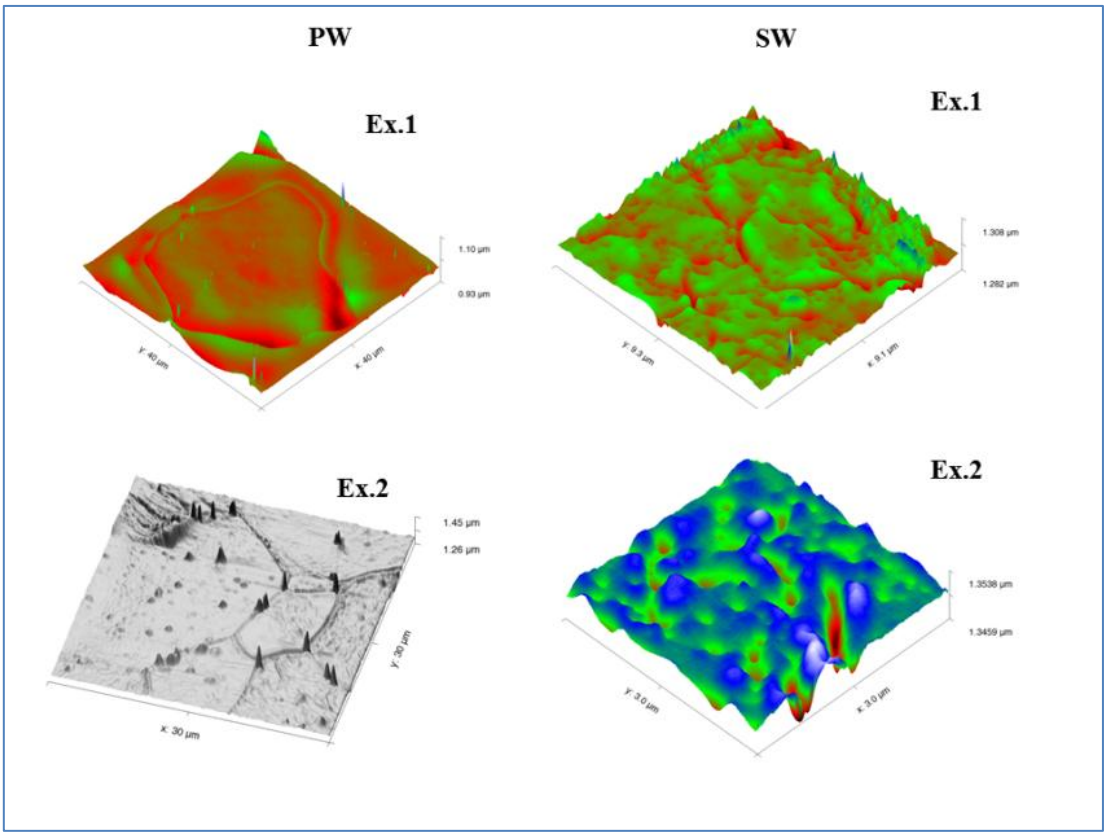


***Figure 14 – AFM images obtained on both PW and SW samples***

The roughness measured on the two types of samples (evaluated on area up to 40x40 $mm^2$) is noticed to be higher for the polycrystalline tungsten: the roughness for PW samples are about 7 ± 3 nm, while the roughness for SW is about 1 ± 0.3 nm. No significant change of the roughness was observed as a result of the implantation/desorption cycles for deuterium implantation. For nitrogen, post implantation images are not available and it cannot be said whether the roughness was modified as a result of nitrogen bombardment or not.

SEM images obtained on different samples are presented in the figure 15 (the upper part). On the lower part, AES measurements are shown for an “as introduced” sample vs. an annealed sample, in order to show the reduction effect that the annealing step has on the native oxide layer.

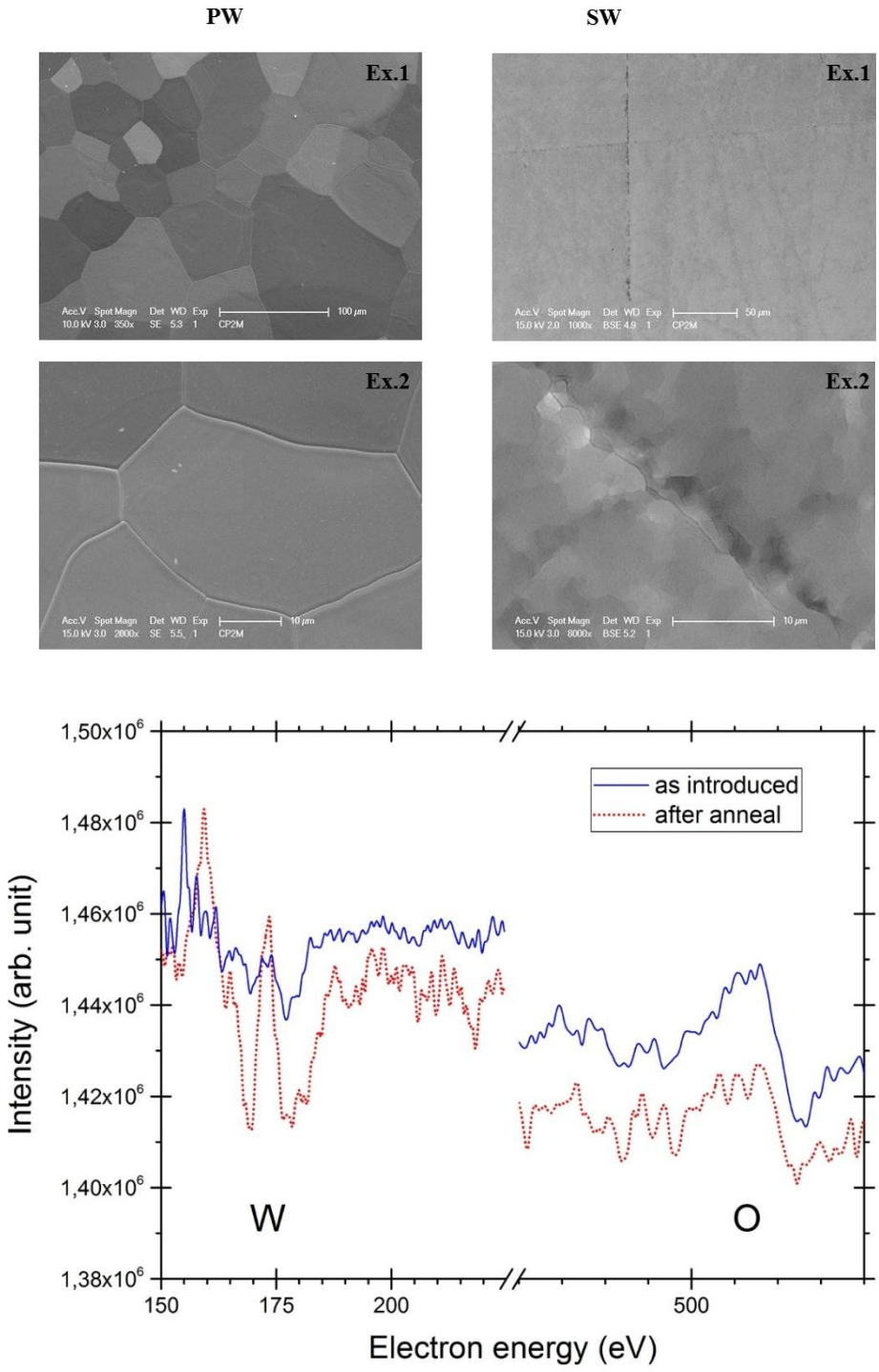


***Figure 15 – SEM images obtained on both PW and SW samples – upper part; AES spectra obtained on an as introduced vs. annealed sample – lower part***

The size of the grains for the PW samples is observed to be in the range of 10 – 30 microns, while for the SW sample no grains are observed. A better quality of the surface preparation is observed for the PW samples (figure 15, left) as compared to the single crystal one. This difference is probably the result of the electro-polishing performed on the PW samples, while the SW sample is introduced in UHV as received (only dry nitrogen is used in order to remove the dust). Various defects can be observed on the SW sample, like scratches that are noticed on various locations of the SW surface (figure 15, up-right image), and can extend laterally up to the micrometer range (figure 15, down right image). These defects observed on the SW sample are not observed on electro-polished PW samples and thus they should be the signature of the mechanical polishing of the SW sample.

From the lower part of figure 15, a reduction of the oxide layer is observed, as a result of the annealing procedure performed on a typical sample, as a part of the preparation step.

# Chapter 3

# Deuterium retention in tungsten

The fuel for the fusion reaction that will be exploited in ITER [59] and in future fusion devices will consist in the hydrogen's isotopes, deuterium (D) and tritium (T) [60]. It was proven experimentally [61] that the fusion of these two isotopes produces the highest energy gain while keeping the temperature at the lowest value possible. Since tritium is radioactive (with a half-life of around 12.5 years), its use raises concerns related to nuclear safety. For ITER the maximum amount of tritium allowed inside the machine at any time is regulated by the French laws at 700 g [62]. As a consequence, another concern, for both tritium and deuterium, is related to their retention inside the machine and in particular to the retention in the plasma facing materials, which will consist of beryllium (for the plasma vessel) and tungsten (for the divertor area) [63]. For nuclear safety reasons, the retention of tritium inside the tungsten material needs to be assessed for both the short and the long term. The purpose of investigating this issue is related, on the short term to the limit imposed for the total amount of tritium inside the reactor, and, for the long term, the amounts of tritium inside the tiles needs to be assessed in the event of tile decommissioning.

These concerns are addressed in this chapter by studying the interaction of deuterium with tungsten, and in Chapter 5 where the sequential implantation of nitrogen and deuterium will be studied. The use of tritium is not possible in our laboratory but the results obtained for deuterium should be safe to extrapolate to the use of both deuterium and tritium.

In this thesis, tungsten samples were subjected to a series of deuterium implantations followed by thermo-desorption ramps, in an all *in-situ* experimental apparatus (described in Chapter 2.3), under ultra-high vacuum. The amounts of retained deuterium were determined by using a mass spectrometer to count the rate of desorption as the temperature of the sample is increased linearly from ambient temperature up to around 1300 K. In order to simulate conditions relevant for fusion reactors, ion implantations were performed for samples at room temperature as well as for higher temperatures of the samples. The concerns related to the long term retention were approached by delaying the execution of the temperature programmed desorption (TPD) after ion implantation.

Deuterium molecular ions ($D_2^+$) with an energy of 500 eV were implanted in tungsten at an angle of 45°, at low flux (~$1.6\times10^{16}$ D/$m^2$s) in both single crystal tungsten and

polycrystalline tungsten. The implantation in single crystal tungsten was performed at ambient temperature whereas the implantation in polycrystalline tungsten was performed for different values of the implantation temperature.

The polycrystalline tungsten samples were commercially provided by ALMT Corp. Japan with a specified 99.99 wt.% purity, recrystallized and with dimensions of 10×10×4 $mm^3$. The single crystal sample, with an (111) orientation, was provided by Surface Preparation Laboratory (The Netherlands) with dimensions of 14×12×2 $mm^3$.

The polycrystalline samples used for this chapter are designated as: ALMT#4, ALMT#5, ALMT#6 and ALMT#9 (since they are all from the same batch of ten). The consistency of the results was also checked on sample ALMT#8. In the preparation step, polycrystalline samples were electro-polished while the single crystal sample was introduced in vacuum as received. All samples were blown with dry nitrogen before being introduced to vacuum, in order to remove any dust. All samples were mounted on a molybdenum platen. For the polycrystalline samples a molybdenum mask and four molybdenum screws were used, while for the single crystal, only two screws were used and no mask was applied. All the molybdenum parts were sequentially cleaned in an ultrasonic bath with acetone and ethanol. When a sample was introduced from air to vacuum, it was degassed by running a temperature ramp from ambient temperature up to $T_{ov}$ = 1300 K with a 10 minutes annealing at 1300 K. This procedure was then repeated for at least two more times.

For most of the measurements, the electron energy inside the QMS ionizing stage was set to 25 eV, giving a good resolution for the signal of HD and $D_2$. For the measurements performed on ALMT#5 and for the tests performed on ALMT#8, the electron energy was set to 50 eV. The switch to 50 eV was performed because sets of sequential implantations (nitrogen and deuterium) were performed in parallel with the implantation of deuterium only. It was necessary therefore to have a high enough electron energy to detect other products (like $ND_3$ – presented in Chapter 5). For every case a proper calibration was used in order to convert the desorption rate from counts/second in $D_2$ molecules/second. The total amount of deuterium released from the sample was determined as the sum of deuterium atoms released in the forms of HD and $D_2$ molecules. The signal for m/z = 19 and m/z = 20 showed no desorption peak, suggesting that no significant amount of deuterium was being released in the form of HDO molecules or $D_2O$ molecules.

The parameters that were varied for the polycrystalline samples were the incident fluence, the temperature of the sample during ion implantation and the storage time in UHV after ion implantation. The dependency of deuterium total retention with the incident fluence

was investigated over five orders of magnitude, between $10^{17}$ and $10^{21}$ D/m$^2$. The effect of the implantation temperature was verified for 4 different temperatures between 319 ± 12 K and 600 ± 10 K. The amounts of trapped deuterium were quantified after storage time intervals ranging from 2 hours up to 315 hours. The dependency of total retention with the storage time was verified for two different fixed values of incident fluence ($2.81 \times 10^{19}$ D/m$^2$ and $1.23 \times 10^{20}$ D/m$^2$).

For the single crystal sample the parameters that were varied are the incident fluence and the storage time in UHV. The investigated range of incident fluence was smaller, with the highest value being $3.2 \times 10^{20}$ D/m$^2$. The dependency of retention with the storage time was obtained for a single fixed value of the incident fluence ($2.81 \times 10^{19}$ D/m$^2$). The implantation temperature for the single crystal sample was ambient temperature for all cases.

The study of deuterium interaction with tungsten is divided in two main sections, one focused on the results obtained for the polycrystalline samples and the second one focused on the single crystal. After investigating each of these two cases separately, they are compared side by side and a complete analysis is presented.

### 3.1 Deuterium retention in polycrystalline tungsten

Deuterium retention is first investigated as a function of the incident fluence for implantation at room temperature. Then the temperature of the sample during implantation is modified and the dependency of retention with the same fluence is studied for higher implantation temperatures. Finally, the dynamic behavior of deuterium retention and deuterium release is studied by performing the TPD after different storage times. The goal of this group of experiments is to identify the trapping mechanisms that lead to deuterium retention in polycrystalline tungsten and to assess the importance of each identified trapping mechanism for both the short and the long term retention.

#### 3.1.1 The effect of deuterium fluence on its retention in polycrystalline tungsten

The deuterium retention in tungsten (in D/m$^2$) was studied for an incident fluence range spread on five orders of magnitude ($10^{17}$ – $10^{21}$ D$^+$/m$^2$). The increase in fluence is obtained by increasing the duration of implantation and keeping the ion flux constant. Since the ion gun delivers a low flux (~$1.6 \times 10^{16}$ D$^+$/m$^2$s), the molecular ion flux was kept constant for all measurements. The lowest incident fluence, obtained using this flux, corresponds to an ion implantation of several seconds while the highest fluence was reached after 40 hours of ion implantation. The advantages of this low flux are twofold. Firstly, the low ion flux

combined with the relatively low kinetic energy of the ions (500 eV) avoid the local heating of the sample during implantation which would determine a thermal gradient on the implanted surface and may produce a difference of retention behavior throughout the sample. The expected heating rate induced by the ion bombardment was determined to be around ~$1.23 \times 10^{-4}$ K/s, meaning that it is negligible. Secondly, the low deuterium ion flux combined with the implantation temperature (319 ± 12 K) and the annealing step at the end of each TPD also avoids the evolution of the sample as more measurements are being performed. As shown in [64] at a flux that is four orders of magnitude higher, and also at higher fluence (~$10^{26}$ D/m$^2$) defects are induced, consisting in the creation of blisters near the surface and a with a more significant accumulation of deuterium in the blisters formed at the interface between grains. In our experiments a good reproducibility of the measurements is observed, when performing numerous replicate measurements on the same sample. This experimental observation shows that is unlikely that the low flux used in our measurements would induce the creation of blisters. The disadvantage of the low flux is, as already mentioned, the long duration of implantation necessary to reach the highest fluence, which, in our case is in the order of several tens of hours.

The results are shown first as the values of total retention plotted as a function of the incident fluence and are then followed by the TPD spectra corresponding to the same measurements. The durations of storage between implantation and desorption (the storage time), for all the results shown here fall between 2 and 2.5 hours.

In figure 16, deuterium retention in tungsten is plotted as a function of the incident fluence. The graph shows three different curves obtained for three samples (ALMT#4, ALMT#6 and ALMT#9). The curves are fitted with a square root power law which was determined to be the best fit for the three curves. The statistics are different from point to point, but each point corresponding to an incident fluence of $3.2 \times 10^{20}$ D/m$^2$ and smaller is an averaged value of at least three measurements. The two highest points shown for the sample ALMT#6 represent individual measurements; therefore no error bars are being shown. For all the other points, the error bars represent the standard deviation of the mean.

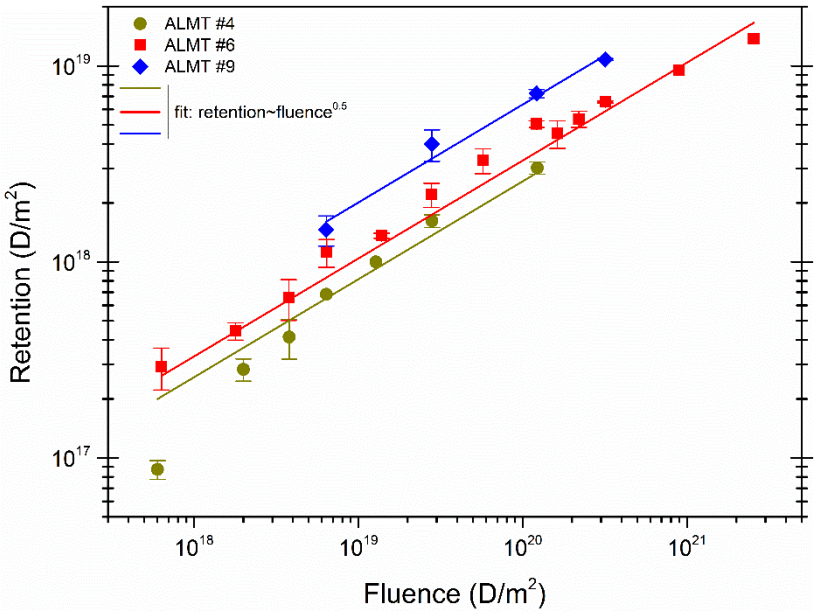


***Figure 16 - Deuterium retention in tungsten as function of incident fluence; Samples: ALMT#4, ALMT#6, ALMT#9***

The three samples show a consistent trend for retention as a function of incident fluence. However, from sample to sample the absolute retention varies within by a factor of 2 at most.

Actually, we observed that our results [16] are in good agreement with similar experiments from literature [24]. In figure 17, the curve of retention as a function of fluence published in [24] by Ogorodnikova *et al.* from the Max Planck Institut für Plasmaphysik in Garching (IPP) is compared to our results. The range of incident fluence investigated in [24] goes up to $10^{24}$ D/m$^2$, adding in this way 3 orders of magnitude to the general image presented in figure 16. The differences between our experiments and the ones from the literature are obviously the higher flux used by IPP (3 orders of magnitude higher) and also by the shorter storage time used in their experiments (around 5 minutes as opposed to our minimum storage time of 2 hours).

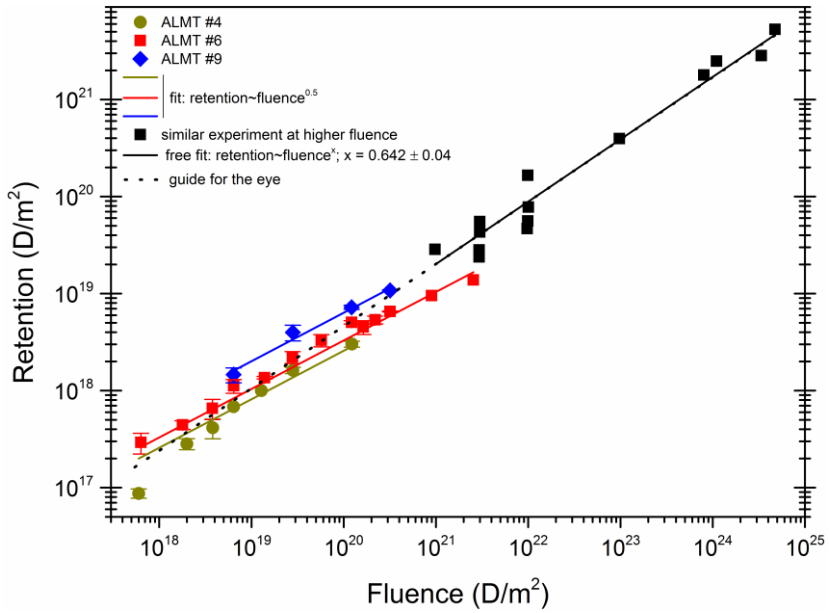


***Figure 17 - Deuterium retention in tungsten as function of incident fluence; Samples: ALMT#4, ALMT#6, ALMT#9 – comparison with results obtained by Ogorodnikova* et al. *[24]***

In our 2015 publication [16] the IPP data are compared only to the results obtained on ALMT#6. When we look solely at data sets obtained on our samples, it is noticed that they are closer to a square root dependency between retention and incident fluence. However, when combining our data with the ones of Ogorodnikova *et al.* [24] a slightly different 0.64±0.04 power law is found. The source of these variations may be found in the differences of sample preparations as it is also suggested in [24].

The desorption spectra corresponding to the curves of retention as a function of fluence plotted above, are shown in the figure 18. The results obtained on each different sample are plotted on an individual graph: a – ALMT#6, b – ALMT#9 and c – ALMT#4. The order of these graphs is the chronological order in which the sets of measurements were obtained. Each one of these spectra is an average of at least three replicate measurements. The spectra for the two highest values of incident fluence are not shown in this figure.

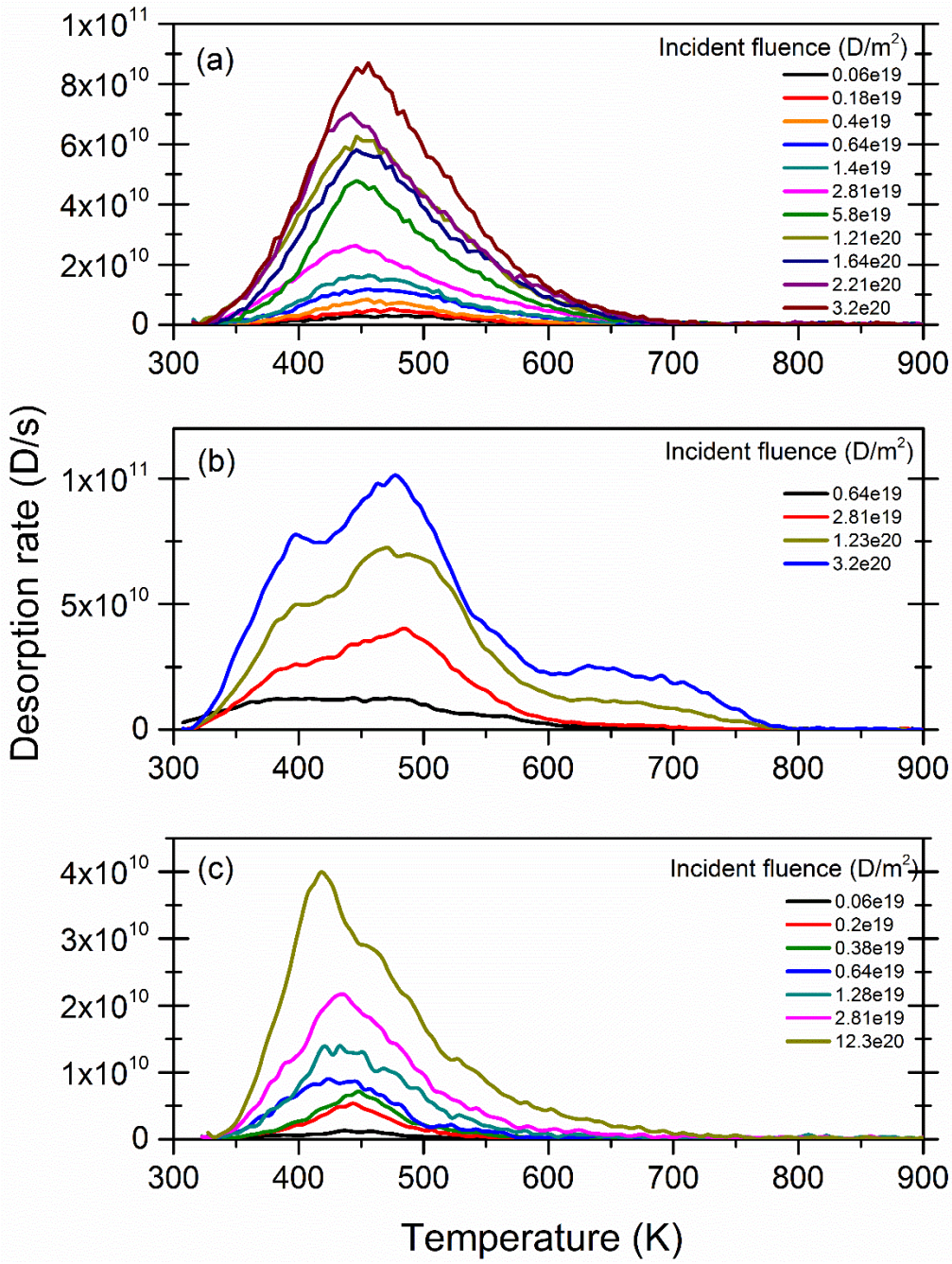


***Figure 18 - TPD spectra for different fluences of deuterium – a) ALMT#6; b) ALMT#9; c) ALMT#4***

The three different sets of measurements show some differences in the shape of the desorption peaks. The spectra obtained on the sample ALMT#6 (figure 18, a) show only one peak of desorption, with the maximum located at 450 ± 30 K and with the width increasing when the incident fluence is increased. It is also observed that the position of the peak maximum gradually decreases for around 30 K, when the fluence is increased. This shift occurs gradually up to an incident fluence of $2.81 \times 10^{19}$ D/m$^2$, and no shift is observed anymore above this value. The shape of the peak is slightly asymmetric, with the decreasing tail being longer than the leading edge.

In figure 18 (b) the spectra obtained on the sample ALMT#9 are characterized by what seems to be multiple peaks of desorption. The source of these peaks was suspected to be presence of irregularities in the temperature ramp (see Chapter 2.3.3 for the temperature calibration method) which would generate oscillations in the desorption rate, leading to the apparition of these extra peaks of desorption. This ramp misbehavior occurs when the contacts of the heater assembly evolve over time. To confirm that this is indeed the origin of these desorption peaks and to rule out the presence of higher energy traps which could explain such behavior, the same calibration of the temperature ramp was used for TPD measurements on the sample ALMT#4 just after the set of measurements on the sample ALMT#9. The ALMT#4 TPD spectra had the same oscillatory behavior (figure 19 (b)). The confirmation that these oscillatory behavior was due to a faulty temperature ramp were given by a performing a new temperature calibration and a new set of measurements on the sample ALMT#4. The obtained TPD spectra returned to the one desorption peak behavior observed on ALMT#6 (figure 19 (a) and (c)), dismissing the higher energy traps hypothesis and showing that the ALMT#9 TPD spectra display fake extra desorption peaks.

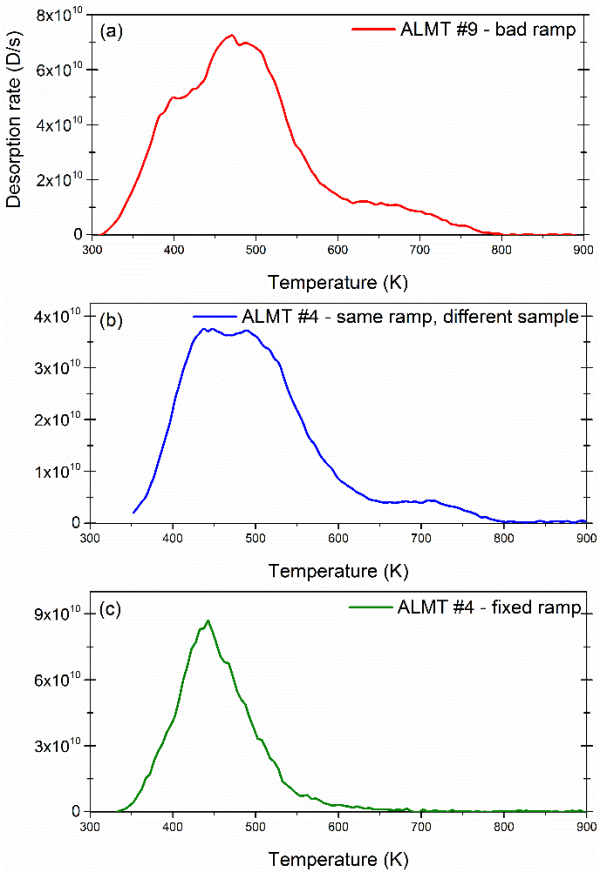


***Figure 19 - TPD spectra showing good vs. bad temperature ramp calibration; a – ALMT#9, b – ALMT#4, c – ALMT#4***

TPD spectra that suffer from an oscillating temperature ramp cannot be used to deduce information from the temperature of desorption peak maximum or on the width of the peak. Indeed, such characteristics of TPD spectra can give information about the trapping energies. Nevertheless, the deuterium retention, which is determined by integrating the area under the desorption peak, should not be affected by the faulty temperature ramp since all the deuterium atoms that get desorbed will be counted by the mass spectrometer, regardless of the peak shape.

We note that, in the third set of measurements, the spectra for the sample ALMT#4 presented in figure 18 (c) show small oscillations. Since it is clear from figure 19 (c) that, just after the ramp calibration, sample ALMT#4 yields only one peak of desorption with no oscillation, the small oscillations noticed on spectra in figure 18 (c) are most likely explained by an evolution of some of the thermal contacts within the heater assembly. Nevertheless, spectra measured on sample ALMT#4 are very similar to the spectra obtained on the sample ALMT#6. There is one peak of desorption, whose maximum position and shape evolve similarly with deuterium fluence i.e. the desorption peak's position shifts to lower temperatures when the incident fluence is increased. Finally, the absolute temperature position of the desorption peak is slightly lower for ALMT#4 than for ALMT#6. This difference could be related to the tightness of the screws that hold the mask and the sample onto the transfer platen. When the sample is changed, it is likely that the tightness of the screws will not be exactly the same.

### 3.1.2 The effect of sample temperature during implantation on retention

The effect of the implantation temperature on deuterium retention was studied for four values of the temperature: 319 ± 12 K, 400 ± 10 K, 500 ± 10 K and 600 ± 10 K. The desired value of sample temperature was set by using the calibration method described in Chapter 2.3.3. When the temperature reached stability at the target value, the desired fluence of deuterium was implanted in the tungsten sample. The power to the filament of the heater assembly was cut off 3 to 5 seconds before turning off the ion beam and the TPD were acquired after the sample has cooled down to room temperature.

The results are presented first as desorption spectra (figure 20). Due to the fact that the set of measurements presented here is affected by the faulty temperature ramp, an additional discussion will be necessary regarding the utility of these spectra in interpreting the results. Then, the total retention will be first represented as a function of incident fluence for these four different values of implantation temperatures (figure 21). The results will then be plotted

as total retention versus implantation temperature, for the different cases of fixed incident fluence that were tested. Finally, a set of experiments consisting in interrupting a temperature ramp around 400 K before acquiring a new TPD spectrum starting from room temperature will be shown with the aim of better understanding the correlation between the implantation temperature and the characteristics of the desorption peak (figure 24).

The TPD spectra obtained after the implantation at different temperatures are shown below. The sample used for these experiments was sample ALMT#9. The spectra of desorption are grouped by the incident fluence in four different plots. The rate of desorption is shown as the release rate of D atoms (D/s) and it is determined as the sum of all the D atoms released in the forms of $D_2$ and HD. Each spectrum is an average of at least three individual spectra. In order to perform the averaging, each spectrum was previously binned for intervals of 5 K.

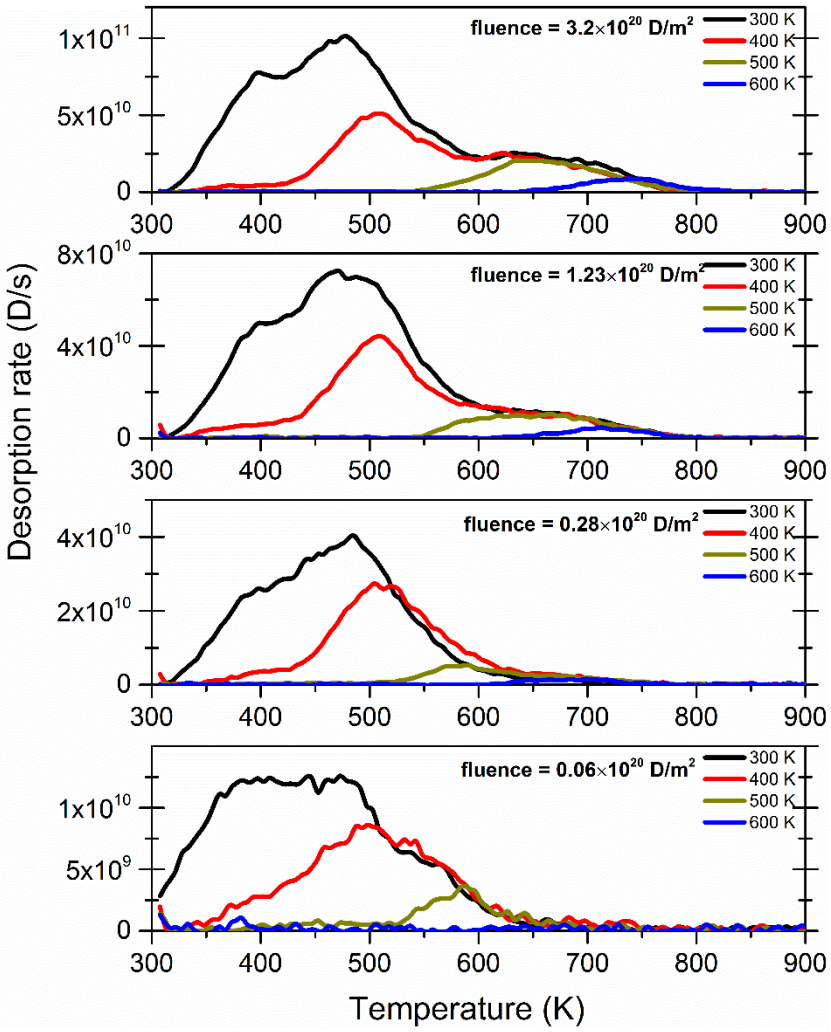


***Figure 20 – TPD spectra for different fluences of deuterium implanted at different temperatures of the sample; sample ALMT#9***

Since these spectra are affected by the faulty heating ramp they cannot be used to obtain accurate information on peak characteristics like the width and position. The evolution of the peaks with the implantation temperature should be therefore investigated only qualitatively.

The dependency of retention with the incident fluence, as a function of the implantation temperature, is shown in figure 21 (solid symbols). Each curve corresponds to a power law fit for a fixed value of the implantation temperature. The range of the incident fluence is covering three orders of magnitude from $6.4\times10^{18}$ up to $3.2\times10^{20}$ D/m$^2$. For each solid point presented on the graph, at least three replicate measurements were performed. The curves are fitted with a square root power law function. Ion implantation at different temperatures was also performed on sample ALMT#4, for one fixed value of the incident fluence ($1.23 \times 10^{20}$ D/m$^2$). The results corresponding to this second sample are plotted in figure 21 as empty symbols.

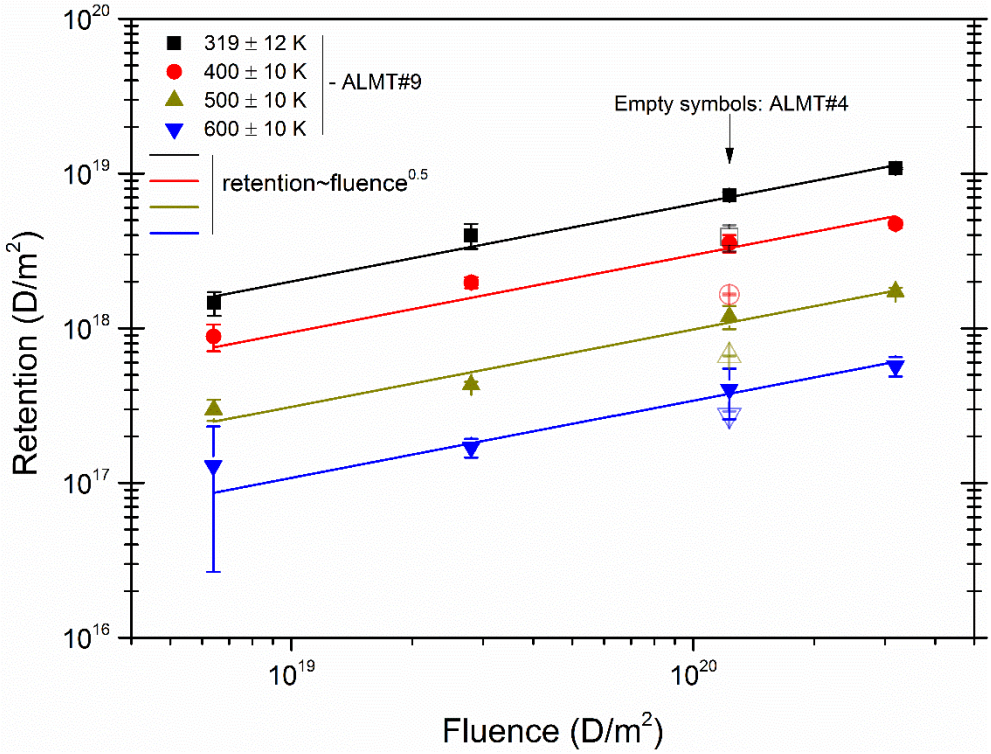


***Figure 21 – Deuterium retention as a function of incident fluence for different implantation temperatures; samples: ALMT#9 and ALMT#4***

It is noticed that total retention decreases by at least one order of magnitude when the temperature is increased from 319 ± 12 K to 600 ± 10 K. The dependency between total retention and incident fluence is found to follow the same 0.5 power law for the four values of implantation temperature. From sample to sample the retention varies within a factor of 2 at most, as was also observed in figure 16 for implantation at 319 ± 12 K.

In the figure below the total retention obtained on ALMT#9 are presented in a different way, with the temperature on the x-axis and with a side by side comparison of the effect that the incident fluence has on retention for the different implantation temperatures. The purpose of using this layout is to follow which of the two parameters (incident fluence and implantation temperature) has the most significant effect on the total retention. The columns represent the amount of deuterium retained after different values of the incident fluence. The columns are then grouped by their corresponding implantation temperature.

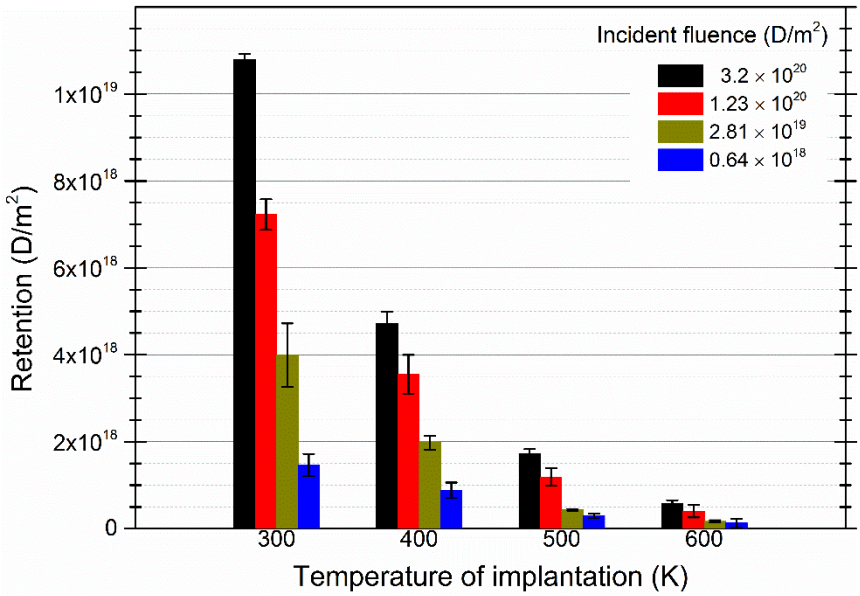


***Figure 22 – Retention as a function of implantation temperature for different incident fluence; sample: ALMT#9***

On the one hand, it is noticed that for each 100 K step of increasing the implantation temperature there is a decrease in the total retention by more than a factor of 2. For the implantation at 600 ± 10 K the retained amounts are reduced by more than a factor of 20 as compared to the implantation at 319 ± 12 K. On the other hand, increasing the fluence by a factor of 500 only increases the retention by a factor of about 20. Therefore, by comparing the smallest incident fluence at 319 ± 12 K implantation with the highest incident fluence at 600 K implantation, it is found that the importance of the temperature outweighs the one of fluence in the parameters range studied here.

Finally, the same values can be plotted as the total retention normalized to the value of retention corresponding to implantation at 319 ± 12 K (figure 23).

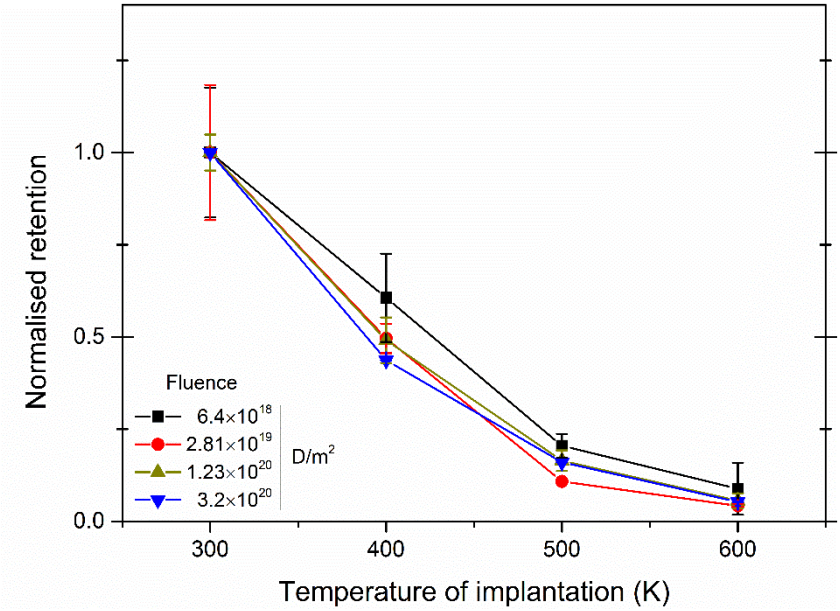


***Figure 23 - The effect of implantation temperature on deuterium retention***

This representation shows that, for each step of the implantation temperature, retention is reduced by a similar percentage, independently of the fluence.

Additionally, a set of experiments consisting in interrupted ramps were performed (figure 24 – upper part) in the following manner:

- a TPD ramp was started from room temperature up to a chosen temperature fixed below 450 K
- the power to the heater assembly was cut off and the sample cooled down to room temperature
- a second ramp was started from room temperature up to 1300 K

If we consider that heating the sample up to around 400 K has the same effect on retention as the implantation at 400 K, then the spectra for these interrupted ramps (figure 24) will show the connection between the temperature of the sample during ion implantation and the characteristics of the desorption peak. The analysis of the peak will then provide information about the activation energies characterizing the trapping mechanisms. On the lower part of figure 24, three TPD spectra obtained for individual measurements are presented. These measurements were performed after the temperature ramp was fixed (see figure 19(c)). Even though they cannot be used for rigorous quantitative analysis, due to lack of statistics, some qualitative information could be extracted.

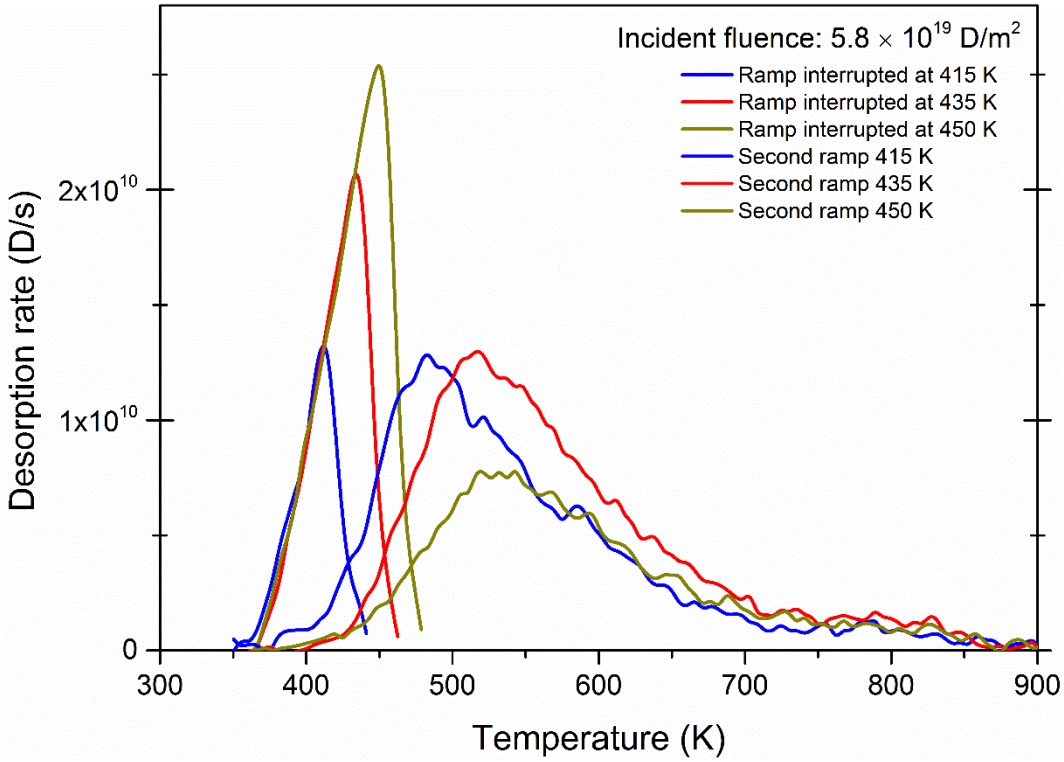


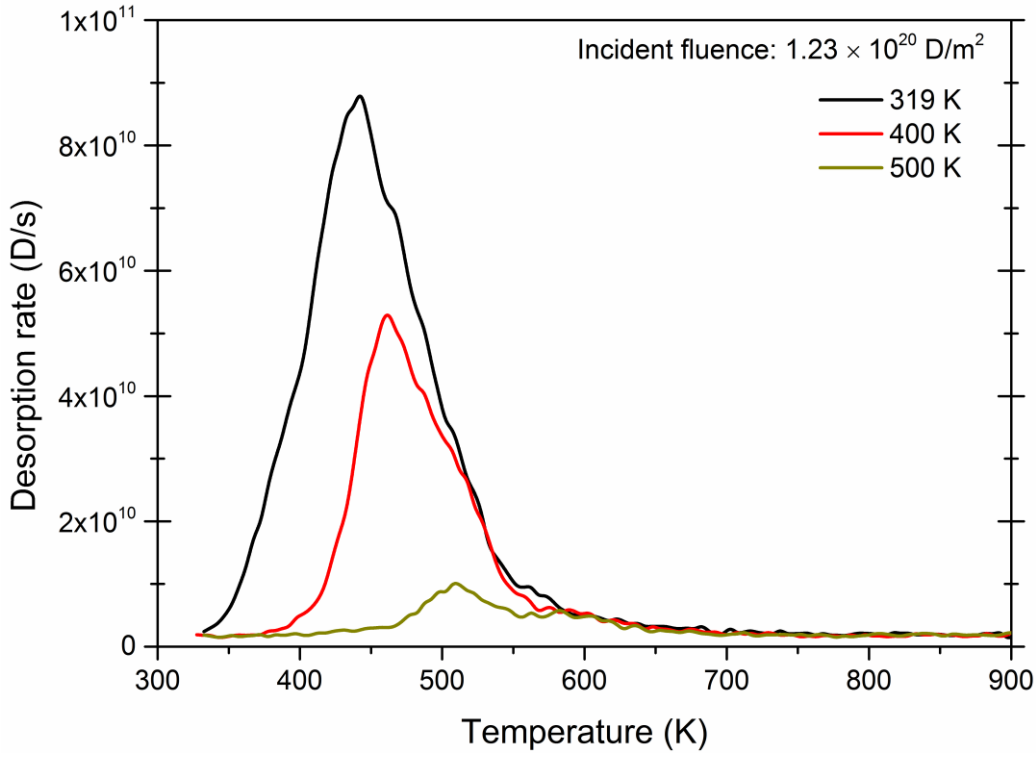


***Figure 24 – upper part: TPD executed in two steps: first an interrupted ramp and second a complete ramp;***

- ***lower part: TPD spectra obtained with a good ramp for implantations at higher temperature (only 3 individual measurements available)***

The temperature at which the heating is cut-off for the three interrupted ramps is increased in steps of roughly 15 K. It is observed that the released amounts increase for each

step (at 435 K and 450 K as compared to the 415 K). For the full ramps (second step of the experiments), the desorption peak maximum shifts to higher temperature in a consistent manner with the cut-off temperature. These shifts in temperature should inform us on how the average activation energy of the traps has changed as a result of the partial-depopulation of traps occurred during the first step (interrupted ramps). A similar shift is observed in the lower part of the figure, where, for each 100 K step of the implantation temperature, a ~30 K shift in temperature is observed for the peak position.

### 3.1.3 The evolution of trapped deuterium with the storage time in polycrystalline tungsten

Deuterium retention in polycrystalline tungsten was investigated so far by performing the TPD after a storage time of about 2.5 hours after ion implantation. In this section the influence of an important parameter is presented, namely the storage time in UHV. As already described in chapter 2, the storage time is defined as the time interval between the end of ion implantation and the start of the TPD ramp. The quantity that is measured in this case is the number of deuterium atoms that are still trapped in the sample after the respective storage time. Regardless of the implantation temperature, the sample is stored at 300 K (ambient temperature). For the highest implantation temperature case the sample needs 1 to 1.5 hours to cool down to ambient temperature.

The investigation of storage time evolution for deuterium retention was performed for two values of fluence ($2.81 \times 10^{19}$ and $1.23 \times 10^{20}$ D/m$^2$) and for two values of implantation temperature (319 ± 12 K and 500 ± 10 K).

The results are presented first as the total deuterium retention as a function of storage time in UHV. The variations from sample to sample are investigated by comparing replicate experiments on two different samples (experiments performed for the same fluence – $2.81 \times 10^{19}$ D/m$^2$ – and the same implantation temperature – 319 ± 12 K). Then the storage time evolution is investigated first for a higher value of incident fluence and second for a higher implantation temperature.

In figure 25 the deuterium retention is plotted as a function of the storage time in UHV for the samples ALMT#5 and ALMT#6, after ion implantation performed at room temperature. Both samples were implanted with the same incident fluence of $2.81 \times 10^{19}$ D/m$^2$. The curves are fitted with an exponential decay. Each point on the plot is an average of at least three individual measurements and represents the number of deuterium atoms that were still trapped in the sample after the respective storage time. This number is determined

as the sum between the deuterium atoms counted by the mass spectrometer as $D_2$ and HD molecules. The error bars represent the standard deviation of the mean.

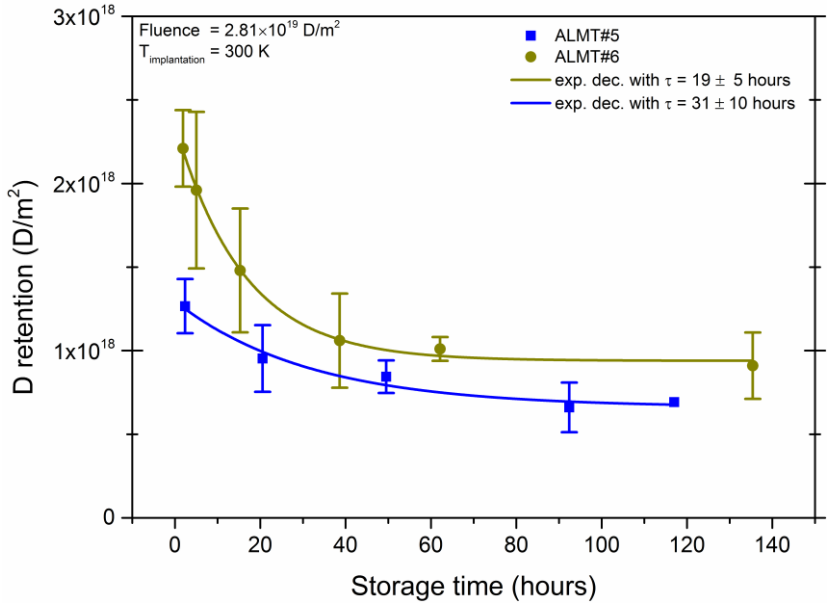


***Figure 25 - The evolution of retained deuterium with storage time in UHV – sample to sample variations***

It is found that after 140 hours there is still a significant amount of deuterium trapped in the polycrystalline tungsten sample. Nevertheless for the time interval for which the evolution of this amount is tested, starting from storage times as short as 2.5 hours and then increasing it until 140 hours, the presented curves show the existence of two types of retention. At first deuterium retained amounts drop exponentially during the first 20 to 40 hours, and then, on the second part of the curve, meaning for a longer storage time of around 60 hours and higher, the retained amounts of deuterium remain essentially constant.

Concerning the sample to sample variations, a difference within a factor of two is noticed between the two curves presented in figure 25. This difference is similar to the difference observed for the curves of retention as a function of fluence obtained on different samples. In this case however, the difference is more pronounced for the short term retention and decreases within statistics for longer storage times. The difference noticed for the short time retention seems to be related to the initial retained amount of deuterium (after $T_{storage}$ = ~ 2.5 hours), which seems to be higher for the sample ALMT#6 than for the sample ALMT#5.

Figure 26 shows how the deuterium retention evolves with storage time when the fluence is increased by a factor of roughly 4 (from $2.81 \times 10^{19}$ to $1.23 \times 10^{20}$ D/m$^2$ – full black squares), measurements being performed on sample ALTM#4. The retention follows the same trend as for the lower fluence, with a short term exponential behavior and a constant long term retention. The amounts are increased for both short and long term retention, when the

incident fluence is increased. The storage time evolution of retention was tested in this case for a storage time as long as 313 hours.

By making use of the square root power law found for retention as a function of fluence, the results for the sample ALMT#4 are scaled down in order to simulate how the curve would resemble for the lower fluence (empty black squares). The square root power low is applied for all the points, independent of their storage time. The purpose of this down scaling is the comparison with the two curves obtained on ALMT#5 and ALMT#6, and to simplify this way the investigation of the sample to sample variations. In order to verify that the scaled curve correctly describes the storage time evolution of retention on the sample ALMT#4 after ion implantation with the lower incident fluence, the curve is verified against two experimental data obtained on ALMT#4 for the same parameters (full black stars): these two points correspond to storage times of 2.5 hours and 93 hours, and they show a very good agreement with the scaled curve.

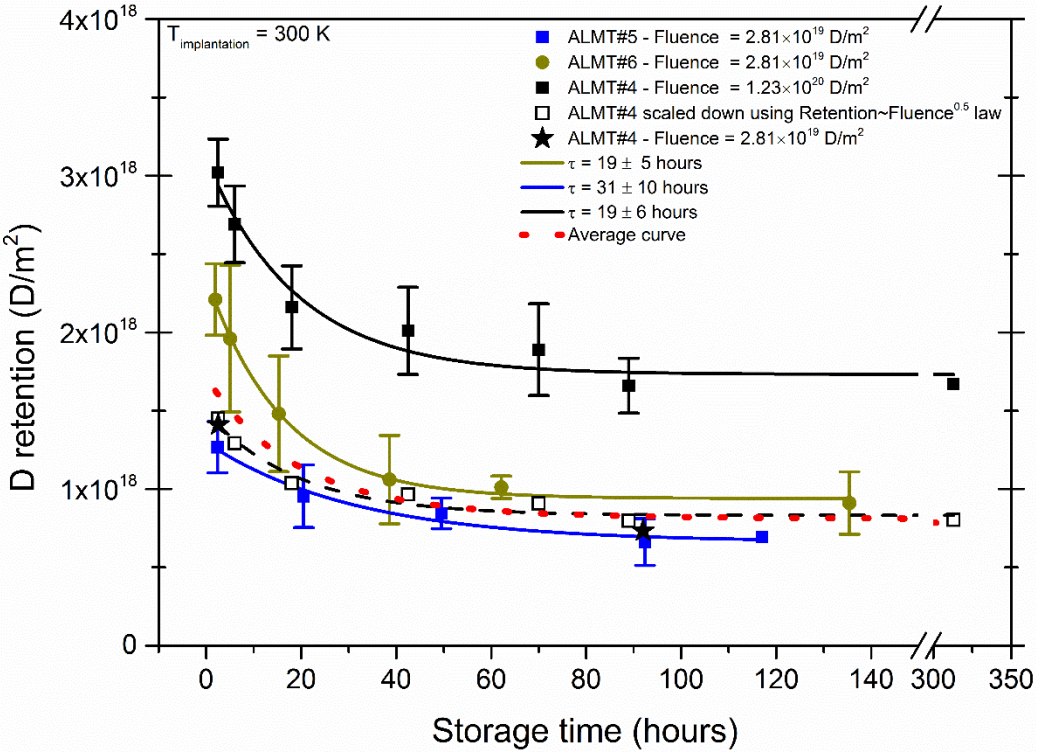


***Figure 26 - The evolution of retained deuterium with storage time in UHV - effect of fluence***

The scaled curve also fits well with the curves obtained on both ALMT#5 (full blue squares) and ALMT#6 (full olive circles), with the initial retention (after $T_{storage}$ ~ 2.5 hours) being closer to the one for ALMT#5, and with the long term retention falling somewhere in between. Nevertheless, by taking into account the scattering of data for replicate measurements, represented by the standard deviation of the mean, the three curves are in good

agreement. Therefore, another way to better describe the evolution of the retained deuterium is to average them (red dotted line in figure 26).

Concerning the long term retention, the amount of deuterium still found in the sample after storage times of 60 hours or more remains constant for each case of incident fluence. When the two levels of long term retention are compared in relation to the incident fluence it is found that a square root power law could also be used to describe the dependency between the incident fluence and the long term retention.

The experimental data displayed in figure 26 were obtained after implantation at ambient temperature. Nevertheless, it is of interest for fusion devices to investigate also how the implantation temperature will affect the evolution of retained deuterium with storage time. In figure 27, the total retention is plotted as a function of the storage time for ion implantations performed at 500 ± 10 K on the sample ALMT#4. On the same graph, the curve for the implantation at 319 ± 12 K for similar parameters is plotted. We are able to compare this way two curves obtained on ALMT#4 for the same incident fluence ($1.23 \times 10^{20}$ D/m$^2$), at two different temperatures (319 ± 12 K and 500 ± 10 K), the only modified parameter being the implantation temperature. Both curves are fitted with an exponential decay. For the curve corresponding to the implantation at 500 K, the first point ($T_{storage}$ = 2.5 hours) corresponds to a storage where the sample temperature decays radiatively from 500 K (implantation temperature) to ~326 K. For the others points of storage time, the sample cools down for the first 2.5 hours and is further stored at ambient temperature. It results then that the fit performed starting from the 2.5 hours point corresponds to the evolution of trapped deuterium with the storage time in UHV at ambient temperature.

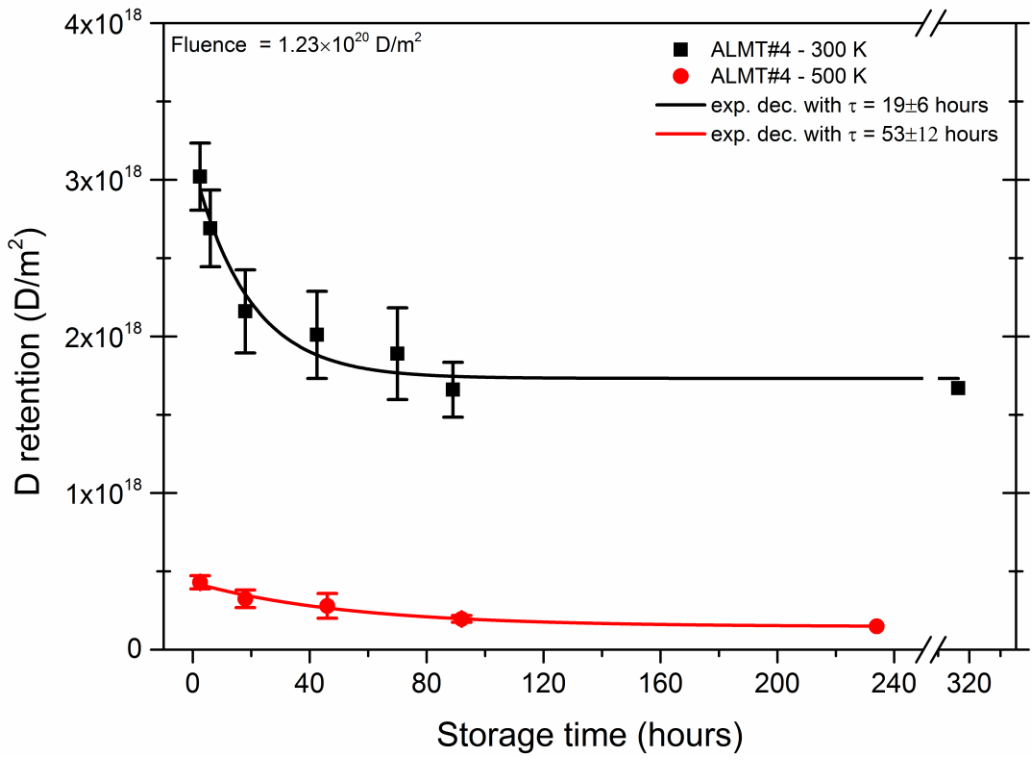


***Figure 27- The evolution of retained deuterium with storage time in UHV - effect of implantation temperature; sample ALMT#4***

The higher temperature of implantation decreases the amount of retained deuterium, in agreement with the already shown results for the retention as a function of fluence at higher implantation temperatures. Nevertheless, it does not change the presence of the two distinct types of retention behavior (short term and long term). For the 500 K implantation, the time constant of the exponential decay is higher than in the 319 K case but it stays in the range of a few tens of hours.

The TPD spectra corresponding to the points presented in this section are plotted for different values of storage time in figure 28, grouped in a way that allows direct visual comparison as follows: (a) and (b) for sample versus sample effect; (a) and (c) for the effect of fluence, and for the sample vs. sample effect; (c) and (d) for the effect of implantation temperature. The y-axis scales were not kept identical in order to allow the efficient display of peak characteristics regardless of the peaks relative intensities (between the four different sets).

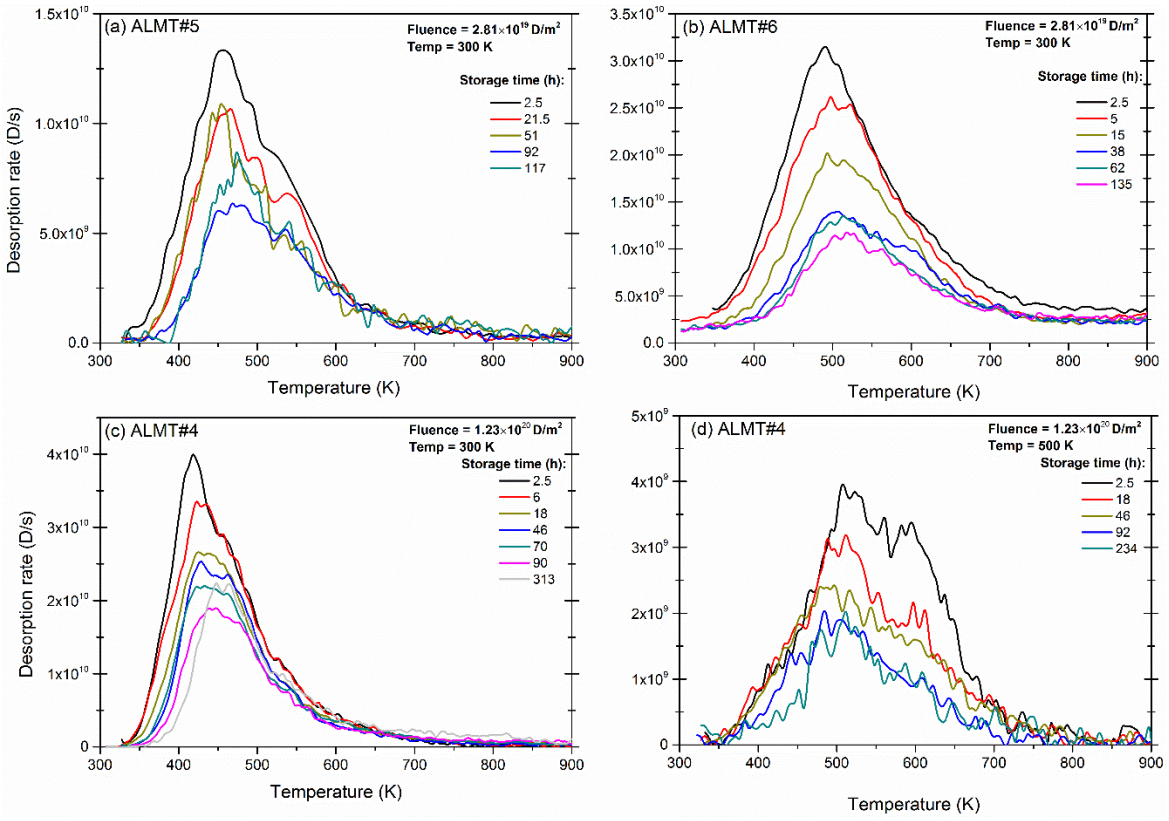


***Figure 28 - TPD spectra for the evolution of retained deuterium with storage time in UHV; samples: a) ALMT#5, b) ALMT#6, c) ALMT#4 and d) also ALMT#4***

The sets of spectra corresponding to implantations at 300 K are all showing a consistent 30 K shift towards higher temperature, as the storage time is increased for both the peak maximum position and for the leading edge. For the implantation at 500 K no peak shift is observed and there is no obvious difference for the start of the leading edge.

### 3.1.4 Analysis and interpretation

The purpose of the experiments presented in this section is to identify the trapping mechanisms for deuterium in tungsten and to determine their significance for both short and long term storage of the sample.

Following the ion implantation of polycrystalline tungsten samples, the use of the TPD technique provides two main results: the number of deuterium atoms that are trapped in the sample for a given time after implantation and the position in temperature of the desorption peak. The trapping mechanisms will be identified by analyzing the evolution of these two results when different parameters are changed (incident fluence, implantation temperature and storage time).

The factors that may influence the density and type of trapping mechanisms inside the sample are the preparation process of the sample, the incident fluence [16], [65], [66] and the ion flux [67]–[69]. Following our preparation steps, the samples are described by the intrinsic defects of polycrystalline tungsten: vacancies, grain boundaries, dislocation loops and interstitial defects, for the bulk, while the surface of the sample is characterized by the presence of a thin layer of oxide of a few nanometers. The low flux and low fluences used here should not lead to the creation of new defects as explained in section 3.1.1. This hypothesis is further supported by the reproducibility of TPD measurements for our samples, where more than 100 cycles of implantation and desorption are usually performed for each sample.

In the literature, the activation energy for each type of trap presented in the tungsten bulk are calculated using computer modeling based on the Density Functional Theory (DFT) [14], [15], [19] . What was shown in these studies is that the activation energy to escape a bulk defect is in general a function of the number of hydrogen isotopes bound to the defect site (the so-called filling level of a trap). The usual trend that is found is a decrease of the activation energy when more atoms are populating a trap. Therefore, when an atom gets released from a trap, the activation energy for the remaining atoms is increased.

Heinola et al. [19] and Fernandez et al.[14] showed that single vacancies can accommodate up to 6 [19] or even up to 12 [14] atoms with the highest activation energy for the case when it accommodates only one atom, and with a decrease of the activation energy as more atoms become trapped.

Xiao et al. [15] showed that a grain boundary (Σ3(111) tilt) can accommodate up to 7 atoms, with the activation energy following the same increasing trend up to a number of 4 atoms per defect, and decreases with additional atoms. For the dislocation loops the maximum number of accommodating atoms is shown to be 6 and the activation energy decreases when more atoms get trapped [15].

The correspondence between the number of atoms accommodated by a trap and its activation energy will be used for the analysis of our TPD spectra. During the TPD step, when the temperature of the sample is increased extra thermal energy is added to the system and deuterium atoms will start to be released from their traps. Since the temperature is increased linearly with a slow rate of 1 K/s, the atoms will be released one by one as the sample temperature is increased. According to the number of atoms that are yet to be released from a trap, the activation of the release process will take place at a certain value of sample temperature [14], [15], [19]. The released atoms will diffuse (from an interstitial to another),

against a diffusion barrier of around 0.2 [14] – 0.39 eV [17], and will reach the surface where they will be desorbed as soon as they recombine with another atom. Some of the released atoms can also get re-trapped, but since the temperature is increasing they will quickly get re-released and reach the surface where they will desorb.

The analysis of total deuterium retention will be performed for the two timescales of retention (short term and long term). For a short storage time of 2.5 hours the filling level of the traps is analyzed as a function of the incident fluence and as a function of the implantation temperature. The variations of these parameters should both lead to variations of the filling level of traps which should be noticed on the TPD spectra. For the longer storage times (60 hours and above) the filling level of traps is expected to be related to phenomena like desorption at ambient temperature, diffusion, initial incident fluence and implantation temperature.

The desorption spectra obtained for different incident fluences, presented in figures 18(a) and 18(c), are both showing a shift, of around 30 K, of the peak maximum towards lower temperatures as the incident fluence is increased. This shift is in good agreement with the correspondence between the filling level of the traps and the activation energies describing them [14]–[16]. For the lower fluences, the number of atoms per trap is small; therefore the activation energy is higher. Increasing the fluence also increases the number of atoms in each trap. More atoms per trap will translate to a decrease of the activation energy and further to a lower temperature of the peak maximum. The fact that there is always one peak of desorption can be interpreted as a continuous overlap of the peaks corresponding to each filling level, as well as an overlap of the peaks for different types of trap (vacancies, grain boundaries, and oxide layer, etc.).

The fact that the shift is not observed above an incident fluence of $2.81 \times 10^{19}$ D/m$^2$ suggests that the maximum filling level is reached at this implantation temperature for most of the traps of our samples, for this incident fluence and above. The position of the peak is, in these cases, at its lowest possible position, for the sample at the ambient temperature.

The asymmetry of the peak can also be interpreted in term of filling levels of the traps combined with the depth profile of the trapped atoms. In our 2017 joint experimental-theoretical communication, we present NRA results showing that the density of deuterium atoms decreases with the depth of the sample [18]. It is easy to imagine that the smaller density at higher depths in the sample translates into a lower level of filling for these traps. The depth of these traps should be higher for higher incident fluences. Due to the time it will take for the atoms to diffuse towards the surface upon releasing from these traps, on the TPD

spectra the higher depth will lead to a higher temperature of desorption actually not related to a higher activation energy. The decreasing tail suffers a stretch due to this delay caused by diffusion.

When deuterium retention in polycrystalline tungsten is plotted as a function of the incident fluence, we find a power law dependency well described by a square root (0.5 power law) in every case: from sample to sample and for several implantation temperatures. This dependency points to the diffusion of the implanted deuterium towards higher depths in the bulk as the process that limits the total retention during the ion implantation process.

By comparing all of our results with the ones obtained by Ogorodnikova et al. [24], we observe a similar trend with the retention following a power law dependency with the incident fluence. The small difference for the power coefficient can be justified by the difference in ion flux and incident fluence. A slightly higher power coefficient can be interpreted as the creation of extra defects due to the higher flux [28], [70] and higher fluence [16], [65], [66]. The consistent value of 0.5 found for the power coefficient in our measurements would support the idea that our samples do not evolve following numerous cycles of implantation and desorption. In other words, no extra defects are generated for our values of ion flux and incident fluence.

Fernandez et al. [14] showed the presence of two regimes of diffusivity, according to the temperature of the tungsten specimen. For all the implantation temperatures that were used in this thesis, the rate limiting step for the effective diffusion should be the trapping and de-trapping from defects [14]. Therefore, for the higher temperatures of implantation used in this thesis, where the diffusivity of the implanted atoms is higher, it is not expect for the power law coefficient to increase, which is consistent with our observations.

From the curves of retention as a function of the storage time (figure 25 and figure 26), the presence of two types of retention can be analyzed in order to identify the trapping mechanisms leading to this behavior. To do this one needs to find the source of retention which gives the decaying trend for the short term retention and also to find the source of retention responsible for the constant amount that stays in the sample for longer storage times.

From the chemical kinetics point of view, deuterium desorption during TPD can be described by the Polanyi-Wigner equation as follows [16]:

***Equation 17***

$$r = -\frac{d\theta}{dT} = A \times \theta^{n} \times e^{-\frac{E_a}{k_B T}}$$

where $r$ is the $D_2$ desorption rate, $A$ is the attempt frequency divided by the linear heating rate, $\theta$ represents the concentration of deuterium atoms as reactants, $n$ is the kinetic order, $E_a$ is the activation energy for the release process, $k_B$ is the Boltzmann constant and T is the surface temperature.

The evolution of deuterium retention with the storage time is obtained for a constant storage temperature of 300 K. It results that the atoms that get released while the sample is being stored in UHV suffer an isothermal desorption [16]. By using equation 17 for a constant temperature T = 300 K, and assuming a first order kinetic process [16], it becomes possible to estimate the activation energy for the process responsible for the decaying behavior which describes the short term retention. The activation energy will be given by the following relation [16]:

***Equation 18***

$$E_a = k_B \times T_{storage} \times \ln(\mathrm{A} \times \tau)$$

where $\tau$ is the time constant of the exponential decay (obtained from the exponential fit of the curve of retention as a function of the storage time).

For all the curves in figure 26 we get an activation energy $E_a$ = 1.06 ± 0.01 eV, meaning that this value does not change when the sample is changed or when the fluence is increased. The value of the pre-exponential factor $A$, used for this calculation was taken from Fernandez et al. [14], and it is equal to $1 \times 10^{13}$ $s^{-1}$.

The same analysis is performed for the implantation at 500 K. Retention is significantly reduced in this case for both short and long term retention but the short term retention shows the same exponential behavior as for the implantation at 300 K. The time constant is slightly higher and the estimated activation energy in this case is $E_a$ = 1.09 ± 0.01 eV, which is almost the same as for implantation at 300 K when considering indicated uncertainties.

The presence of these similar exponential decay shows that the source of short term retention is not removed when implantation is performed at 500 K. Even more, the activation energy for the process responsible for the decay of the short term retention barely changes. Since the filling level of all the traps found inside the bulk should be small after an implantation at 500 K, the activation energy for bulk defects should be expected to be higher. But for higher activation energy, the time constant which would result would be infinitely long. For example, using the energy values listed in Chapter 1, section 1.4.3 (found by DFT [14], [15], [19], [20]), one can notice that the 1.06 ± 0.01 eV value corresponds to vacancies

accommodating 5 to 6 atoms, and grain boundaries with roughly 3 atoms. If the filling level is decreased by just one atom, the activation energy increases to values between 1.24 eV and 1.30 eV. Considering a rough average value of 1.27 eV, the time constant from equation 18 should be around $7 \times 10^4$ hours. This is not what is observed for the implantation at 500 K. Thus, bulk retention seems to not be able to describe the similar short term retention for 300 K and 500 K implantation temperature. From the possible sources of retention, presented in the beginning of this section, the most likely candidate for the short term behavior is suggested to be the thin oxide layer present on the surface of the sample (see AES measurement in Chapter 2).

The TPD spectra corresponding to the storage time experiments are also analyzed in order to verify if they support or disprove the importance of the oxide layer as trapping mechanism. For implantation at 300 K, all sets of measurements show a shift of 30 K towards higher temperatures for the peak maximum and a decrease in intensity. This behavior would correspond well to the release from bulk defects, meaning that the shift is the result of a lower filling level of traps. A second factor that would contribute to the shift is the diffusion of the released atoms. Some of them will go deeper in the bulk and will get re-trapped, while some of them will reach the surface and will get desorbed.

The spectra for the implantation at 300 K obtained for different storage times are somehow different than the spectra obtained by increasing the fluence. The leading edge shifts to higher temperature while the decreasing tail remains fixed. At the same time the peak maximum has a less dramatic decrease. These observations can be interpreted by considering the filling level of traps. When the storage time is increased, at room temperature, only the traps with a high filling level (low activation energy) will release atoms, which will determine an increase of the average value of the activation energy. This will, therefore, shift the leading edge to higher temperatures (similar to what was observed for the interrupted ramps, where the traps were depopulated in steps of temperatures and determined a shift to higher temperatures for the following complete ramps – figure 24).

The TPD spectra for implantation at 500 K show a different behavior. The only characteristic that changes with the storage time is the decreasing tail which seems to drop for longer storage time. From the point of view of the bulk defects, this would correspond to an isothermal desorption (at 300 K) from the traps accommodating less atoms, and therefore being characterized by a higher activation energy, rather than the opposite. This is not physically possible without breaking the second law of thermodynamics [71]. As a trapping mechanism located on the surface, the oxide layer will fit this behavior of the spectra if we

consider that, in order for one atom to find another atom and to be released, it must diffuse through the oxide layer. The high implantation temperature makes it that there are fewer atoms going through the oxide layer and that these atoms are relatively far away from each other. During TPD the atoms will take longer to get closer to each other and to be desorbed. This will translate into the higher apparent position in temperature.

To summarize on the sources of deuterium retention in polycrystalline tungsten, it was shown in this section that the short term retention is described by an exponential decay, independent of the implantation temperature, which is in disagreement with the activation energies determined by the filling level of bulk defects. Nevertheless, it was shown that the short term retention can fit better with a trapping mechanism located in the near-surface region in a form of an oxide layer.

Results on polycrystalline tungsten are not sufficient for discriminating the traps responsible for the long term retention. Furthermore, a confirmation that the source of the short term retention decay comes from an oxide surface layer would be appreciated. In the next section, similar experiments performed on single crystal tungsten are presented.

### 3.2 Deuterium retention in single crystal tungsten

From the experiments performed on polycrystalline tungsten we obtained a description for deuterium retention which corresponds to deuterium atoms being trapped across all the intrinsic trapping mechanisms found naturally in tungsten like vacancies, grain boundaries, dislocations and the natural oxide. In order to better discriminate the impact of each type of trapping mechanism on deuterium retention, the study was extended from polycrystalline tungsten to single crystal tungsten. A simple schematic is shown in figure 29 to illustrate the difference between the two types of samples. Since the single crystal consists in one big grain of tungsten atoms, there are no grain boundaries found inside the tungsten bulk. There will be therefore no trapping of deuterium atoms in grain boundaries but all the other trapping mechanisms should behave the same as for the polycrystalline sample. By performing similar experiments on the single crystal sample and by comparing them to the ones obtained on the polycrystalline sample, it becomes possible to discriminate the effect of grain boundaries as trapping mechanism for deuterium in tungsten.

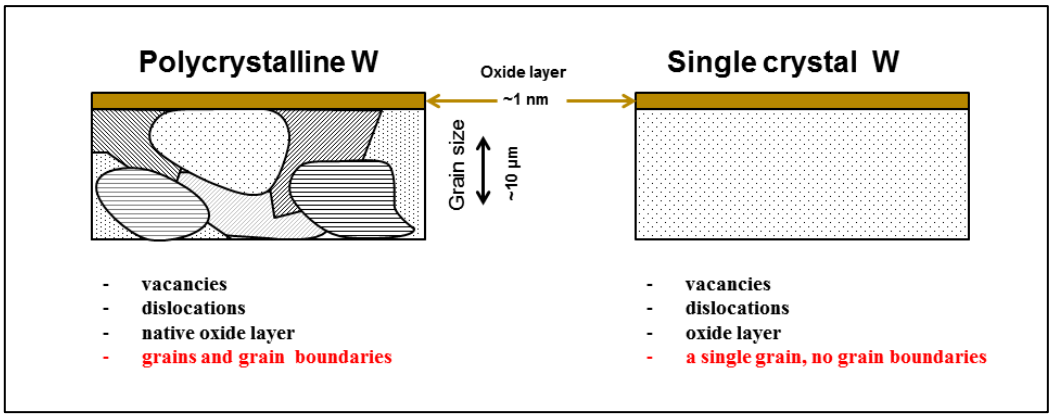


***Figure 29 – Schematic of tungsten samples: polycrystalline versus single crystal; multiple grains and grain boundaries for the polycrystalline sample while the single crystal has no grain boundaries***

Deuterium retention in single crystal tungsten was studied as a function of incident fluence and as a function of storage time in UHV. These dependencies were measured only for implantations at ambient temperature. The sample used for these experiments was a single crystal tungsten with an (111) orientation with dimensions of 14×12×2 $mm^3$.

### 3.2.1 The effect of deuterium fluence on its retention in single crystal tungsten

Deuterium retention in single crystal tungsten was investigated for a range of incident fluence covering 4 orders of magnitude ($10^{17}$ – $10^{20}$ $D/m^2$) and which corresponds to durations of ion implantation no longer than 5 hours. This way, the duration of implantation is kept below the typical time constant for deuterium release from tungsten (see chapter 3.1.2).

The results were obtained in one series of measurements (no exposure to air between any of the measurements) and they are shown first as TPD spectra and then as integrated amounts, i.e. as retention plots.

The deuterium desorption curves obtained on the single crystal sample are plotted in figure 30 for the entire range of incident fluence that was investigated. These spectra are obtained for a storage time of around 2.5 hours. Each spectrum is an average of at least three individual spectra obtained for replicate measurements.

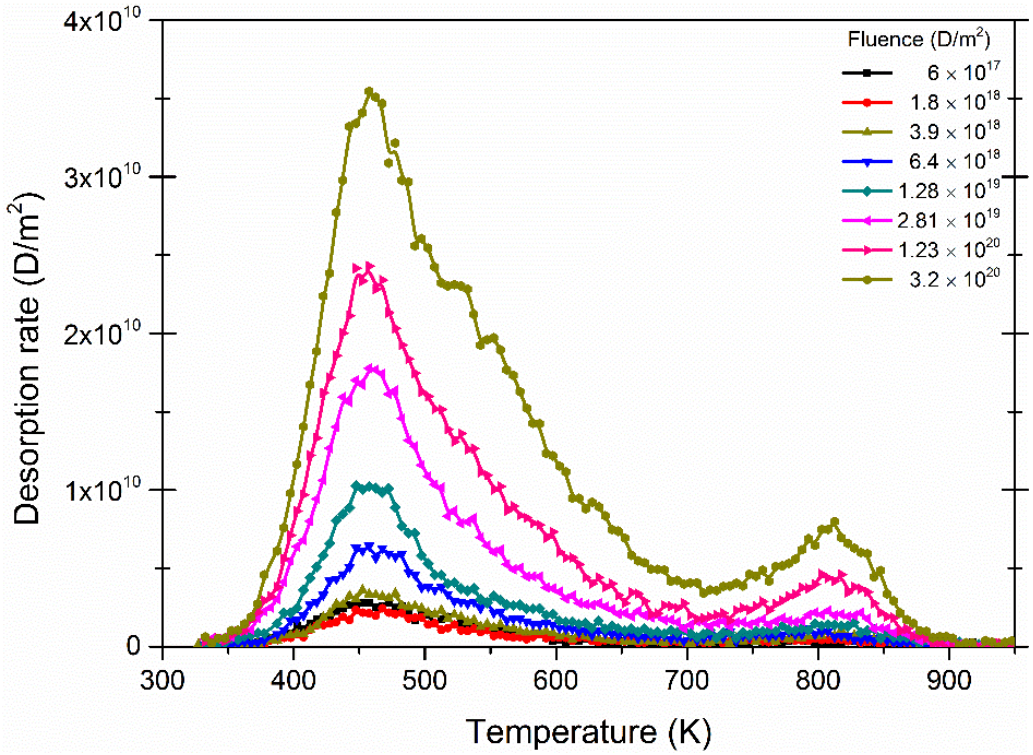


***Figure 30 - TPD spectra for deuterium retention in single crystal tungsten - effect of fluence***

It is noticed that the desorption curves reveal the presence of two main peaks. The characteristics of the first peak are similar to those observed for the polycrystalline tungsten, with roughly the same position in temperature for the peak maximum, and a similar shape and with a similar width. The second peak of desorption noticed on these spectra is characterized by a higher temperature of desorption and a smaller intensity as compared to the first peak.

The position of the maximum of desorption for the first peak is situated around 450 K ± 30 K. When the incident fluence is increased, there is no shift in position for the desorption maximum, contrary to the observation made in the case of the polycrystalline sample (figures 18,a and 18,c). The peak position remains constant for all fluences. The desorption peaks are slightly asymmetric with a longer decreasing tail.

The source of the second peak for the single crystal needs to be investigated in order to determine whether this second peak appears due to a certain trapping mechanism different from polycrystalline tungsten or if it is caused by a irregularities of the temperature ramp, as it was the case for some sets of measurements on polycrystalline tungsten (see chapter 3.1.1). In order to test the first possibility, namely the presence of extra trapping mechanisms as a source for the second peak of desorption, it is necessary to investigate all the available results which include the evolution of this peak with the storage time. Since the evolution of total

retention with the storage time is presented in the next section, this possibility will be checked there.

In order to test the second possibility, namely that an eventual faulty ramp is the source of the second desorption peak, we will use spectra of desorption obtained on polycrystalline tungsten, before and after the present set of measurements performed on the single crystal sample. Both before and after these measurements, experiments were being performed on the sample ALMT#4. In figure 31, the spectra of desorption obtained on ALMT#4 are plotted with the purpose of verifying the presence of a faulty ramp.

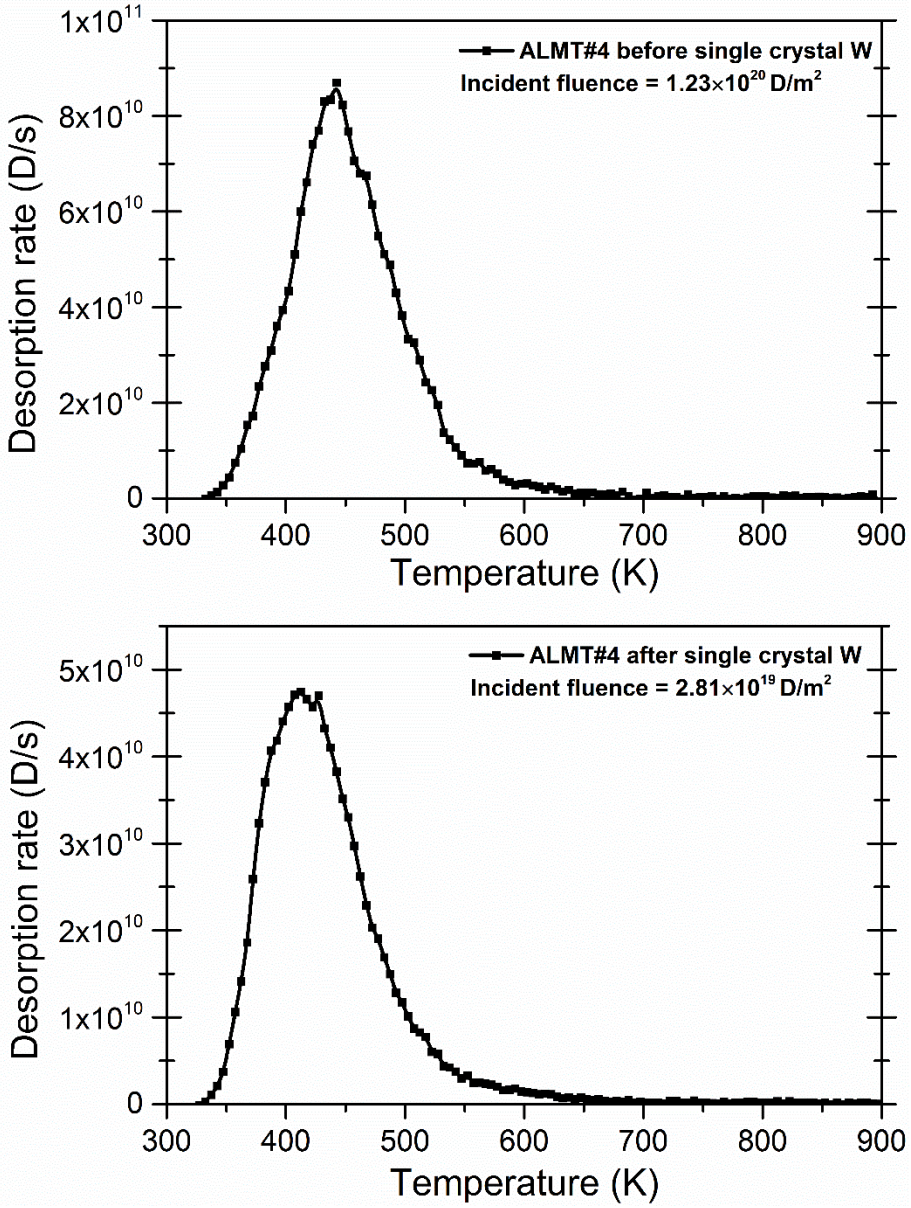


***Figure 31 – TPD spectra obtained before and after the set of measurements on single crystal; the spectra show a good quality of the temperature ramp in both cases; sample: ALMT#4***

The two spectra presented above show no sign of irregularities, pointing to a good quality of the temperature ramp. Since the temperature calibration was the same for the spectra obtained on both ALMT#4 series and for the spectra obtained on the single crystal sample, and since this calibration is shown to be of good quality both before and after the measurements performed on the single crystal, it is clear that the temperature ramp is not the source of the second peak observed on the single crystal. The good quality of the temperature ramp was also verified for individual measurements by searching for the presence of oscillations (irregularities) on the temperature trace of the heater assembly, leading to the same conclusion: the quality of the temperature ramp was good throughout the single crystal series of experiments.

The deuterium retention in single crystal tungsten as a function of incident fluence is presented in figure 32. The three curves that are shown represent the total retention calculated by integrating the full desorption spectra (black hexagons), and the retention calculated for each separate peak of desorption (blue square and red triangle).

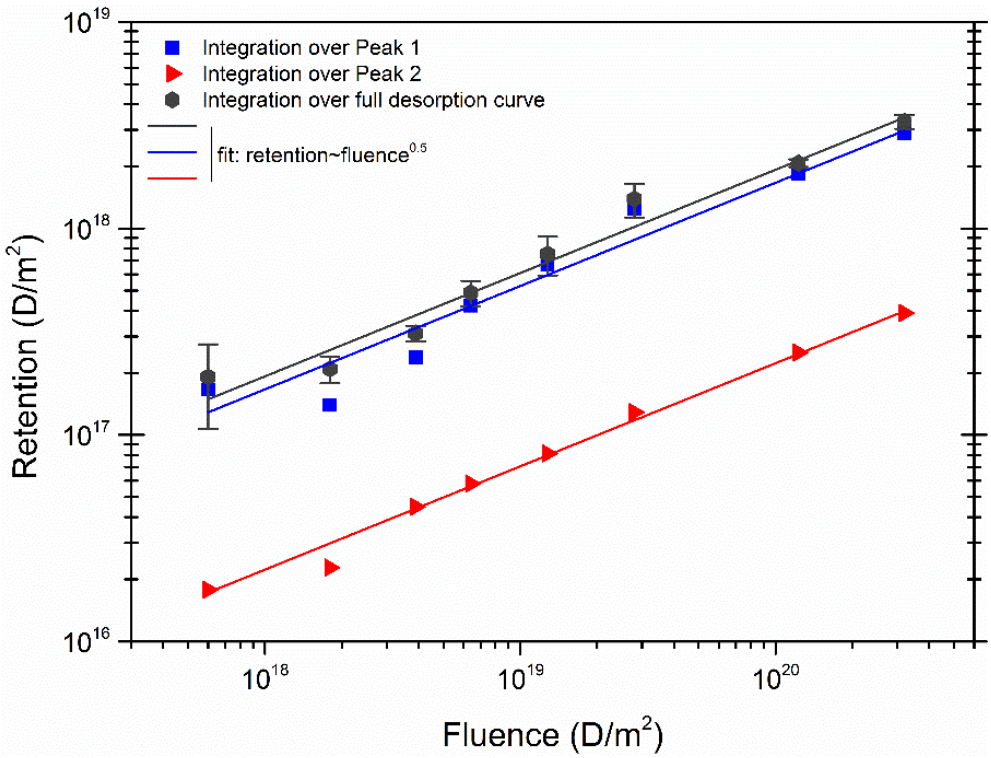


***Figure 32 - Deuterium retention as a function of fluence in single crystal tungsten***

It is found that, similar to the polycrystalline tungsten case, the deuterium retention in single crystal tungsten follows a square root dependency with the incident fluence. This is valid for the retention calculated from the full spectra but also when each of the two peaks is integrated separately and their corresponding retention is plotted as a function of the incident fluence. It

is also noticed that for all the fluences studied here, the retention corresponding to the second peak is always ~15% of the retention for the first peak. This constant ratio would indicate a rather uniform density distribution of this second type of trapping mechanism while a more localized defect would be characterized by reaching to saturation when the fluence is increased.

In figure 33, the values corresponding to the integration of the full TPD spectra for the single crystal sample are compared to the retention curves obtained on the three polycrystalline tungsten samples studied in the first part of Chapter 3. The retention on the single crystal is shown here without subtracting the retention values coming from the second peak. By keeping this conservative approach one avoids the errors induced by a poor evaluation of where the first peak ends and the second peak begins, especially for the higher fluences where the peaks overlap.

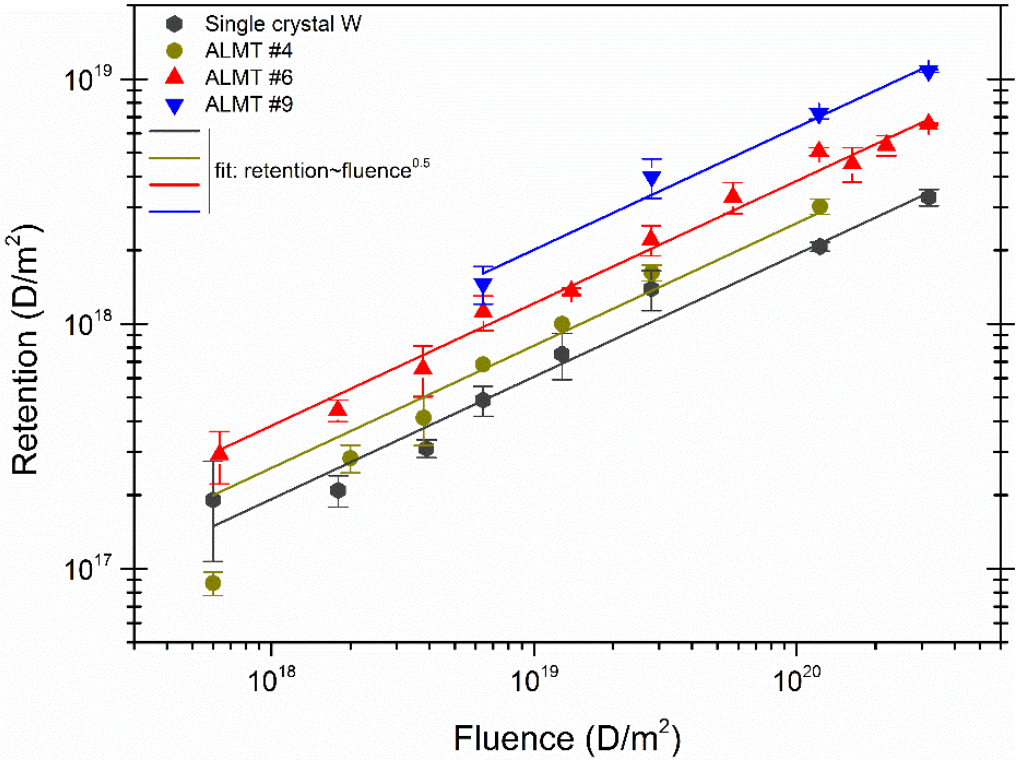


***Figure 33 – Deuterium retention as a function of fluence: polycrystalline tungsten vs. single crystal tungsten***

If the retention values corresponding to the second peak would be subtracted from the total retention values obtained on the single crystal, the curve would slightly shift to lower values. Following the purpose of investigating how removing the grain boundaries as a trapping mechanism will influence total retention, it is observed that removing grain boundaries leads to a decrease in total retention when the retention is measured after the storage time of 2.5 hours. Depending on the polycrystalline sample that is being compared to, the decrease

noticed on the single crystal can be more or less significant, the highest difference being noticed when compared to ALMT#9, and the lowest difference when compared to ALMT#4.

### 3.2.2 The evolution of trapped deuterium with the storage time in single crystal tungsten

The evolution of retained deuterium in single crystal tungsten was studied for storage times ranging between 2.5 and 140 hours. The ion implantation was performed at room temperature (300 K) for an incident fluence of $2.81\times10^{19}$ D/m$^2$. The results presented here were obtained in a single set of measurements, which is the same set that includes the measurements from the previous subsection (4.2.1). This means that all the results for the single crystal sample were obtained with the sample being under UHV at all times. Since the retention measured after a storage time of 2.5 hours showed only a small decrease as compared to the polycrystalline tungsten case, a direct comparison of the storage time evolution of retention for the two types of sample should help to determine how significant the grain boundary trapping is for deuterium retention in tungsten.

The results will be shown first as TPD spectra which will allow the analysis of both peaks of desorption and their evolution with the storage time, then the integrated values for the full spectra and for each of the two peaks will be plotted as a function of the storage time in UHV.

The amount of trapped deuterium atoms in single crystal tungsten was investigated for six different values of the storage time. The averaged TPD spectra corresponding to this experiment are presented figure 34. Just like for other set of measurements, each spectra is an average of at least three individual spectra, except the one obtained after 137 hours which is averaged only on two spectra. A zoom on the second desorption peak is being shown on the right side of the figure in order to allow a better assessment of the characteristics of this second peak.

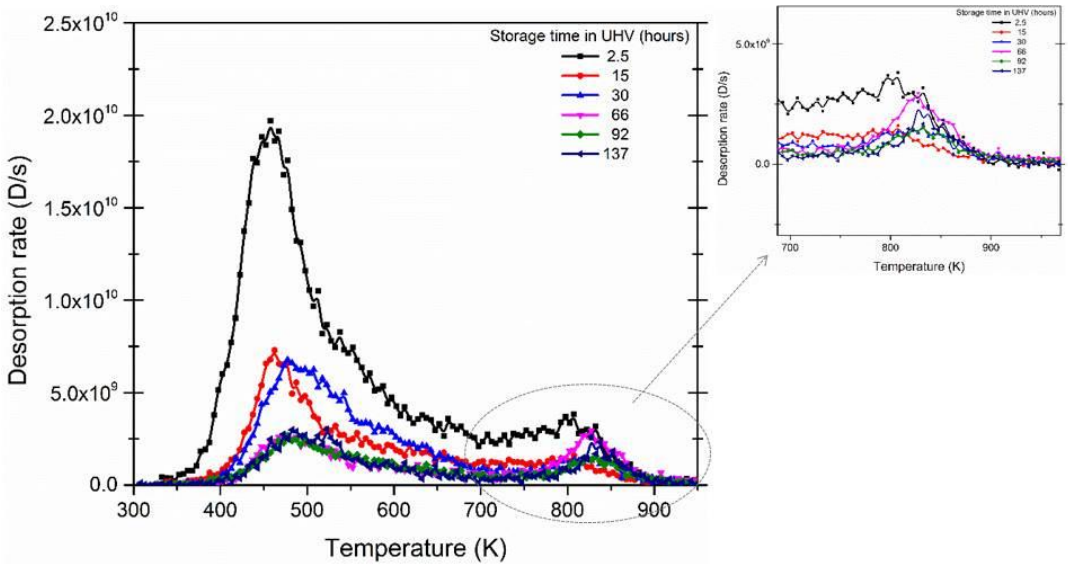


***Figure 34 - TPD spectra for different storage times after deuterium implantation in tungsten***

Analyzing the first peak only, it is observed that the intensity is greatly reduced when the storage time is increased from 2.5 hours up to 92 hours or above. The position of the desorption maximum suffers a shift of around 30 K towards higher temperature when the storage time is increased from 2.5 hours up to 92 hours and above. The shape of the peak is asymmetric with the decreasing tail extending towards higher temperature.

As it can be seen on the zoom of the figure, the intensity of the second peak remains constant with the storage time in UHV. For a storage time of 2.5 hours there is an overlap of the two peaks due to the higher intensity of the first peak, making the shape of the second peak less distinguishable. From the evolution of the two peaks with the storage time it becomes clear that the origin of the second peak is related to the presence of defects in the sample and it is not related to the quality of the temperature ramp. The position of this peak at higher temperature points to a trapping mechanism described by a higher de-trapping activation energy as compared to the one observed in polycrystalline tungsten. The high activation energy describing these extra defects impedes the deuterium from getting completely released at ambient temperature, for all the range of the examined storage time.

The fact that the second peak has a constant intensity allows the calculation of the exact amount of deuterium that is being trapped in the extra defects, for a fixed value of incident fluence. The safe way to do this is to average between the values of integration over the second peak for the TPD spectra recorded after a storage time of 30 hours or longer since the TPD spectra recorded after 2.5 and 15 hours respectively do not allow an accurate

discrimination of the two peaks because the two peaks overlap. The number of deuterium atoms trapped in the extra defects of the single crystal tungsten sample was determined to be: *total retention* = $8 \times 10^{16} \pm 3 \times 10^{16}$ D/m$^2$ for an *incident fluence* = $2.81 \times 10^{19}$ D/m$^2$. By subtracting this value from the retention calculated for the full desorption curve, we obtain the evolution of trapped deuterium in pristine single crystal tungsten (defects free) with storage time in UHV. These results are plotted as black hexagons in figure 35 next to the points obtained by integrating each peak separately and also by integrating over the full desorption curve (blue, red and green, respectively). The difference between the blue and the black curves, which are exponential decay fit lines to the corresponding colored symbols, shows that the error made in discriminating the two peaks for the shorter storage times is rather small.

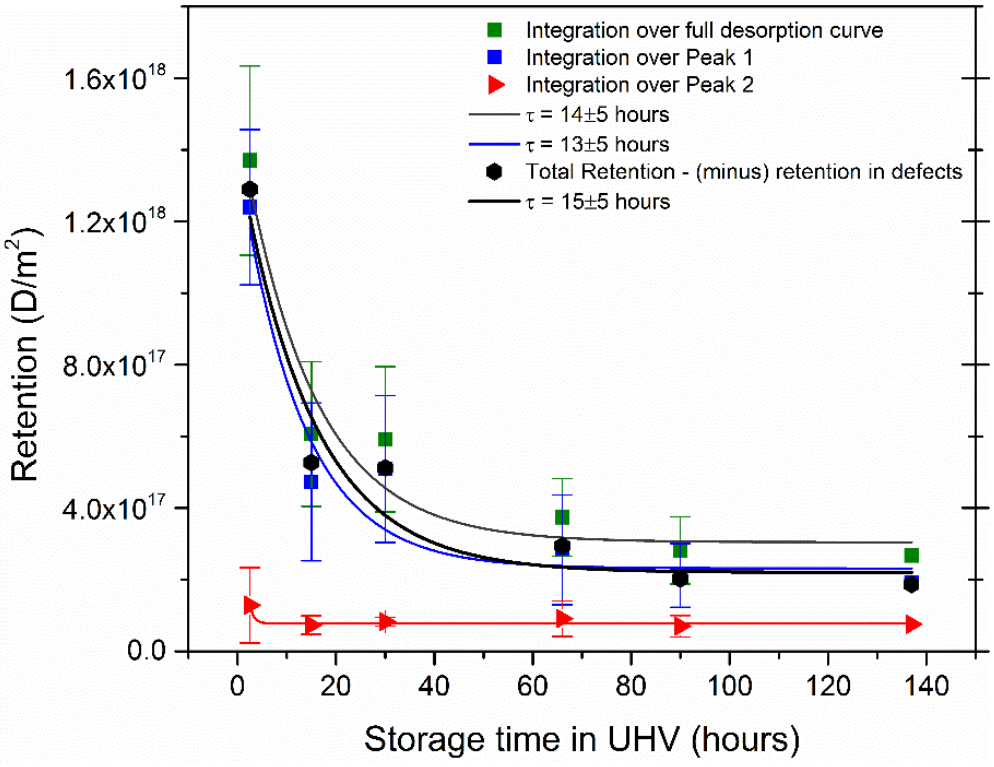


***Figure 35 – Storage time evolution of deuterium trapped in single crystal tungsten***

Analyzing the evolution of retained deuterium in single crystal tungsten with the storage time, it is noticed that retention follows the same trend as the one obtained on the polycrystalline tungsten, meaning the presence of two types of retention: short term and long term retention. The short term retention is characterized by a quick decay in the first 15 hours, which translates in a significant amount of deuterium being released in a short time interval after ion implantation, while the long term retention is characterized by a steady value above the 60 hours point.

### 3.2.3 Analysis and interpretation

The purpose of performing similar experiments on single crystal was to investigate how the absence of grain boundaries, as a trapping site influences the total retention amounts and the curves of desorption. It would be more tedious to control the density of other types of defects, like vacancies, dislocation loops or the oxide layer.

The results for the single crystal tungsten are analyzed in the same manner as for the polycrystalline sample following the influence of incident fluence and storage time. An investigation on the influence of implantation temperature was not performed.

The analysis has the same starting point as the one for the polycrystalline sample, meaning the known correlation between the filling level of a trap and the activation energy that describes it [14], [15], [19] and will be performed for both short term and long term retention.

When retention is plotted as a function of incident fluence, the same square root dependency is found. It was argued that retention is a process limited by diffusion, during the ion implantation step (see chapter 3.1.4). The implantation zone corresponds to a depth of around 10 nm and the diffusion length of atoms in polycrystalline samples during storage goes up to around 1 µm. The grain size for the polycrystalline samples is around 10 µm. It results that the diffusion towards higher depths in single crystal should be similar to the one in polycrystalline tungsten.

Looking at the effect of fluence on the TPD spectra, and especially on the position of peak maximum (figure 30), no shift in temperature is observed in the case of the single crystal. These spectra were obtained for a storage time of around 2.5 hours. With no grain boundaries being present, the most significant trapping mechanisms inside the bulk remain the vacancies and the dislocations. The absence of the shift for these spectra (obtained at short storage time) suggests that neither vacancies nor dislocations are that significant for the total retention amounts measured at short storage time. With no good candidate for the short term retention inside the bulk, it is suggested again that the oxide layer found on the surface of the sample could be responsible for the short term retention.

Analyzing the retention as a function of the storage time, the retention is significant only in short term, starting from 5% after 2.5 hours and dropping to roughly 1% after 60 hours, when compared to the incident fluence. The activation energy estimated from the exponential decay is found to have the same value as for the polycrystalline tungsten, i.e. $E_a$= 1.06 ± 0.02 eV. With the vacancies and dislocations having no significant influence on short

term retention, as it was shown by the TPD spectra, and with no grain boundaries present, the remaining possibility for the process responsible for the decay is the diffusion through the oxide layer.

The long term retention is small but it is not null, nevertheless. It can be argued that this non null amount is related to the trapping in vacancies accommodating 1 or 2 atoms, having therefore a high activation energy, to the trapping in dislocations accommodating also 1 to 2 atoms, and also related to atoms trapped in the oxide layer. Considering the idea that atoms trapped in the oxide layer need to diffuse through the oxide in order to reach another atom and to be released, when more and more of these atoms get desorbed, the remaining ones will become more and more distanced. The long term retention in single crystal tungsten should be related to these distanced atoms in the oxide layer, to the vacancies with low filling level, and to retention in dislocations.

Finally, the fact that the low temperature part of the spectra are described by a single peak of desorption, for all the durations of storage is in disagreement with the expected peak positions determined by using the activation energies for vacancies obtained by DFT [14], [19], [20]. If retention would be related only to the vacancies and, two peaks of desorption should become more distinguishable when the storage time is increased. The fact that this is not observed can be interpreted as an overlap of the two peaks with an extra peak related to the oxide layer. The activation energy as a function of the filling level ($l$) of dislocations is found in Xiao et al. [15]. Using the Redhead analysis [52], filling levels $l$ = 3 and l = 4 (with de-trapping energies around 0.90 to 1.00 eV) are expected to give the peak positions around 400 - 450 K. Regarding filling levels $l$ = 1 and $l$ = 2 (with de-trapping energies around 1.96 and 2.06 eV), it is expected that they will give peaks with positions around 700 - 750 K [52]. The difference in temperature between these two groups of filling levels should be big enough to give a clear shift of at least 250 K at longer storage times, which is not observed. Additionally, it is not clear if the second peak, noticed on the TPD spectra around 800 - 850 K, is related to the low filling levels of dislocations or not, since the Redhead analysis of the DFT studies of Xiao et al. [15] suggest that such peak positions should be around 700 - 750 K, i.e. 100 K lower than our experimental observations. However, dislocations could be present close to the surface as a result of the mechanical polishing, since the sample was not electro-polished, and could result in the presence of this second peak, at higher temperature. The point to be emphasized here is that the energy gap between the filling levels of dislocations could not explain the shift of the peak towards lower temperature, when the fluence is increased, for the polycrystalline tungsten experiments, since the peak noticed there

happens more gradually. Therefore, we conclude that the oxide layer found on the surface of the tungsten must also play an important role in retention, especially for the short term retention.

To summarize the measurements on single crystal tungsten, we found that the trapping mechanisms responsible for deuterium retention in a pristine sample are the oxide layer, vacancies, and dislocations.

### 3.3 Synthesis on deuterium retention in tungsten for both polycrystalline and single crystal cases

The investigation of the two types of tungsten samples was performed separately in the previous sections (3.1.4. and 3.2.3). The presence of two zones of retention, in relation with the storage time was shown. The two analyses lead to similar conclusions on the type of trapping mechanisms that are responsible for the short term retention in tungsten. For the short term retention it was proposed a higher impact of the oxide layer from the surface of the sample and a less important effect related to vacancies. For the long term retention, a significant difference in total amounts was noticed between the two samples.

The results obtained for the two samples are compared in this section side by side with the purpose of reaching a definitive conclusion on the importance of each type of trap for both short term and long term retention.

For the single crystal, only implantations at ambient temperature were performed, therefore a complete comparison between the two types of samples for implantation at higher temperatures will not be available for the present work.

In terms of retention vs. fluence dependency, the two samples were already compared on the same plot in section 3.2.1 (figure 33). In this section, the evolution with the storage time for the two types of samples will also be plotted together for the comparison of the two.

The switch to single crystal showed that, when there are no grain boundaries in the sample the total retention is smaller but it follows the same square root power law as for the polycrystalline sample. This observation supports the comparison of the two samples as valid for discriminating the type of trapping mechanisms and their importance. It also suggest that the comparison performed here should be valid for other orientations of a single crystal sample as well, in terms of retention trends for both short and long term retention.

The evolution of retention with storage time for the two types of tungsten samples are compared in figure 36. It is observed that the long term retention (60 hours and longer storage time) is reduced drastically when grain boundary trapping is absent. From the non-null

amount of retention observed for the long term part in single crystal and from the long term retention in polycrystalline tungsten, the trapping mechanism with the highest significance for the long term is easily associated with grain boundaries.

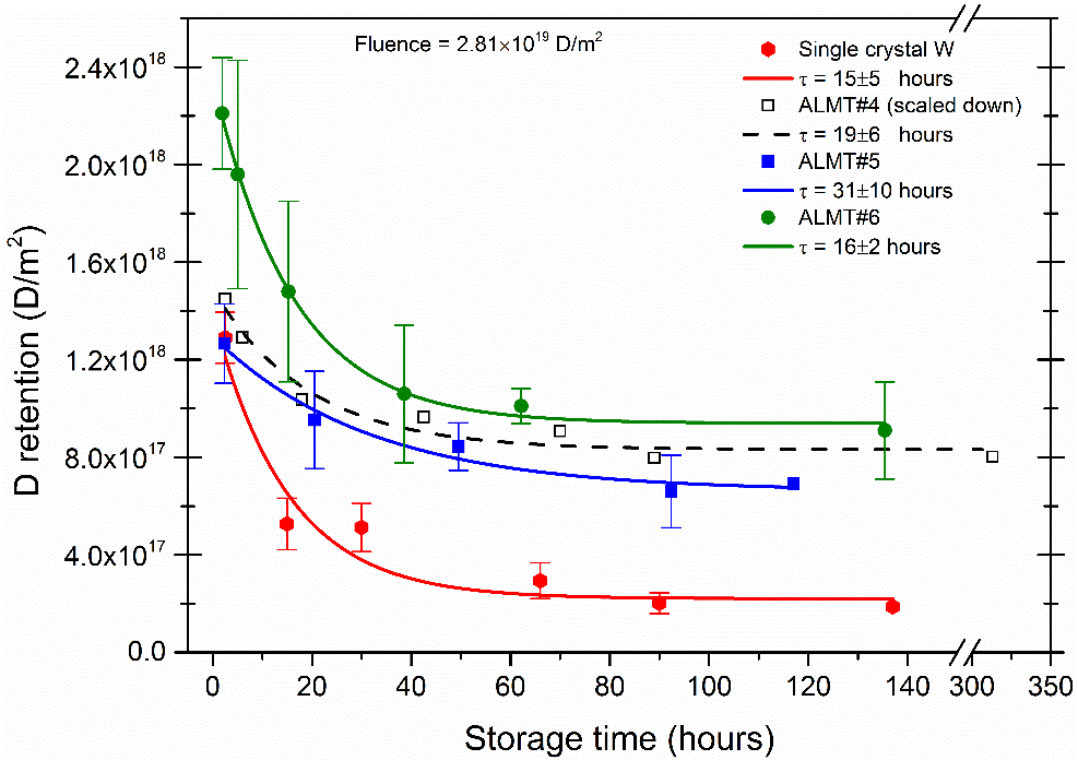


***Figure 36 - Storage time evolution of deuterium in two different types of tungsten (polycrystalline W vs. single crystal W)***

To support this conclusion, it suffices to sum up the storage time curve for single crystal with the difference of the long term retention levels between polycrystalline tungsten and the single crystal (retention level for single crystal vs. average retention level for polycrystalline tungsten). This operation corresponds to adding the (long term) effect of grain boundaries onto the curve of the single crystal tungsten. The resulting curve is an almost perfect match to the storage time curve for polycrystalline tungsten (figure 37).

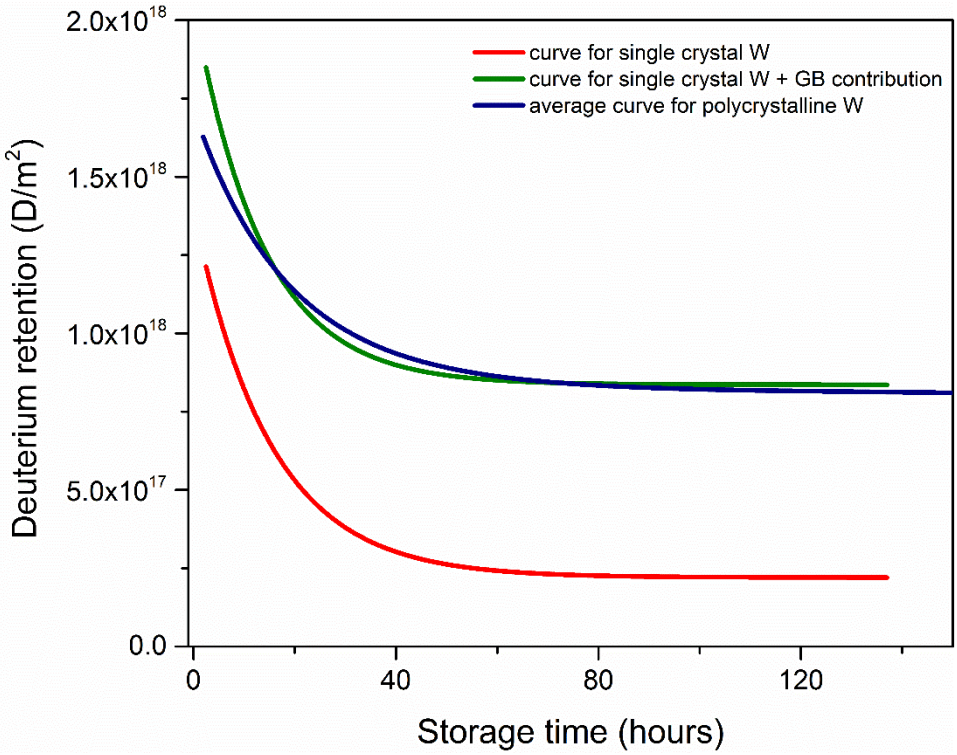


***Figure 37 - Graphic representation of grain boundary trapping superposed to retention in single crystal tungsten***

This match also shows graphically that the decaying behavior of the short term retention is not related significantly to the release from grain boundaries since their presence has little effect on the short term behavior.

The source of retention for the non-null amount for the long term part, observed for the single crystal could be related to vacancies, dislocations and to the oxide layer. The experiments presented here do not offer enough evidence favoring any of the two in particular. For future works, the non-null amount of the long term retention could be verified for samples with a controlled density of vacancies and/or dislocations, and for samples with a controlled thickness of the oxide layer. From the present results it can be said that this amount is related to vacancies and dislocations accommodating a low number of atoms and to atoms trapped in the oxide layer.

The thickness of the oxide layer was not being controlled for the experiments presented in this thesis, but it was reduced by an initial degassing procedure of at least two heating ramps (up to around 1300 K). Furthermore repeated annealing was performed after each individual measurement for about 10 minutes. It was noticed that just after a sample is introduced in UHV and is implanted with deuterium, for a typical fluence ($2.81\times10^{19}$ D/m$^2$), the retention for the first 2 to 3 measurements is higher by a factor of 1.5 to 2 compared to all the following measurements. This behavior suggests that the impurities present on the surface

are being removed either by the ion bombardment or/and due to sublimation at higher temperature, during the TPD heating ramps for the first measurements on a certain sample. To illustrate this evolution of impurities, the first TPD spectrum obtained on the single crystal sample is compared to the spectrum obtained by averaging all the following replicate measurements:

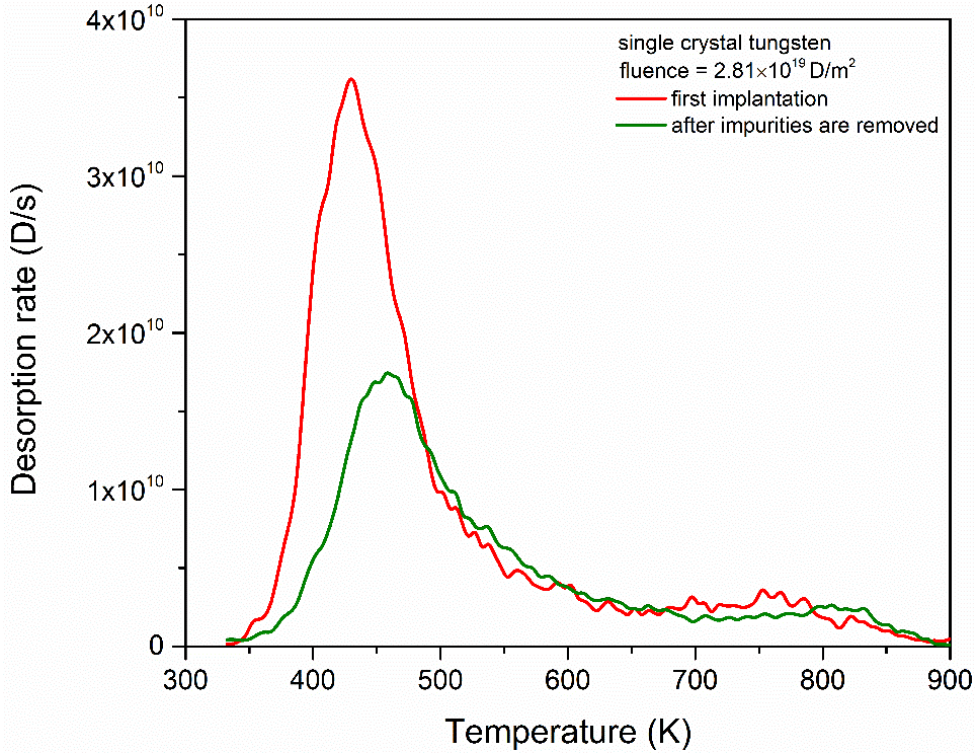


***Figure 38 - Impurities effect on TPD spectra***

The lower position in temperature of desorption peak maximum for the first implantation matches well with the trend obtained through calculations, presented by Hodille et al. [18] where it is shown that the addition of a 5 nm thick oxide layer leads to a shift of the peak towards lower temperatures. At the same time, for the calculations presented in [18], the presence of the oxide layer is shown to be the missing piece for a really good match of the calculations with our experimental results.

A graphical representation of the sources of retention corresponding to both the short and the long term is presented below, in figure 39. The storage time evolution of retention for the two types of samples are plotted by using the curve obtained on the single crystal and an average curve obtained on all the polycrystalline samples. The correspondence between different types of trapping mechanisms and the curves characteristics are shown.

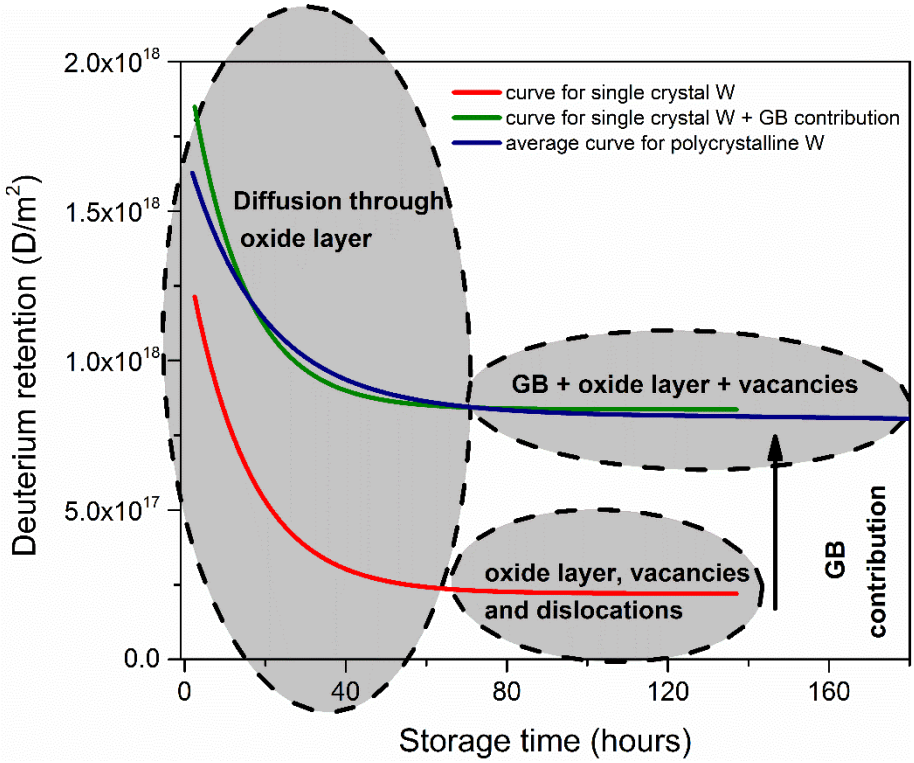


***Figure 39 - Identification of different types of traps and their contribution to deuterium retention in tungsten***

This representation summarizes the results obtained in this chapter for the retention of deuterium in tungsten, for the case where the trapping mechanisms are represented only by the natural defects. The analysis pointed out to grain boundaries, the oxide layer, vacancies and dislocations as being the main sources of deuterium retention. This fact remained true for the fluence range that was tested, for the ion flux and for the experimental method used during these measurements, which all insured that the density and the type of traps did not evolve with the repetition of measurements. The two types of retention that were defined as short term and long term were shown to be related to the retention in the oxide layer for the short term retention and to the retention in grain boundaries (if present), vacancies and dislocations for the long term retention. The contribution of trapping in vacancies, dislocations and in the oxide layer for the long term retention was shown to be non-null but also to be less significant when compared to the incident fluence.

To get a better idea about how much deuterium is retained due to each trapping mechanism and how this amount evolves with the storage time in UHV, in table 1 retention is presented as a percentage of the incident fluence for the case of *fluence* = $2.81 \times 10^{19}$ D/m$^2$ impinging a polycrystalline sample:

***Table1: Deuterium retention in polycrystalline tungsten expressed as percentage of the incident fluence of $2.81 \times 10^{19} D/m^2$***

| | Total retention | Oxide layer | Oxide layer, Vacancies and Dislocations | Grain boundaries |
|---|---|---|---|---|
| Short term | 5% | 3% | | 2% |
| Long term | 3% | | 1% | 2% |

The numbers presented in table 1 can be translated into percentage of the total retention for either the initial value of the storage time or for the long term retention, for the grain boundary trapping. The contribution of grain boundaries as a trapping mechanism counts for 30 - 40 % of the short term retention and for 66 % for the long term retention.

The switch from polycrystalline tungsten to single crystal tungsten and the comparison between the two cases proved to be a useful tool for determining the sources of retention (traps) and for following the evolution of the deuterium atoms accommodated on each type of trap.

The applications of these results to ITER, DEMO and other fusion devices based on tungsten as the divertor material come firstly as the identification of the trapping mechanisms that have the higher contribution to deuterium retention, as a dependency on specific storage times (defined as the durations between plasma exposure and any other action that is desired to be performed on a tungsten tile). The two types of retention (short term and long term) can be easily imagined as being related to situations when it is desired to know what happens with the fusion reaction fuel during a discharge and the immediate time after (short term retention) or related to situations when it is desired to know the tritium content in a tile after a longer time interval since plasma exposure, an example being the commissioning of tiles.

The findings presented in this chapter are also suitable to be used in wall models. The improvements to any wall model would consist in relating the changes in different exposure parameters to their actual physical effect. For example, the fluence can be related to the filling level of traps, which will help to use a more accurate value for the activation energy of the respective trap. This can be further used to assign the right temperature for the activation of the release process for a single atom. Furthermore, the bulk and the surface can both be taken into account for the retention and the release of deuterium by implementing the presence of the oxide layer as a trapping mechanism.

# Chapter 4

# Nitrogen retention in tungsten

The plasma facing materials that are planned to be used for the ITER fusion reactor are beryllium, for the 440 modules that constitute the blanket which completely covers the interior walls of the plasma vessel on a surface with an area of 600 $m^2$ [11], and tungsten for the plasma facing components of the divertor (inner and outer vertical targets and the dome) with a surface area of around 210 $m^2$ [1],[2]. Other experimental fusion machines, which were previously built with carbon based plasma facing components (graphite), have also switched to tungsten as a first wall material (ASDEX Upgrade changed from graphite to tungsten coated graphite [72], JET switched from graphite to beryllium walls and a tungsten divertor [73], Tore Supra switched from a carbon limiter to a tungsten divertor and became WEST [74]). The change was applied as a solution for the high fuel retention associated to the carbon first wall [75]. Under the action of plasma, carbon was being sputtered and some part of it would re-deposit and trap a significant fuel amount in the form of co-deposits. The experiments carried out with tungsten as first wall material (for the divertor area or for the vessel) have shown significant reduction of fuel retention compared to carbon based devices [76]. The main factor contributing to this improvement is the low sputtering yield of tungsten. At the same time, the low sputtering yield of tungsten leads to less impurities compared to the carbon case. The power density reaching to the wall is much higher in the absence of these impurities which were previously acting as radiating centers for the high power loads. The puffing of extrinsic impurities was proposed as a solution, with nitrogen being one of the candidates [77]. Experiments have shown that the use of nitrogen also improves plasma performance on top of efficiently radiating away the power loads [8],[9]. The concerns generated by the use of nitrogen in the divertor area are related to the eventual increase of fuel retention in the plasma wall, namely in tungsten, due to changes of the material following the exposure to energetic nitrogen ions generated inside the plasma. These concerns are addressed in this chapter, which presents the study on the interaction of nitrogen with tungsten, and also in Chapter 5.

In order to obtain results relevant for fusion devices, tungsten samples were subjected to a series of nitrogen implantations followed by thermo-desorption ramps, in an all *in situ*

apparatus, under ultra-high vacuum. The nitrogen retention amounts in tungsten were investigated by means of mass spectrometry.

Nitrogen molecular ions ($N_2^+$) with an energy of 500 eV were implanted in polycrystalline tungsten at an angle of 45°, at low flux (~$1\times10^{16}$ N/$m^2$s) with the sample at ambient temperature. The samples were provided by ALMT Corp. with a specified 99.99 wt.% purity, recrystallized and with dimensions of 10×10×0.4 $mm^3$. Since they were delivered in a batch of ten, they are identified throughout this chapter by their corresponding number. The results presented in this chapter were obtained on samples ALMT#4 and ALMT#5. In the preparation step, the samples were electro-polished and mounted on a molybdenum platen with the use of a molybdenum mask and four molybdenum screws. All the molybdenum parts were previously cleaned in an ultrasonic bath with acetone and ethanol. When a sample was introduced from air to vacuum, it was degassed at least three times by running a temperature ramp from ambient temperature up to $T_{oven}$ = 1300 K with a 10 minutes annealing at 1300 K.

The electron energy inside the QMS ionizing stage was set to 50 eV which allowed the counting of both m/z = 14 (for $N_2^{2+}$ and $N^+$) [56], [57] and m/z = 28 (for $N_2^+$) with a good signal to noise ratio. As explained in Chapter 2, when the signal for m/z = 28 is recorded, apart from the $N_2^+$ detection, the QMS also detects residual CO. The presence of CO appears as a desorption peak that overlaps with the peak given by the desorption of nitrogen. This fact makes it difficult to determine accurately the number of counts generated by the $N_2^+$ detection, therefore the use of the signal for m/z = 14 is preferred. Due to the way of calibrating the QMS sensitivity (Chapter 2), the use of the signal for m/z = 14 gives accurate results for the detection of desorbed N atoms, despite the lower intensity of the recorded signal determined by the lower ionization cross section.

The parameters that were varied for the study of nitrogen's interaction with tungsten were the incident fluence and the storage time in UHV after ion implantation. The implantation temperature was always room temperature. The evolution of the retained amounts of nitrogen (in N/$m^2$) with the storage time in UHV was studied for two different values of fluence. Additional experiments were performed in order to investigate the effect of nitrogen bombardment on the surface of the sample, by sequentially combining ion implantation and gas leaking.

The study of the nitrogen interaction with tungsten is divided in the following sections accordingly to the studied parameters. The first section is dedicated to the effect of the incident fluence on nitrogen retention, and it is then followed by the investigation on how

different storage time intervals affect retention. In the last section the eventual surface changes induced by nitrogen implantation are investigated.

### 4.1 The effect of nitrogen fluence on its retention in polycrystalline tungsten

The retention of nitrogen in polycrystalline tungsten was studied for an incident fluence range between $1\times10^{19}$ and $2.34\times10^{21}$ N/m$^2$. The low molecular ion flux of ~$1\times10^{16}$ $N_2^+$/m$^2$ provided by the ion gun leads to relatively long durations of implantation in order to reach the higher fluences. The lowest value of incident fluence is reached after 15 minutes of ion implantation, while the highest value requires 64 hours of ion implantation. The expected heating rate induced by the ion beam, calculated for a typical sample, is around ~$7.4 \times 10^{-5}$ K/s. This heat will be lost both by black body radiation and by conduction towards the heater assembly on which the sample is mounted. When the entire assembly composed by the heater and the sample is considered, the ion bombardment will determine an insignificant increase of the sample temperature even for a 64 hours implantation.

The quantification of the total retained amount of nitrogen was performed using the TPD technique. The results are shown first as desorption (TPD) spectra, i.e. as the release rate of the individual nitrogen atoms plotted as a function of the sample's temperature during TPD. Then, by integrating these spectra and by applying the quantification method detailed in chapter 2, section 2.4, the values for total retention are obtained and plotted as a function of incident fluence. The influence of the storage time will be discussed in the following section.

Figure 40 shows the TPD spectra obtained after ion implantation of different values of nitrogen incident fluence, on sample ALMT#5. The spectra show the desorption rate of nitrogen as it is detected by the mass spectrometer, meaning that the curves show only 4% of the total number of released nitrogen atoms (absolute amounts are considered when total retention is determined – method is explained in Chapter 2). Since these curves correspond to the release of nitrogen in the form of $N_2$, a factor 2 is applied to the y-axis in order to show the desorption rate as N atoms per second. Such a representation is consistent with the way TPD curves will be presented in the next two chapters where, for the evaluation of total retention, multiple types of molecules need to be considered (for example $N_2$ and $ND_3$ for the release of nitrogen or HD, $D_2$ and $ND_3$ for the release of deuterium). The x-axis represents the sample temperature (the sample is heated with 1 K/s from ambient temperature up to 1300 K). These spectra were obtained in a single set of measurements and each spectrum is, in general, an average of at least two replicate measurements, except the spectra for the highest value of incident fluence. The spectrum shown for $4.5 \times 10^{20}$ N/m$^2$ represents an individual

measurement since the average of the two available measurements (on sample ALMT#5) were leading to a fake second peak of desorption. The reason for this fake peak is a difference of 70 K between the peaks maxima of the two measurements. This difference is coming from ramp irregularities noticed for one of the two measurements, which makes the maximum of the peak suffer the approximately 70 K shift in temperature position.

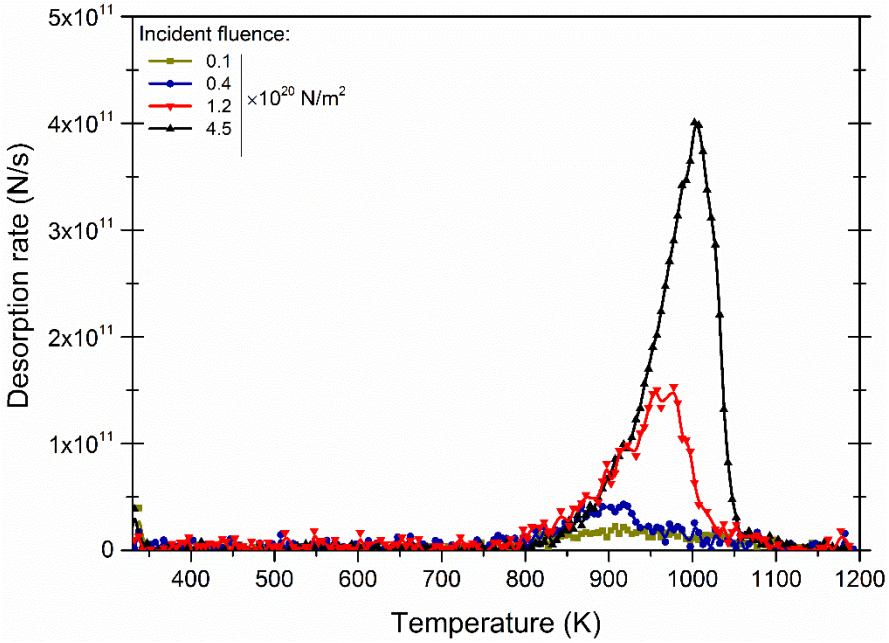


***Figure 40 - TPD spectra: release rate of nitrogen from tungsten for different incident fluences; Sample: ALMT#5***

The same faulty behavior of the temperature ramp has affected the implantation performed for the highest incident fluence, rendering the desorption spectrum unusable for the above figure. Due to the long duration of implantation necessary to reach this highest fluence (64 hours for $2.34 \times 10^{21}$ N/m$^2$), the measurement was performed only once, and therefore no desorption curve is included in the figure.

In order to illustrate the effects of recurrent ramp problems mentioned above, the TPD spectra plagued by the faulty ramp are compared with TPD spectra obtained with a functional ramp. To do this, all the individual spectra obtained from replicate measurements (i.e. measurements with identical parameters) for fixed incident fluence are plotted in Figure 41. On the left side, are shown spectra obtained with a good ramp on sample ALMT#4 with an incident fluence of $1.23 \times 10^{20}$ N/m$^2$. On the right side, spectra affected by a bad ramp are plotted and correspond to an incident fluence of $4.5 \times 10^{20}$ N/m$^2$ obtained on sample ALMT#5. It should be noted that spectra on ALMT#5 were obtained during experiments for sequential implantation of nitrogen and deuterium, except for the two thicker curves which correspond to the implantation of nitrogen alone, and which are added for comparison

purposes. The spectra obtained from sequential implantations are used here only as a mean to show the differences between a good ramp and a faulty one. The results corresponding to these measurements are presented and analyzed in Chapter 5, and some will be mentioned in the next section as well.

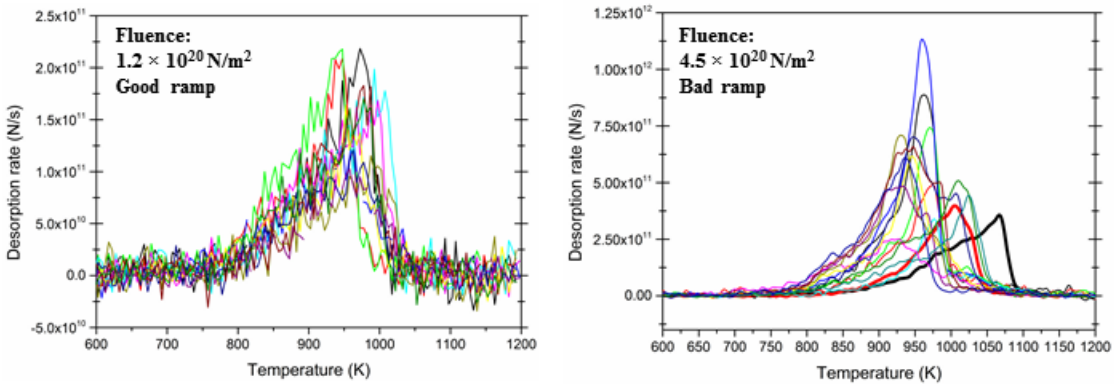


***Figure 41 – Individual TPD spectra for a fixed fluence of 1.23 × $10^{20}$ N/$m^2$ obtained with a good ramp on ALMT#4 – left; Individual TPD spectra for a fixed fluence of obtained with the faulty ramp (ramp with irregularities) on ALMT#5 – right.***

For ALMT#4 (left side of the figure), shape and position of the peaks remained consistent throughout the measurement series. In contrary, the spectra on the right side (ALMT#5) show large variations in width, position and intensity, with the appearance of double peaks in some cases. These inconsistencies suggest irregularities of the sample temperature ramp for the ALMT#5 series, as it was confirmed with the analysis of the time derivative of the oven temperature ramp (not shown). When measurements are verified chronologically, it is noticed that the ramp irregularities started to occur sometime during the experiments on sample ALMT#5, which were performed after the experiments on ALMT#4. From the experience gained while calibrating the heater assembly in order to get the linear temperature for the sample, it is known that any mechanical evolution of the heater has a certain effect on the quality of the ramp's linearity. It is suspected therefore that the contacts of the heater assembly have suffered a certain evolution, and therefore many of the ramps were affected by irregularities. Since the data set from ALMT#4 showed consistent TPD spectra, and the data from ALMT#5 are partially affected by a faulty ramp, in the following we will only discuss TPD spectra for which a faulty ramp can be excluded by analysis of the time derivative of the oven ramp, i.e. the ones presented in Figure 40. Nevertheless, TPD spectra with faulty ramp will be used for retention studies.

In Figure 40, it is observed that nitrogen atoms are being desorbed from tungsten starting from around 800 - 850 K and that the maximum of desorption rate is situated between

950 and 1050 K (depending on the incident fluence). The peaks of nitrogen desorption are described by an exponential increase of the desorption rate up to the peak maxima followed by a steep drop in desorption rate. The width, the intensity and the peak position are all increasing when the incident fluence is increased. This behavior will be discussed in section 4.4.

The evolution of nitrogen retention with the nitrogen incident fluence is plotted in figure 43. At first, only the results from nitrogen-only implantations were considered. Later on, the measurements for sequential implantation of nitrogen and deuterium were performed and it was noticed that the results show a higher scattering for the retention value. It was considered at this point if the nitrogen retention values obtained for the sequential implantation could be used in order to have better statistics for the results show in figure 43. The data are shown later on, in this thesis in Chapter 5, where the sequential implantation of nitrogen and deuterium in tungsten is presented. But the main idea, that needs to be confirmed here, is the fact that deuterium implantation does not determine a significant loss of the implanted nitrogen. If this is the case, then the nitrogen retention values observed for the case of sequential implantation can safely be used for better statistics in figure 43. This is shown in figure 42 below, where nitrogen retention is compared for the two types of implantation: individual – $N_2^+$ only, and sequential – $N_2^+$ followed by $D_2^+$.

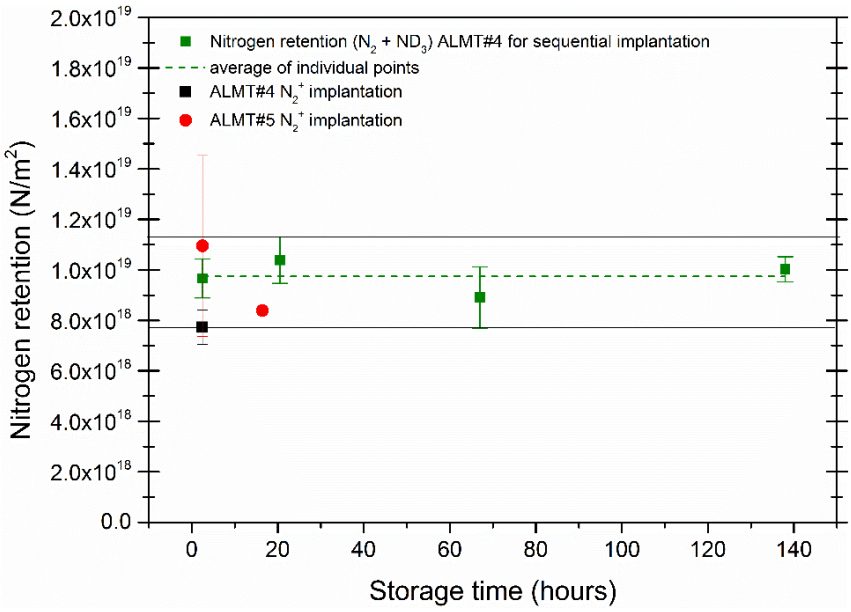


***Figure 42 – Nitrogen retention compared for the two types of implantation: individual – $N_2^+$ only (red circle and black square), and sequential – $N_2^+$ followed by $D_2^+$(green square); Incident fluence used: 1.23 × 10$^{20}$ N/m$^2$and 2.81 × 10$^{19}$ D/m$^2$; Samples: ALMT#4 and ALMT#5; The average value of the four points for the sequential implantation is plotted as a green dashed line. The black continuous lines represent the highest deviations from this average value, and it can be noticed that they incorporate all the points for individual nitrogen implantation***

The above figure confirms that deuterium implantation does not remove a significant amount of the previously implanted nitrogen (actual values/percentage are discussed in Chapter 5). Briefly, the nitrogen retention values obtained for individual nitrogen implantation, fall within the standard deviation of the values of nitrogen retention obtained for the sequential implantations. Therefore, in figure 43, datasets from both ALMT#4 and ALMT#5 samples, and measurements for both individual and sequential implantation, are used in order to determine the average values of retention with improved statistics. The individual retention values corresponding to each of these measurements are also shown in figure 43 as red and blue stars with the purpose of illustrating their scattering. To avoid confusion on why both datasets are used, the following facts need to be pointed out: even if a TPD spectrum is affected by oscillations, this doesn't affect the calculation of retention, when the peak is integrated (this explanation concerns measurements with a faulty ramp obtained on ALMT#5); the samples belong to the same batch, therefore they are very similar, which justifies the use of the replicate results from both samples, in order to obtain better statistics.

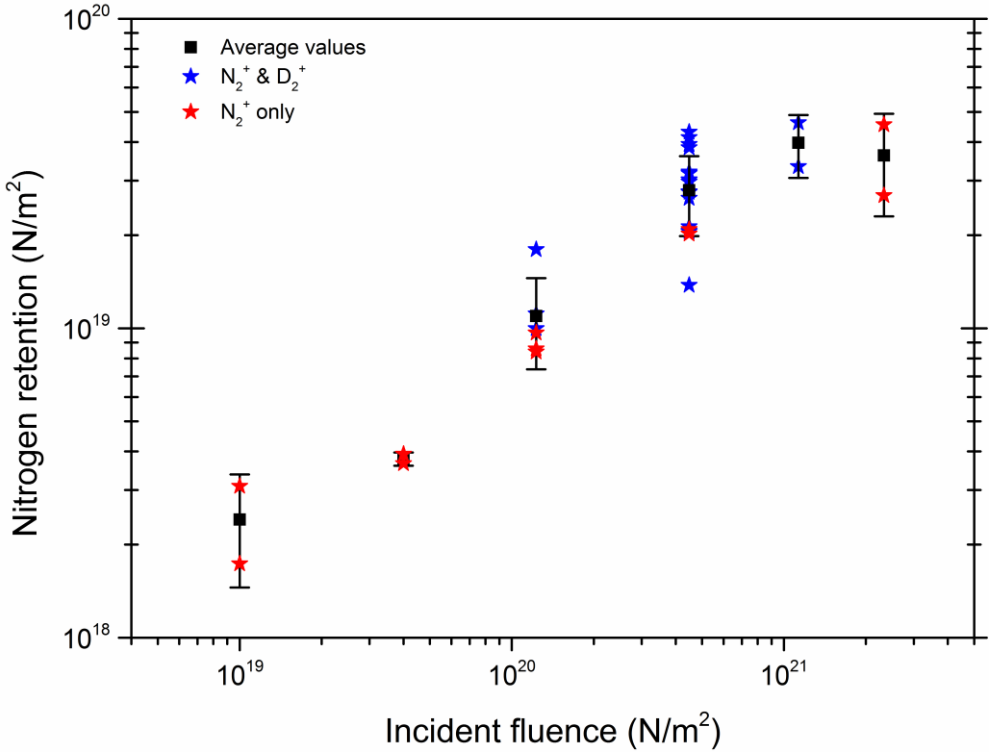


***Figure 43 - Nitrogen retention in polycrystalline tungsten as a function of incident fluence; Samples: ALMT#4 and ALMT#5; The bars represent the standard deviation of the mean, obtained by using all the available points for a specific incident fluence***

As the incident fluence is increased, retention shows two different trends. Up to an incident fluence of $4.5 \times 10^{20}$ N/m$^2$ retention is increasing, but above this value the number of retained nitrogen atoms seems to saturate and to remain constant for the rest of the fluence range that

was investigated. The rather high scattering of the individual points could be explained/justified in different ways. There is a possibility that not all nitrogen atoms are desorbed during TPD. In our set-up, the temperature of the oven goes as high as 1250 - 1300 K, but King and Wells have shown that nitrogen could be desorbed at temperatures higher than that in case of a significant adsorption on clean tungsten [80]. Nevertheless, a clear indication in this direction is not available in our case. A second reason could be represented by a "memory effect", which would mean that the sample will have slight evolutions from one measurement to another, when exposed to higher fluences of nitrogen, or simply to nitrogen. More precisely, for our measurements, a ten minutes annealing at a temperature of around 1250 K is performed at the end of every ramp. From experience, this step leads to a good reproducibility for deuterium cycles of implantation and desorption, and it was considered that it could insure the same reproducibility for nitrogen experiments. It could be possible that, for these high fluences of nitrogen, this annealing step is not sufficient to insure that the sample does not evolve from one measurement to another and therefore a wider scattering of the retention values for nitrogen is obtained. A last explanation could be related to the impinging nitrogen flux which could be unstable when performing long implantation duration. Indeed, ion flux was measured on a regular basis during the day but not overnight. In the calculation of nitrogen fluence, we assumed that the ion flux varied linearly between the last ion flux measurement of day N and the first ion flux measurement of day N+1, but this could be not the case.

### 4.2 The evolution of trapped nitrogen with storage time in polycrystalline tungsten

The number of nitrogen atoms retained in tungsten following ion bombardment was quantified after different durations of storage in UHV. The investigated storage time intervals fall between 2.5 and 140 hours. The dependency of the retained nitrogen amount with storage time is presented for two different values of the incident fluence ($1.23 \times 10^{20}$ and $4.5 \times 10^{20}$ $N/m^2$).

No complete set of measurements dedicated to the storage time evolution of the nitrogen atoms implanted in tungsten, for the case of "nitrogen only" implantation, is available. The results presented in this section were obtained during two sets of measurements with the sample being sequentially bombarded with nitrogen and deuterium, both of them in the form of molecular ions. These results were compared to the few available results for "nitrogen only" implantations for storage times longer than the usual minimum of 2.5 hours (see figure 42). It was observed that the points obtained for the sequential implantation can

safely be used to describe the evolution of the implanted nitrogen with the storage time. The two cases show similar nitrogen retention, within the error bars.

In order to quantify the total number of retained nitrogen atoms, the following released products were taken into account: $N_2$ and $ND_3$. The measurements were performed on two different samples as follows: the results for the lower fluence were obtained on the sample ALMT#4 while the results for the higher fluence were obtained on the sample ALMT#5.

The results are shown first as desorption spectra which are then compared for the two different values of incident fluence. Then, the nitrogen retention values are plotted as a function of the storage time in UHV, for the two fluences. In this case, the retention value is calculated as the sum of all the nitrogen atoms released in all forms.

The curves of nitrogen desorption rate recorded after various storage time intervals between implantation and TPD are plotted in figure 44 (a). These spectra correspond to an incident fluence of $1.23 \times 10^{20}$ N/m$^2$. On the right side of figure 44 (b) the same spectra are averaged and plotted as a single curve. This averaged curve illustrates the similarities between the four separate spectra corresponding to the four different storage times tested. In figure 44 (c), the two of the spectra from 44 (a) corresponding to storage times of 68 and 138 hours are zoomed and plotted together with their standard deviations of the mean for each temperature bin (5 K intervals).

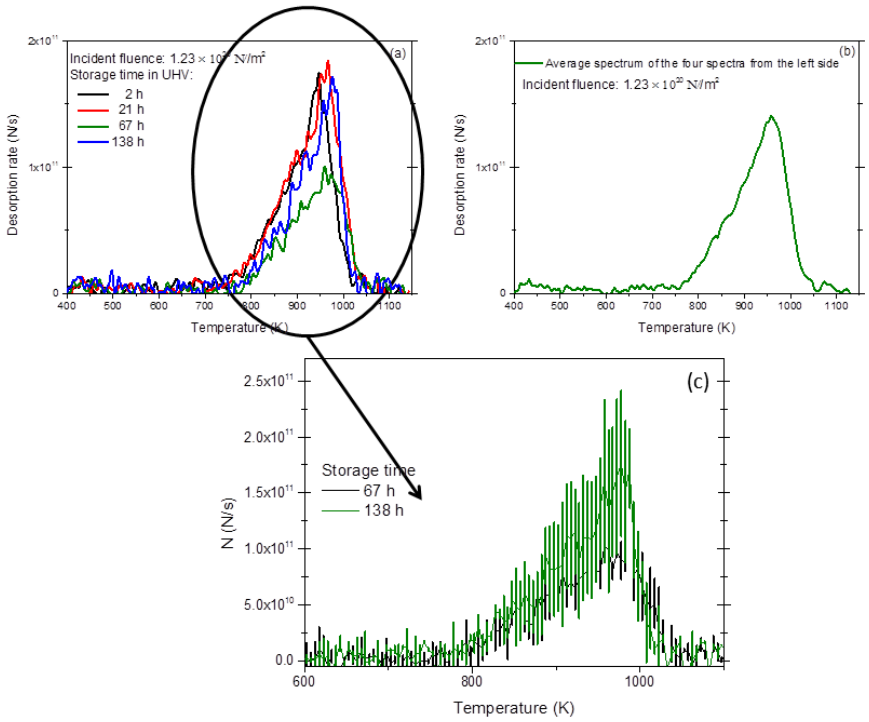


***Figure 44 - TPD spectra for nitrogen desorption from polycrystalline tungsten; Incident fluence = 1.23 × $10^{20}$N/m; Sample: ALMT#4***

The characteristic of the peaks in figure 44 (a) are similar for all the values of the storage time, except the one for a storage time of 67 hours. The spectra for 2.5, 21 and 138 hours are clearly overlapping and they all have the same shape, the same intensity within small variations and their peak maxima are described by the same position in temperature. Given that the spectrum for the storage time of 68 hours is obviously smaller than the other ones in figure 44 (a), one could think that there is a problem with this spectrum. However, when one plots the spectra for 68 and 138 hours together with the standard deviations for each temperature bin (in figure 44 (c)), one finds overlapping TPD spectrum too. Therefore, one can average all the four spectra (for all the four storage time values) in one single curve (figure 44 (b)) which should describe the release of nitrogen from polycrystalline tungsten, for the case of the aforementioned incident fluence, and independent of the storage time.

For the second value of nitrogen incident fluence ($4.5 \times 10^{20}$ N/m$^2$) four storage time intervals were tested: 2.5 hours, 24 hours, 68 hours and 119 hours. For each of the three higher values, the measurements were performed two times while for the storage time of 2.5 hours, the measurement was performed three times. The TPD spectra of nitrogen for which the storage time evolution was tested were obtained on sample ALMT#5 and their shape and position are affected by the irregularities of the temperature ramp. As it was shown in figure

41 (right side), in such a case, the spectra are unusable for averaging or for providing accurate information about the position and the width of the peak.

Nevertheless, the retention of nitrogen is determined by integrating the spectra described in the previous two paragraphs, for the two incident fluences, and the values are plotted in figure 45.

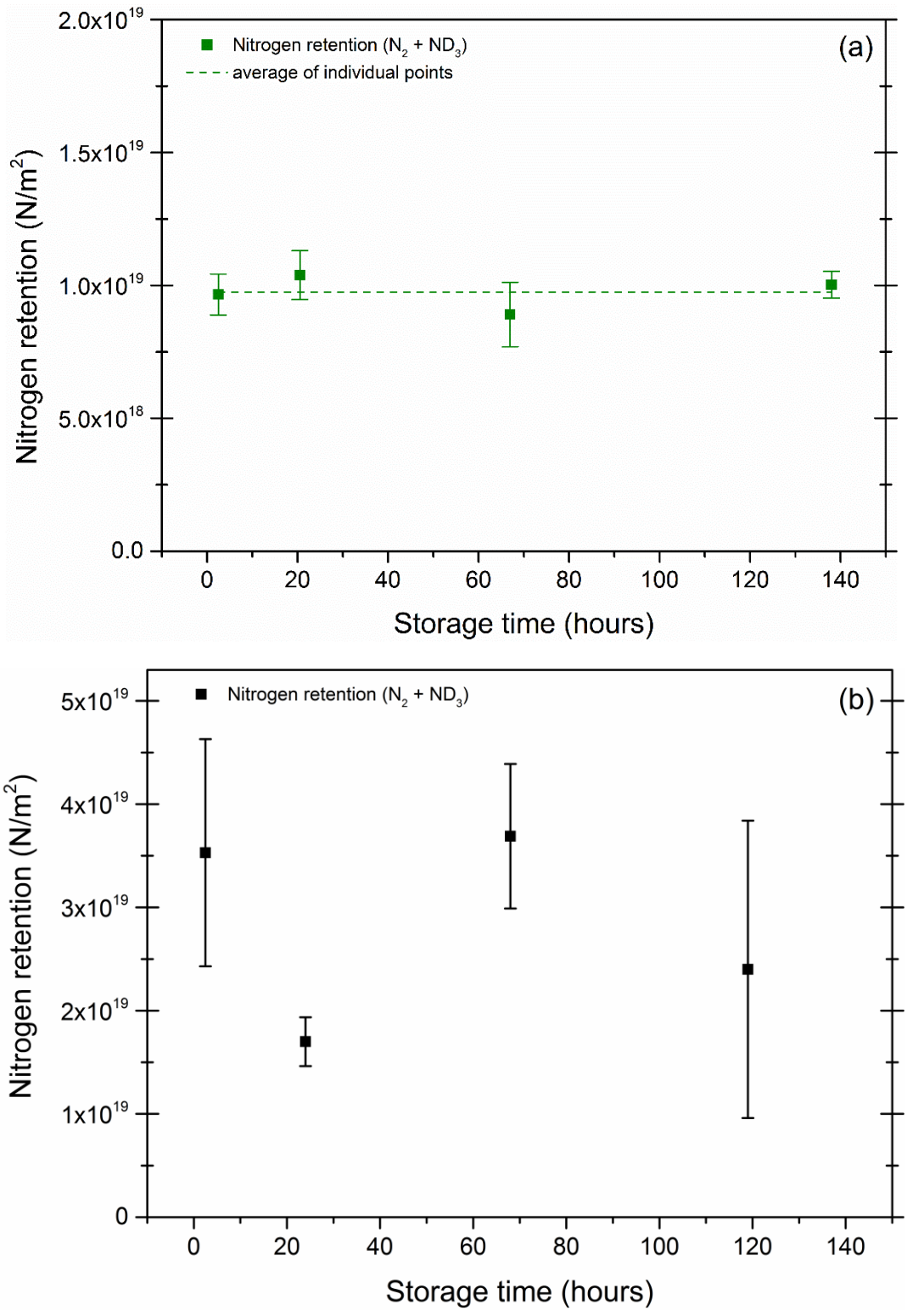


***Figure 45 – The evolution of trapped nitrogen atoms with storage time for two different fluences: $1.23\times10^{20}$ $N/m^2$ – up -– ALMT#4; and $4.5\times10^{20}$ $N/m^2$ - down – ALMT#5***

In the top of Figure 45, nitrogen retention values remain constant for all the storage time intervals, after exposure to an ion incident fluence of $1.23 \times 10^{20}$ $N/m^2$ (green square points). The dotted green line represents the average value of the green square points, meaning the

retention value calculated as the average of the four individual points. For the exposure to higher ion incident fluence (figure 45 bottom), the nitrogen retention values seem to show a less good reproducibility, and to vary within a factor of 2. They do not show, nevertheless any clear sign of decrease, within experimental uncertainties.

### 4.3 Surface changes and their effect on retention

With the perspective of the study on the synergetic interaction of nitrogen and deuterium with tungsten, in Chapter 5, a preliminary experiment was performed in order to determine if the bombardment with nitrogen molecular ions ($N_2^+$) affects the morphology and the reactivity of the tungsten surface. The idea of the experiment consists in exposing the sample to nitrogen ion bombardment and to see how this preliminary step affects the further interaction of deuterium with the surface. Any eventual change of the surface due to pre-exposure to nitrogen was evidenced by leaking molecules onto this ion-exposed surface and by looking at how the sticking of molecules ($D_2$) is changing. The quantification of the molecular sticking is achieved using the TPD technique. At first reference TPD spectra were recorded on an unmodified sample without any exposure to gas or molecular ions. Then, for various combination of exposures to molecules or/and molecular ions, the desorption of HD, $D_2$, $N_2$ and $ND_3$ was quantified.

Two types of exposures were carried out:

- $D_2$ molecules were leaked on an unmodified sample
- $N_2^+$ molecular ions were implanted in the unmodified sample, followed by a $D_2$ molecules leaking

The TPD spectra of HD, $D_2$ and $N_2$ for these two experiments are presented in figure 46 a) – HD, b) – $D_2$, and c) – $N_2$). A reference curve that shows the signal in the absence of any exposure is also plotted.

It is observed that:

- The number of HD molecules increased after $D_2$ leaking as well as after $N_2^+$ bombardment followed by $D_2$ leaking
- $D_2$ molecules are present only after the $N_2^+$ bombardment followed by $D_2$ leaking
- $N_2$ molecules are clearly detected only after $N_2^+$ ion bombardment
- The presence of ammonia will not be discussed here and it will be instead presented in Chapter 5; Nevertheless, no desorption peak was observed for m/z = 20, for any of the cases presented in the figure below.

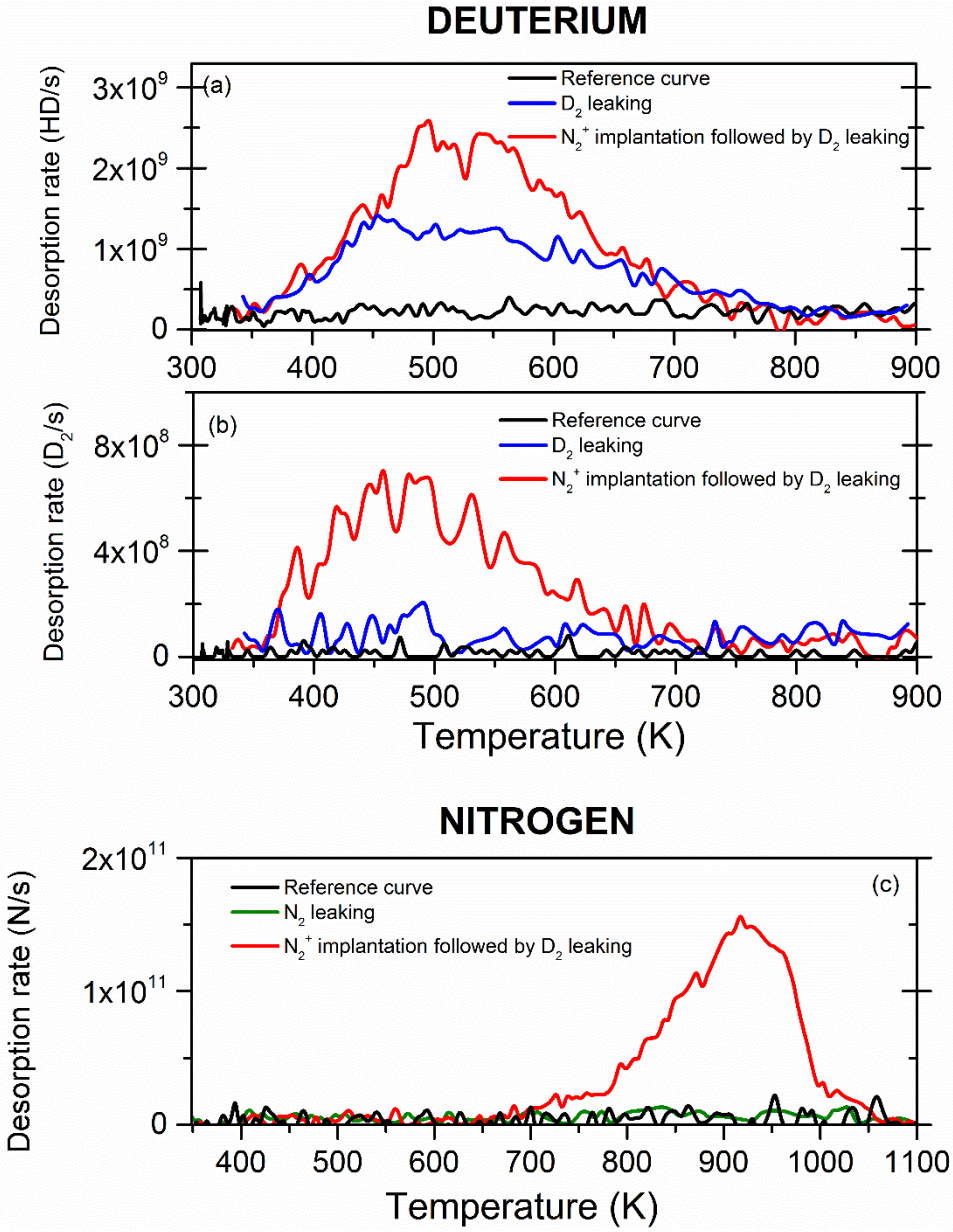


***Figure 46 – TPD spectra of: a) HD; b) $D_2$; c) $N_2$; various types of exposure***

We interpret the presence of deuterium desorption after $N_2^+$ implantation followed by $D_2$ leaking as the result of the dissociative chemisorption of $D_2$ on $N_2^+$ modified W surface. A more detailed discussion of these observations is included in the next section.

The number of deuterium atoms which get chemisorbed on a tungsten surface is determined to be around $4.7 \times 10^{17}$ D/m$^2$. This value is obtained for a storage time in UHV of 2.5 hours. If the storage time is increased to 120 hours (not shown in the figure), there is a decrease of the number of chemisorbed deuterium atoms, to around $2.6 \times 10^{17}$ D/m$^2$. These amounts are calculated by taking into account the release of deuterium as both HD and $D_2$.

The values are around two orders of magnitude smaller than the typical tungsten surface density, which is roughly $1 \times 10^{19}$ W/m$^2$, meaning that only a small (2 – 4 %) percent of the $N_2^+$-modified W surface chemisorbs deuterium atoms.

Since during a $D_2^+$ ion implantation (flux density = $1.6 \times 10^{16}$ D/m$^2$s), there is an important background pressure of $D_2$ neutral molecules (typically around $3.5 \times 10^{-7}$ mbar which gives a flux density = $7.5 \times 10^{18}$ D/m$^2$s), these neutral species will contribute to the retained amount by increasing the inventory of retained deuterium atoms (surface + bulk). Therefore, chemisorbed amounts need to be compared to typical values of deuterium retention in tungsten, obtained as a result of sequential nitrogen and deuterium molecular ion implantation (presented in chapter 5). It is observed that the chemisorption contribution is significant only if the deuterium fluence is small. For example, for the incident fluences used in this thesis, they will account for roughly 20 – 25 % of deuterium retention when a $2.81 \times 10^{19}$ D/m$^2$ incident fluence is used, but will become less important as the fluence is increased. It means that, when the retention is analyzed as a function on incident ion fluence for the sequential implantation of nitrogen and deuterium these chemisorbed amounts need to be considered as well.

### 4.4 Analysis and interpretation

The experiments presented in this chapter are focused on the amount of nitrogen that is retained in tungsten after ion implantation, as a function of the incident fluence. The evolution of these retained atoms is then followed for different times of storage in UHV. The purpose is to identify the mechanisms for nitrogen trapping in tungsten and to understand how nitrogen ions exposure modifies the tungsten surface and the bulk. In the context of this thesis, these results will be the first step in investigating the interaction of both nitrogen and deuterium with tungsten.

From the TPD spectra obtained after the exposures of polycrystalline tungsten to a nitrogen ion beam, the first things that are noticed are the presence of a single peak of desorption situated at high temperature, with a relatively small width (maximum 200 K for the highest fluence), and with the maximum of desorption varying between 900 and 1010 K depending of the incident fluence (the position of the maximum shifts to higher temperature when the incident fluence is increased). This suggests a trapping mechanism with relatively high activation energy while the small width of this single peak strongly suggests a single type of trapping mechanism [52], [54].

The desorption curves are well described by an exponential increase of the desorption rate up to the peak maxima followed by a steep decreasing tail. The increase of the incident fluence leads to a shift to higher temperature of the desorption peak maximum (figure 40). At the same time, the exponential increase is shared by the spectra corresponding to different incident fluences, meaning that they have the same starting point and they overlap. These characteristics of the TPD spectra correspond well to a zero order reaction mechanism.

The overlapping of the exponential increase suggests an immediate replenish of a desorbed surface layer. It means that as soon as a layer is being desorbed, the atoms below act as an immediately available reservoir for the surface covering layer. Since the diffusivity of nitrogen in tungsten is known to be low [32], this replenishing effect should be the result of the small implantation depth for nitrogen in tungsten. The incident fluence would then be related to the filling level of the implantation range and will not influence significantly the implantation range itself. Higher fluence will result in higher intensity of the desorption peak and with an apparent shift in temperature for the peak maximum. By applying the natural logarithm to the Polanyi-Wigner equation (Eq. 3 in Chapter 1), the expression for $E_{DES}$ can be extracted and it gives:

***Equation 19***

$$E_{DES} = \ln\left(\frac{A \times \theta^n}{r_{des}}\right) \times k_B \times T$$

For a zero order reaction, with n = 0 and $\theta^n = 1$, the expression for $E_{DES}$ becomes:

***Equation 20***

$$E_{DES} = \ln\left(\frac{A}{r_{des}}\right) \times k_B \times T$$

The dependency of nitrogen retention with the incident fluence, presented in figure 43, shows first an increase of the number of trapped nitrogen atoms, with a slope of 0.78 ± 0.12. This increase, nevertheless, occurs only up to an incident fluence of $4.5 \times 10^{20}$ N/m$^2$, where retention starts to saturate. As suggested in [34], nitrogen is implanted in the immediate vicinity of the surface, within a depth that is directly correlated to the energy of the incident particles. From the phase diagram obtained by Schmid et al in [32], it results that, for implantation temperatures below 600 K, nitrogen remains trapped only in the form of WN in the implantation range. The nitrogen atoms trapped in this binding state will be able to accumulate in tungsten only up to a concentration of roughly 50% due to the 1:1 atom ratio. The retention dependency with the incident fluence, shown in figure 43, suggests that

nitrogen saturation is achieved for an incident fluence of roughly $7.5 \times 10^{20}$ N/m$^2$. By introducing in equation 20 the $T_p$ of the peak maximum and the maximum desorption rate $r_{des}$ for the case of close-to-saturation incident fluence, the values of $E_{DES}$ could be estimated.

For the TPD spectrum of the incident fluence = $4.5 \times 10^{20}$ N/m$^2$, from figure 1, $T_p$ = 1007 K and $r_{des} = 4 \times 10^{11}$N/s. To account for all the atoms that get desorbed from the sample, the correction represented by the geometrical factor $G$ (explained in Chapter 2, section 2.3.4.1) is applied to the rate of desorption ($G$ = 0.04). Using the pre-exponential factor published by J. Keinonen et al. [31] for a similar range of temperature as the one of our peak, $A = 4.3 \times 10^{-4}$ m$^2$/s, the value obtained for the activation energy is $E_{DES}$ = 2.71 ± 0.11 eV. But, with the hypothesis of a zero order process, this procedure should be applied for the position in temperature at which the desorption starts (the release is activated). Therefore, the same procedure is applied for the lowest incident fluence for which a position of the peak maxima can be clearly distinguished ($0.4 \times 10^{20}$ N/m$^2$). The maximum of desorption is found around 870 K, and the obtained value for the activation energy is $E_{DES}$ = 2.26 ± 0.1 eV.

Comparing the two values with the activation energy for the diffusion on nitrogen in tungsten published in [31] (2.32 ± 0.16 eV) it can be argued that the activation energy obtained for the desorption of the lower incident fluence shows almost a perfect match with the diffusion activation energy reported by Keinonen et a. [31]. This indicates that the hypothesis of a zero order process should be correct. The temperature of the leading edge start should be therefore a better indicator of the temperature at which the release process is activated, as opposed to the position of the peak maximum, whose shift to higher temperatures is stopped only due to nitrogen saturation

In our experiments, the results of nitrogen retention showed a poorer reproducibility of measurements as compared to the cases of deuterium retention (deuterium retention is discussed in the next chapter), with the individual results being described by a wider scattering. Some hypotheses were discussed already in section 4.1, when the figure was presented. It was pointed out that nitrogen might not get completely desorbed during the TPD that runs up to around 1250 – 1300 K; or there could be a memory effect from one measurement to another, if the annealing step performed at the end of the TPD is not effective; additionally, an experimental uncertainty from "overnight – unmanned implantation" ion flux measurement could induce an error in the fluence estimation. An incomplete desorption of nitrogen during a TPD ramp could be possible if nitrogen adsorbs on the surface: indeed the chemisorbed nitrogen is completely desorbed only at temperatures close to 2000 K [80], [81]. The presence of this adsorption state could lead to an apparent

extra nitrogen accumulation if it diffuses or if it is “pushed” into the bulk during a subsequent implantation cycle, where it could be desorbed during a subsequent TPD.

The evolution of trapped nitrogen atoms with storage time in UHV (figure 45) clearly shows that, at ambient temperature nitrogen does not desorb from tungsten. The TPD spectra obtained for different storage time values, after exposure to a fixed incident fluence, presented in figure 44, show no change in peak intensity or in the position of the desorption peak maximum. These findings show that the trapped nitrogen atoms do not diffuse and remain trapped when the sample is stored at room temperature. This is in good agreement with the position of the desorption peak, found at relatively high temperature, which further points out to a high activation energy for the release of nitrogen atoms from their bulk trapping mechanism (which was already discussed to be the formation of WN).

From the study on the surface modifications induced by nitrogen (section 4.3), it is observed that adsorption of deuterium occurs after nitrogen molecular ions ($N_2^+$) exposures. Our interpretation is that when the surface is exposed to $N_2^+$ molecular ions, some oxygen atoms found in the native oxide layer that covers the surface of the sample are removed, creating active sites leading to the dissociative chemisorption of deuterium.

From the TPD quantitative analysis, it is determined that, for the case of sequential implantation of nitrogen and deuterium, which will be presented in Chapter 5, the amount of adsorbed deuterium needs to be taken into account especially at low fluence. This means that, when considering the retained amount of deuterium as a function of the molecular ions fluence, this amount coming from exposure to the molecular deuterium needs to be subtracted. The reason for this precaution comes from the fact that, during molecular ion implantation, the deuterium partial pressure inside impl/TPD chamber is in the order of $10^{-7}$ mbar, and the sample is therefore exposed to both molecular ions and molecules at the same time.

To summarize on the interaction of nitrogen with tungsten, it was concluded that, following ion bombardment, nitrogen is implanted in a relatively small depth represented by the first few nanometers of the sample. When the incident fluence is increased above an incident fluence of $4.5 \times 10^{20}$, retained nitrogen starts to saturate. The implanted nitrogen atoms do not diffuse and they remain trapped in tungsten when the sample is stored at room temperature. The changes of the surface determined by nitrogen ion bombardment were evidenced showing that on this $N_2^+$-modified sample the sticking of other molecules like $D_2$ will be different than on an unmodified tungsten sample.

# Chapter 5
# Sequential implantation of Nitrogen and Deuterium in Tungsten

In the present operational design of ITER [59] three species of gas will be introduced inside the vacuum vessel: deuterium, tritium and possibly nitrogen. In the previous chapters the interaction of deuterium and nitrogen with tungsten were studied separately. This approach revealed the specific ways of interacting with tungsten for each of these two gas species. In this chapter the interaction of tungsten samples with both these gases is investigated.

Nitrogen was chosen to be used for radiating the energy in the divertor region of ITER vacuum vessel [78]. Despite the improvements noticed in plasma performance following nitrogen puffing [36] the presence of nitrogen and hydrogen isotopes (deuterium and tritium) inside the vacuum vessel leads to new issues. The main concern is the production of ammonia which is both a corrosive and an hazardous substance [82][83]. The formation of ammonia, favored by the catalytic effect of the metal walls [84] will affect directly the fuel balance for the fusion reaction and will also lead to issues related to the recovery of tritium [40] following the condensation of ammonia on the cryostat panels [8][9]. Its corrosiveness [82] raises concerns related to the pumping systems [85] and their lifetime shortening due to exposure to ammonia. Finally, extra concerns are added to the retention issues in the first wall material for both nitrogen and the hydrogen isotopes.

These concerns are addressed in this chapter, which presents the synergetic interaction of nitrogen and deuterium with tungsten, in a configuration of sequential implantation with the nitrogen being the first one to be implanted for all the measurements presented here. This sequence of implantation (first nitrogen and then deuterium) was chosen because nitrogen does not desorb at ambient temperature, as it was shown in Chapter 4. This makes easier, for example, to test higher incident fluences of nitrogen by performing implantations on multiple days and without “losing” the implanted amounts. The production of ammonia is also investigated and all the produced amounts are followed for storage time intervals corresponding to both short and long term as defined in previous chapters.

The goals followed in this chapter are first to determine if the retention behavior is changing for either of the two implanted species when they are both implanted and then to

quantify the eventually ammonia produced amounts and finally to investigate the retention and release behavior of ammonia.

In order to address these three issues, namely deuterium retention, nitrogen retention and the storage time dependent production of ammonia, polycrystalline tungsten samples were subjected to cycles of sequential implantation of nitrogen and deuterium followed by thermo-programed desorption (TPD). The mass spectrometer was set-up to record all the possible resulting products in order to count the retained atoms and to determine the ratios of the formed products.

These experiments were performed on two of the ALMT polycrystalline samples (ALMT#4 and ALMT#5). The sample preparation procedure and the mounting were identical as in previous chapters. The polycrystalline tungsten samples were exposed first to a nitrogen molecular ion beam ($N_2^+$), and in the second step they were exposed to a deuterium molecular ion beam ($D_2^+$). For both types of ions the energy was set to 500 eV/molecular ion, an amount that will be shared by the two charged atoms resulting upon dissociation. The angle of incidence was 45° for both cases, and the fluxes, set at around $1 \times 10^{16}$ N/m$^2$s and $1.6 \times 10^{16}$ D/m$^2$s were kept constant for each type of ion implantation.

The electron energy inside the QMS ionizing stage was set to 50 eV, which allowed the counting of all the released products with good signal to noise ratios. Calibrations were performed with the purpose of obtaining the coefficients of conversion from counts per second to molecules per second for the main products of interest: HD, $D_2$, $N_2$ and $ND_3$. These coefficients were determined directly only for $D_2$ and $N_2$ while, for HD and $ND_3$ the coefficient was deduced from relative ionization cross sections, using the ones determined for $D_2$ and $N_2$ and applying corrections related to the ionization cross sections and the transmission through the QMS entrance orifice (see section 2.3.4).

A typical experiment for the sequential implantation of nitrogen and deuterium consists in first bombarding the tungsten sample with nitrogen molecular ions ($N_2^+$), then moving the sample to the load lock and then degassing the ion gun for at least three times to clean the ion source. The sample is then moved back to the impl/TPD chamber and the implantation of deuterium is performed by bombarding with deuterium molecular ions (essentially $D_2^+$). Before performing the TPD ramp for the sample, the heater assembly is degassed with the sample being again placed in load lock. In the final step of the experiment, the sample is moved back on the heater assembly when the heater assembly has cooled down to ambient temperature, and the TPD ramp is performed.

The main parameter that was followed for the experiments presented in this chapter was the storage time in UHV. This way, the evolution of all the released products with the storage time was obtained. These dependencies were determined for two regimes of incident fluence: a low incident fluence regime and a high incident fluence regime. The high incident fluence regime corresponds to an incident fluence of nitrogen that leads almost to nitrogen saturation in the implanted range, at roughly 90% of saturation (see Chapter 4, section 4.1). The low incident fluence regime corresponds to nitrogen fluence below saturation i.e. roughly 30% of saturation. For all the measurements shown in the present chapter, implantations of both species were performed at ambient temperature. The second parameter that was investigated was the incident deuterium fluence, with the focus being on the fluence of deuterium implanted in a nitrogen almost saturated surface.

The study presented in this chapter begins with the comparison between the implantation of a single species of atoms and the sequential implantation of both species. In order to determine the complete picture of nitrogen and deuterium desorption and the significance of extra products to the total retention of each one of the two species, it was necessary to confirm at first that ammonia is indeed produced. Ammonia was counted inside the mass spectrometer by looking at the signal for the m/z = 20, which corresponds to the $ND_3$ product. Finally, the ammonia was investigated in the same manner as deuterium and nitrogen by monitoring how the ammonia amounts evolve with the storage time and by testing different incident deuterium fluences.

### 5.1 Desorbed products

The atomic species available to form desorbing products are: deuterium and nitrogen, as a result of implantation; oxygen as found in the native tungsten oxide from the surface of the sample; and hydrogen found as a natural solute in the sample. In the table below the mass to charge ratio (m/z) for all the possible compounds counted by the mass spectrometer are shown. The table also includes the fragments of the desorbed products.

***Table 2 – Correspondence between mass to charge ratio and possible compounds***

| **m/z:** | **3** | **4** | **14** | **15** | **16** | **17** | **18** | **19** | **20** | **28** |
|---|---|---|---|---|---|---|---|---|---|---|
| | **HD** | **$D_2$** | **N** | **NH** | **ND** | **NDH** | **$ND_2$** | **$ND_2H$** | **$ND_3$** | **$N_2$** |
| | **–** | **–** | **–** | **–** | **NH2** | **$NH_3$** | **$NDH_2$** | **HDO** | **$D_2O$** | **CO** |
| | | | | | | **OH** | **OD** | | | |

Taking into consideration that the raw signals provided by the mass spectrometer need to be converted from number of counts into number of desorbed atoms (or molecules), by using the conversion coefficients as explained in Chapter 2, section 2.3.4, from the table above, it can be noticed that if this conversion procedure is straightforward in the case of individual implantations, it becomes more complex when both nitrogen and deuterium are implanted.

For the individual implantations, the detection of nitrogen can be achieved by recording the signal for $N_2$ (calibrated for the signal recorded as m/z = 14 – see section 2.3.4), while the detection of deuterium can be achieved by recording the signals for HD (m/z = 3) and $D_2$ (m/z = 4).

For the sequential implantations, apart for the products mentioned above, nitrogen and deuterium can be released also as $NH_3$ (m/z = 17), $NDH_2$ (m/z = 18), $ND_2H$ (m/z = 19), and $ND_3$ (m/z = 20). As it can be seen in table 1, for these values of m/z, the signals will also incorporate extra counts recorded due to the presence of other fragments (NDH and OH for m/z = 17 and OD for m/z = 18) which becomes an issue for the quantification of the implanted nitrogen and deuterium atoms. This difficulty is amplified by the fact that no direct calibration is performed for any of these signals, in order to convert them from counts into number of molecules. To avoid inaccurate results, only the signal of $ND_3$ was chosen in order to investigate the release of nitrogen and deuterium as deuterated ammonia, with the necessary mention that the obtained values will represent only the lower limits of these amounts. Nevertheless, the signal for $ND_3$, meaning the m/z = 20 can also be plagued by the presence of $D_2O$. An extra precaution was therefore taken, in order to verify that the trace of m/z = 20 signal can be used for the correct quantification of $ND_3$. This step consists in showing that the presence of a desorption peak for the signal of m/z = 20 is correlated with the release of $ND_3$ and not with the release of $D_2O$, and this is presented in section 5.4.1. For the case of individual implantations, deuterium retention was calculated as the sum of deuterium atoms desorbed as HD and $D_2$, and for nitrogen the retention was determined by counting the atoms released as $N_2$. In the next two sections the retention amounts resulting from the sequential implantation will be quantified by also taking into account the number of deuterium and nitrogen atoms that desorb as $ND_3$. This means that the following m/z signals will be taken into account: m/z = 3, m/z = 4 and m/z = 20 for deuterium; m/z = 14 and m/z = 20 for nitrogen. Even if this procedure will not give the absolute total retention (due to the omitted $NDH_2$ and $ND_2H$), it will give the number of all the atoms that were counted accurately.

In summary, in order to quantify the retention of nitrogen, deuterium and the production of ammonia, the signals for the m/z values were used as follows:

a) for the detection of nitrogen:
    - m/z = 14 was used for the case where only nitrogen was implanted;
    - m/z = 14 and m/z = 20 were used for the case where both nitrogen and deuterium were implanted;
b) for the detection of deuterium:
    - m/z = 3 and m/z = 4 were used for the case where only deuterium was implanted;
    - m/z = 3, m/z = 4, and m/z = 20 were used for the case where both nitrogen and deuterium were implanted;
c) for the detection of deuterated ammonia only the signal for m/z = 20 was used, as explained above; the quantification of $ND_3$ is possible due to the calibration method which relates directly the signal in counts to the corresponding number of molecules reaching the mass spectrometer, without being affected by the production of fragments inside the mass spectrometer.

Before addressing the question of ammonia production, the retention of nitrogen and deuterium, following sequential implantation, are presented in the next two sections. Then, the production of ammonia and its dependencies with various parameters are addressed in the section 5.4.

### 5.2 Nitrogen retention as a function of the storage time and incident fluence

The results for nitrogen retention obtained in the case of the sequential implantation were already shown in Chapter 4, section 4.2 for the study on the evolution of the trapped nitrogen atoms with the storage time, for the two regimes of incident fluence. The fact that those results are obtained from a set of measurements consisting in sequential implantations is clearly stated in Chapter 4. The choice of presenting the results in Chapter 4 was already justified there, firstly due to the lack of a complete set of measurements for nitrogen retention vs. storage time in the case of the individual implantation of nitrogen, and secondly by the insignificant amount of nitrogen that gets desorbed in the form of $ND_3$ as compared to the amount that is detected as $N_2$ (only 1 to 2 % of the implanted nitrogen gets released as $ND_3$). From figure 42 in Chapter 4, it was observed that the deuterium implantation which follows the nitrogen does not increase the number of nitrogen atoms that are present in the sample,

demonstrating that the ion source is well cleaned with our procedure when switching between the two gases (see previous sections in this chapter). Additionally, it can be demonstrated that the deuterium bombardment does not lead to a significant sputtering of the implanted nitrogen, for the incident fluence used here; otherwise we would measure a lower nitrogen retention. Finally, from the figure 42 it can also be argued that the number of nitrogen atoms that get released as $NDH_2$ and $ND_2H$ is not significant as compared to the total number of retained nitrogen atoms, since no significant difference is noticed between the two types of implantation (individual and sequential).

The main observations presented in Chapter 4 that are of interest for the next sections of the present chapter are:

- the small implantation depth of nitrogen on the order of a few nanometers;
- the saturation of the implanted zone at higher incident fluence;
- the lack of nitrogen desorption at ambient temperature;
- the high desorption temperature of implanted nitrogen;
- surface reactivity modifications determined by the nitrogen bombardment.

These observations will constitute the starting point for an attempt of determining how ammonia is produced.

### 5.3 Deuterium retention as a function of the storage time and incident fluence

Deuterium retention in tungsten resulting from the sequential implantation of nitrogen and deuterium was investigated for storage time intervals between 2.5 hours and around 130 hours, for the two regimes of incident fluence mentioned in the introduction of this chapter. The actual values of incident fluence are:

- Low incident fluence regime: $1.23 \times 10^{20}$ N/m$^2$ and $2.81 \times 10^{19}$ D/m$^2$;
- High incident fluence regime: $4.5 \times 10^{20}$ N/m$^2$ and $1.23 \times 10^{20}$ D/m$^2$.

The two regimes were chosen for the following reasons:

- the low incident fluence regime corresponds to the fluence used for many of the deuterium implantations presented in Chapter 3 and for the nitrogen implantations presented in Chapter 4; this allows a direct comparison between the results of the two types of implantation (individual and sequential);
- the high incident fluence regime was focused primarily on being in the saturation zone for the nitrogen implantation, which means a three times higher incident

fluence; the incident fluence of deuterium was also increased around four times, and again, the value was chosen in such a way that it allows a comparison between the individual implantations and the sequential ones.

The results are presented first as the integrated values of deuterium retention for the two regimes of incident fluence obtained for the sequential implantation, together with the corresponding curves obtained after the implantation of deuterium alone. Then, the spectra of desorption for HD and $D_2$ are also presented, for the two different regimes of incident fluence.

Since measurements were performed on two different samples (ALMT#4 and ALMT#5), the similarity between the samples was tested. In figure 47 the TPD spectra for replicate measurements are shown. Both spectra are obtained for sequential implantations of nitrogen ($1.23 \times 10^{20}$ N/m$^2$) and deuterium ($2.81 \times 10^{19}$ D/m$^2$) for a storage time of 2.5 hours. The spectra are an average of 3 to 4 individual spectra and they show the release of deuterium in the form of HD and $D_2$.

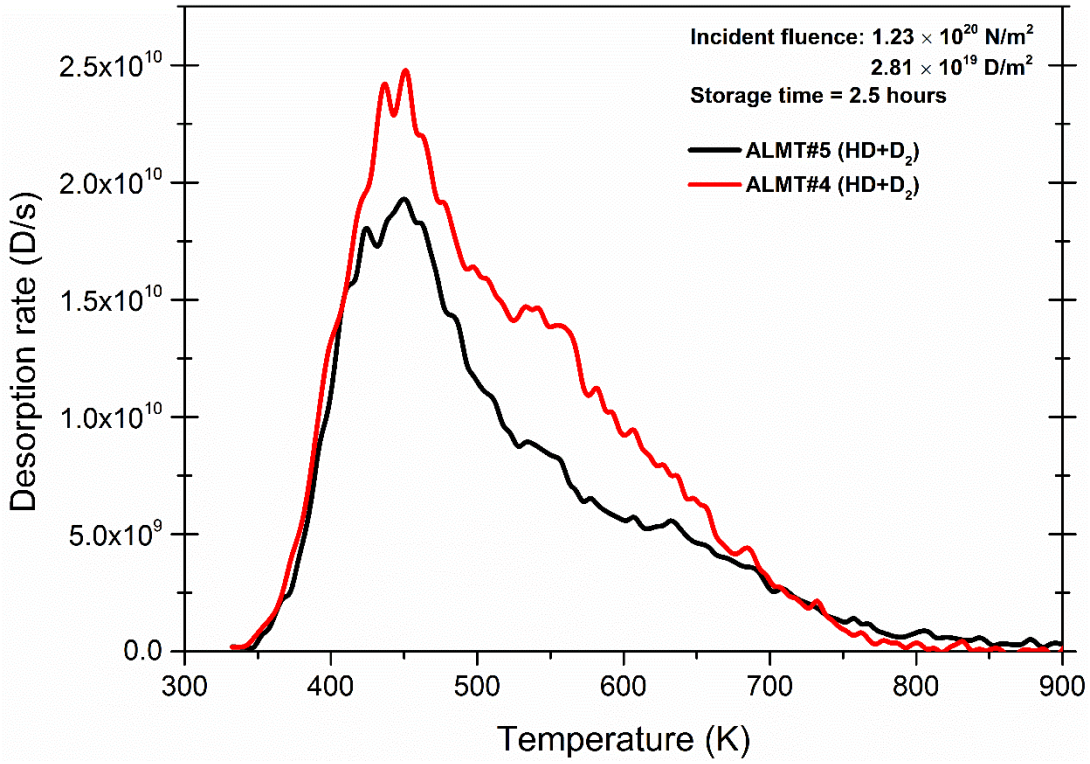


***Figure 47 – Comparison between ALMT#4 and ALMT#5; the two samples show similar behavior of deuterium desorption following the sequential implantation of nitrogen and deuterium***

The two spectra look similar regarding the shape, position and intensity of the desorption peak. It can be noticed, nevertheless, that the integrated intensity of the two desorption peaks is not identical, with the ALMT#4 sample showing a slightly higher deuterium retention. The difference between the integrated values of the two peaks is roughly 22%. This observation is

consistent with the typical sample-to-sample differences shown in Chapter 3, where the dependency of retention with fluence was presented. Usually, the difference in retention between two samples was noticed to vary within a factor of two. Therefore, it can be considered that the comparison from the above figure shows a good similarity between the two samples. This test was performed as a result of the sample ALMT#4 getting accidentally cracked at the end of the set of measurements for the lower fluence range. Since it was not possible to get results for the higher fluence range on the same sample as for the lower fluence range, this comparison insures that the two samples are similar and thus their results can be used together to interpret the results.

In figure 48 the evolution of deuterium retention with the storage time is shown for the sequential implantation of nitrogen and deuterium, at low incident fluence, and for the implantation of deuterium alone. The deuterium incident fluence for these curves is $2.81 \times 10^{19}$ D/m$^2$ and the incident fluence of nitrogen for the sequential implantation is $1.23 \times 10^{20}$ D/m$^2$. All the points are obtained on the same sample, namely ALMT#4. Each point is an average of at least three measurements except for the longest storage time (138 hours) for which only two measurements were performed. What the figure shows in fact is the way nitrogen implantation modifies the behavior of deuterium retention, when nitrogen is being implanted first.

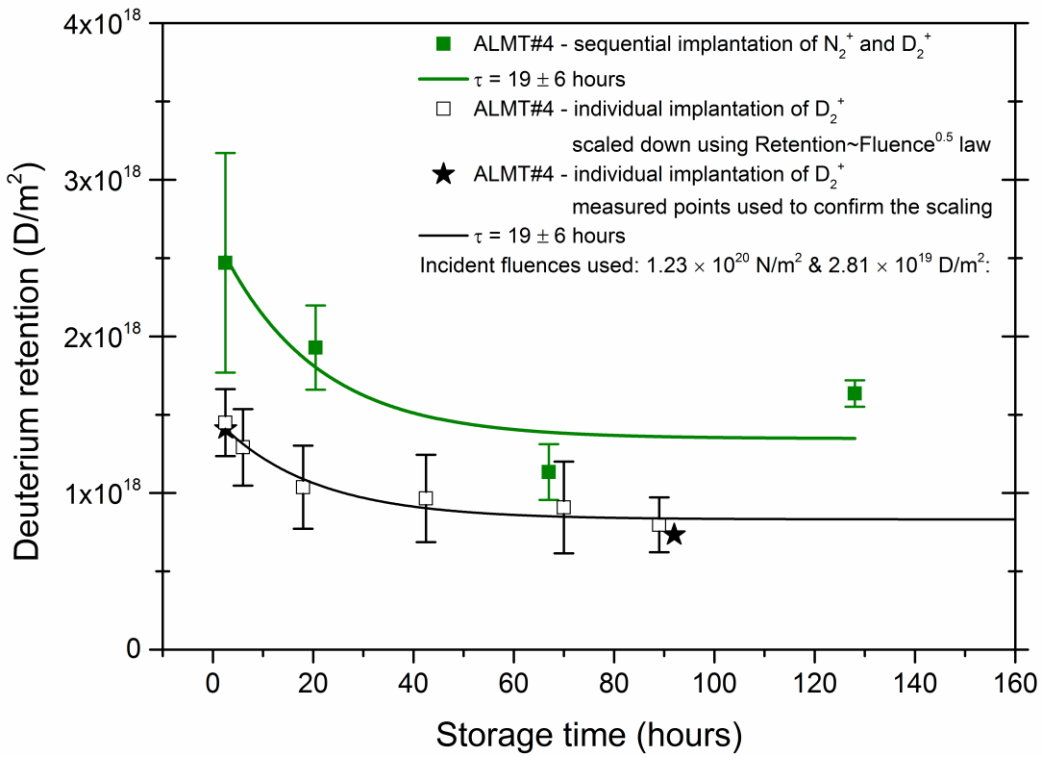


***Figure 48 – Storage time evolution of deuterium following sequential implantation of nitrogen and deuterium (ALMT#4) compared to the storage time evolution of deuterium following implantation of deuterium alone (average on multiple samples); lower incident fluence regime***

It is noticed that the previously implanted nitrogen leads to an increase of deuterium retention for all the measurements, meaning for both short term and long term retention. Regarding the evolution of the retained atoms with the storage time, the curve shows the same behavior noticed for the case of the individual implantation of deuterium. For the short term, retention decreases exponentially in the first 20 to 40 hours after implantation and the long term retention is characterized by a constant level of retention for storage times of around 60 hours after implantation and above.

For the higher incident fluence regime, the incident fluence of deuterium is $1.23 \times 10^{20}$ D/m$^2$ and the incident fluence of nitrogen is $4.5 \times 10^{20}$ N/m$^2$. In this case, nitrogen is first implanted up to saturation, and then deuterium is implanted in a sample which should consist of both W and N with similar ratios, as discussed in Chapter 4. The storage time evolution of deuterium retention with the storage time after sequential implantation of nitrogen and deuterium is compared in figure 49 with the corresponding curve obtained after the implantation of $D_2^+$ alone (already shown in Chapter 4). Each point on the curve obtained for the sequential implantation is an average of at least two measurements. The number of measurements was limited by the long duration of implantation necessary for reaching the desired nitrogen incident fluence. The two set of data are obtained on two different samples:

ALMT#4 for the implantation of $D_2^+$ and ALMT#5 for the sequential implantation. For the sequential implantation measurements, the retention coming from dissociated $D_2$ molecules is subtracted.

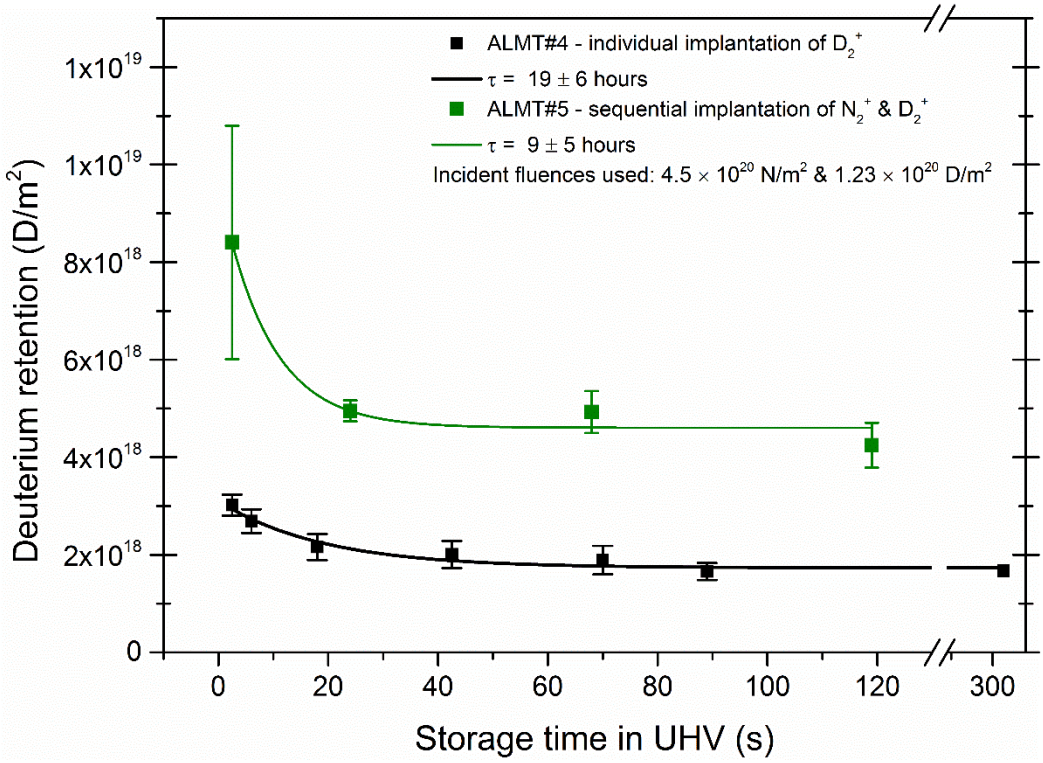


***Figure 49 – Storage time evolution of deuterium following sequential implantation of nitrogen and deuterium (ALMT#5) compared to the storage time evolution of deuterium following implantation of deuterium alone (ALMT#4); higher incident fluence regime***

For the case where the sample was previously implanted with nitrogen up to the saturation in the implantation range, it is noticed that the amounts of deuterium that remains trapped in the sample are significantly increased by the presence of nitrogen. However, the short term retention shows the same exponential decay behavior as for the implantation of $D_2^+$ only. The long term retention also shows a constant amount of deuterium that remains trapped above a storage time of around 50 to 60 hours.

The desorption spectra for deuterium in the form of HD and $D_2$, obtained after the sequential implantation of nitrogen and deuterium are presented in figure 50 for the two regimes of incident fluence (figure 50.a – low incident fluence; figure 50.b – high incident fluence). The spectra are presented for all the storage time intervals that were tested, which fall between 2.5 hours and 138.5 hours. For the low incident fluence case every spectrum is an average of at least three replicate measurements, except the one for the longest storage time which is an average of only two replicate measurements. For the high incident fluence

case the spectra all result from an average of two replicate measurements. Better statistics were not pursued in this case due to the long duration of implantation necessary to reach the desired incident fluence for nitrogen.

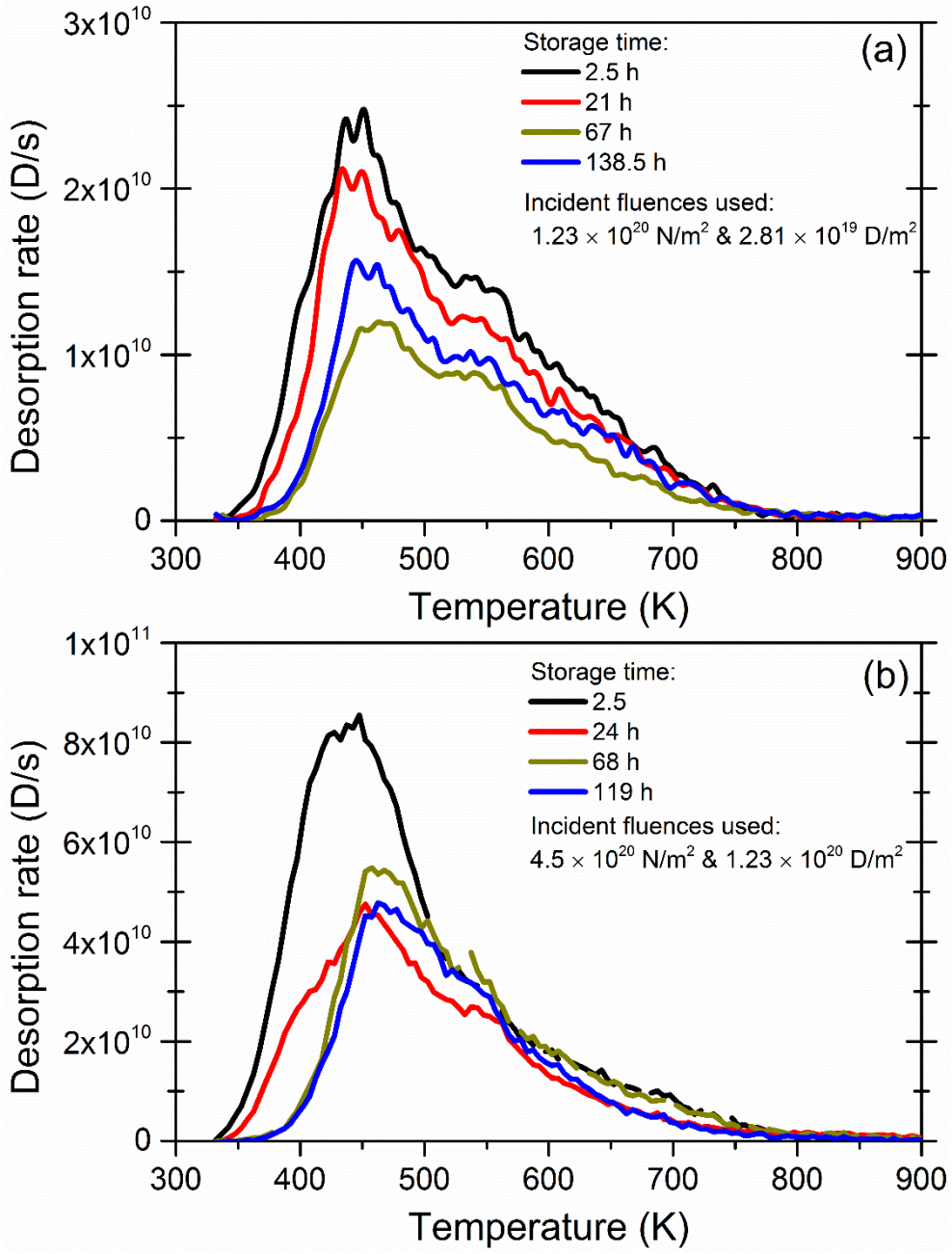


***Figure 50 – TPD spectra for deuterium (signals of HD and $D_2$) obtained for the sequential implantation of nitrogen and deuterium. The spectra are shown for all the storage times tested and for both regimes of incident fluence***

The spectra show one peak of desorption for both regimes of incident fluence, similar to the case of the implantation of $D_2^+$ only. The peaks are asymmetric with a steep increasing tail and a longer decreasing tail. For both cases, the trend is that the maximum of the peak shifts towards higher temperatures when the storage time is increased. This shift is up to 30 K

between the minimum storage time case of 2.5 hours and the longest storage time tested in each case. The evolution of the two tails of the peak is similar to the one observed and described in Chapter 3, for the implantation of $D_2^+$ only, with the leading edge shifting to higher temperature and with the decreasing tail showing a slight decrease but no shift.

### 5.3.1 Analysis and interpretation

In this section deuterium retention in tungsten was investigated for the case of the sequential implantation of nitrogen and deuterium, by counting the released atoms in the form of HD and $D_2$ molecules. The purpose is to see how the presence of nitrogen influences deuterium retention for both the short term and the long term, as compared to the case of the individual implantation of deuterium.

The nitrogen incident fluence was shown to induce modifications on the surface of the sample (see Chapter 4) and it was shown to be a connection between the oxide layer from the surface and deuterium retention (see Chapter 3). As a starting point, these two observations have led to the question whether the nitrogen implantation will result in a change of the exponential behavior for the short term deuterium retention. To fully test this idea, the sequential implantation was performed in the two regimes of fluence with nitrogen being at the saturation level and also below. The main purpose was to verify whether these two situations would provide different results for the behavior of the short term deuterium retention. The long term retention was also studied as a function of the incident fluence.

From the curves obtained for the storage time evolution of the trapped deuterium, following sequential implantations, it is noticed that the exponential decaying behavior is present for both regimes of incident fluence. In both cases deuterium retention is increased by the presence of previously implanted nitrogen. For the lower incident fluence regime, retention is increased by around 1.5 times when nitrogen is previously implanted in the sample. For the high incident fluence regime the increase is more significant being 2.5 times higher than the case of the individual implantation of deuterium. For both cases, the retention coming from dissociated $D_2$ molecules (see Chapter 4) is subtracted for the shown values. The increase noticed in both cases could be explained in different ways as discussed below.

The first idea would be that nitrogen acts as a diffusion barrier for deuterium, as reasoned by Gao et. al in [38]. In [38] nevertheless, this effect is noticed for implantations at 500 K but is not at ambient temperature. This explanation is not applicable in our experimental configuration since there is no change in the exponential behavior of the short term retention and since nitrogen as a diffusion barrier between the bulk and the surface will

result exactly in a change of this behavior. If deuterium desorption would be delayed by the presence of nitrogen (N) and tungsten nitride (WN), the time constant for the storage time evolution should become significantly higher. This is clearly not the case here.

A second possibility that could be invoked to explain the increased deuterium retention would be a change of the reflection coefficient for deuterium implantation on a surface formed of both W and WN. If this would be the case, fewer atoms would be reflected in the case of WN and the number of actual implanted atoms would be higher for a certain value of incident fluence. A slight decrease of the reflection coefficient for the case of deuterium implantation in a nitrogen pre-implanted tungsten surface is found by simulation obtained using the SRIM software [86], and it should also be anticipated simply as resulting from the mass change of the surface atoms that is "seen" by the incident molecular ions. When a deuterium molecular ion hits at 45º a WN surface instead of a W surface, it hits a wall with a smaller averaged mass; therefore the average scattering angle should change, leading to more atoms getting implanted and less atoms reflected.

A third possible explanation, as discussed in [37] is the enhancement of deuterium diffusion into the bulk, when nitrogen is found in close to the surface layers. This diffusion enhacement would lead to a higher deuterium retention for the sequential implantation case, for similar incident fluence as for the individual implantation.

These two later ideas are actually complementary and together could explain well the increase of deuterium retention. The lower reflection coefficient for deuterium results in a higher number of atoms that get implanted during bombardment for the sequential case. It also means that the density of deuterium atoms in the bulk is higher during the bombardment step favoring the enhancement of a diffusion to higher depths in the bulk. The combined effect is therefore a more important higher total retention.

The TPD spectra support this conclusion by showing very similar characteristics to the ones obtained for the implantation of deuterium alone. This suggests that there is no extra trapping mechanism that contributes to deuterium retention and could justify the extra retained amounts. In this section, for the TPD spectra, the release of deuterium was pictured using only the signals of HD and $D_2$, in order to compare them with the spectra obtained for the implantation of deuterium alone. If the m/z = 20 signal is incorporated into the desorption curve, the amount of desorption shows a slight increase in intensity, but no change in shape or position. This is illustrated in the figure below:

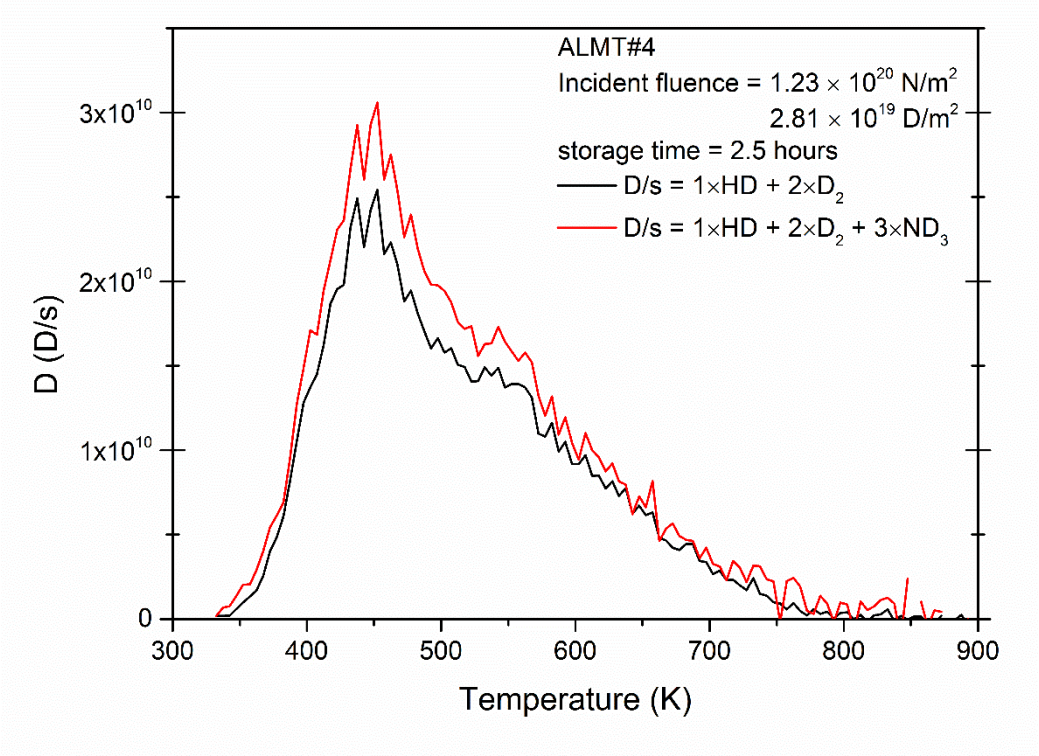


***Figure 51 – TPD spectra for deuterium release with and without incorporating the m/z = 20 signal (atoms released as $ND_3$)***

However, for the calculation of the total retention, these amounts were included, in order to better account for all the deuterium retained. The amounts released as m/z = 20 are also investigated separately in the next sections dedicated to the study of ammonia.

## 5.4 Ammonia production

One of the main purposes of the experiments presented in this chapter is to investigate the production of ammonia for the case where the tungsten sample is exposed to both nitrogen and deuterium. If ammonia is shown to be present, it will then be quantified and its evolution as a function of different parameters will be analyzed.

This section will present firstly how the production of ammonia is evidenced. Secondly, I will show the evolution of ammonia production as a function of storage time and the incident fluence of nitrogen and deuterium. In a final step, all these results will be used to investigate the physical processes that lead to ammonia formation.

### 5.4.1 Attributing the m/z = 20 signal to $ND_3$

As stated before, due to the type of species that are implanted in the sample, the presence of ammonia is monitored by recording the QMS signal corresponding to m/z = 20. This mass to charge ratio corresponds to the signal that will be detected when deuterated

ammonia ($ND_3$) will be formed. The m/z = 17 which corresponds to $NH_3$ should be way less significant in showing the presence of ammonia compared to the signal of $ND_3$ since we implant deuterium and not hydrogen. At the same time, any eventual signal arising from $NH_3$ will be superimposed with the signal from the NDH fragment, and will reduce the accuracy in the results for m/z = 17.

As it can be seen in table 2, the mass to charge ratio used to detect $ND_3$ also corresponds to the detection of $D_2O$. It is necessary then to examine whether the signal recorded as m/z = 20 corresponds to $ND_3$, $D_2O$ or to both of them. In previous set of measurements it was observed that for both m/z = 19 and m/z = 20 there are no peaks of desorption following deuterium implantation. Nevertheless, in the present case nitrogen is implanted before deuterium, and as it was shown in Chapter 3, nitrogen implantation modifies the state of the surface. It is necessary therefore to verify that no peak of desorption is observed when deuterated ammonia is not produced. The method used in order to evidence that the peak of desorption observed for the signal of m/z = 20 corresponds to ammonia production consists in performing a series of controlled experiments with different combinations of the implantation (or exposure) steps. The sample was exposed to different combination of $N_2$, $D_2$, $N_2^+$, $D_2^+$ as both sequential or individual implantations, and the presence of a desorption peak for the signal of m/z = 20 was examined. These measurements are shown in table 3, in chronological order:

***Table 3: Chronological order of measurements used in order to show that the peak of desorption noticed for the signal of m/z = 20 corresponds to the release of $ND_3$ and not $D_2O$***

| 1 | Type of exposure | Presence of desorption peak for m/z = 20 |
|---|---|---|
| 2 | $D_2^+$ | no peak of desorption |
| 3 | $D_2$ | no peak of desorption |
| 4 | $N_2$ | no peak of desorption |
| 5 | $N_2$ followed by $D_2$ | no peak of desorption |
| 6 | $D_2^+$ | no peak of desorption |
| 7 | $D_2$ | no peak of desorption |
| 8 | $N_2$ | no peak of desorption |
| 9 | $N_2$ followed by $D_2$ | no peak of desorption |
| 10 | $N_2^+$ | no peak of desorption |
| 11 | $D_2$ | no peak of desorption |
| 12 | $N_2$ | no peak of desorption |
| 13 | $N_2$ followed by $D_2$ | no peak of desorption |
| 14 | $N_2^+$ | no peak of desorption |
| 15 | $D_2^+$ | peak of desorption is present |
| 16 | $D_2$ | no peak of desorption |
| 17 | $N_2$ | no peak of desorption |
| 18 | $N_2$ followed by $D_2$ | no peak of desorption |
| 19 | $N_2^+$ followed by $D_2$ | no peak of desorption |
| 20 | $N_2^+$ followed by $D_2^+$ | peak of desorption is present |
| 21 | $N_2^+$ followed by $D_2^+$ | peak of desorption is present |
| 22 | $N_2^+$ followed by $D_2$ | no peak of desorption |
| 23 | $D_2$ | no peak of desorption |
| 24 | $N_2$ | no peak of desorption |
| 25 | $N_2$ followed by $D_2$ | no peak of desorption |

It is observed that a peak of desorption for the signal of m/z = 20 is present only when the sample is exposed to both nitrogen and deuterium and only when they are in the form of molecular ions (lines 20 and 21). The only other case where we notice a small peak of desorption for m/z = 20 is on the line 15. This line is preceded by an implantation of $N_2^+$. Two suggestions can be provided in order to infer the presence of the desorption peak for this measurement: nitrogen might not have been fully removed from the sample during the previous TPD step, as it was also suggested in Chapter 4, where the higher scattering of

nitrogen retention values was discussed; the second possibility comes from verifying the lab book where it is noticed that the ion gun was degassed three times before proceeding with the implantation of deuterium, unfortunately in front of the sample still mounted on the heater assembly, suggesting that the contamination of the surface with nitrogen ions has occurred during the ion source degassing. Usually, the ion gun is degassed three times before switching between the implanted species, but always with the sample being located in the load-lock chamber.

For the case of $N_2^+$ followed by $D_2$ no peak of desorption is observed. It was shown in Chapter 4 that this configuration, deuterium sticks to the surface. The absence of the peak in this case suggests that, even though there is a certain amount of deuterium available on the surface none of it gets released as $ND_3$ or as $D_2O$. This observation together with the lack of a peak of desorption for m/z = 20 after implanting $D_2^+$ alone, strongly refute the idea of the desorption peak resulting from $D_2O$. Therefore, by taking into account the observations from table 3, it is demonstrated that the signal recorded at m/z=20 can be used to detect the desorption of $ND_3$, with no detectable contribution arising from $D_2O$ for this signal.

### 5.4.2 Storage time evolution of the produced ammonia

The amount of ammonia, produced as a result of the sequential implantation of nitrogen and deuterium, was investigated by performing the TPD step after different storage times. This type of measurement was performed for both regimes of incident fluence. The results are first shown as TPD spectra for the two regimes of fluence and then the integrated values are shown.

Before showing the TPD results, the baseline subtraction method is presented (figure 52), in order to explain the higher noise towards the end of the temperature ramp (this explanation concerns figures 53 and 54). In order to show that this noise comes indeed from the baseline subtraction procedure, in the figure below a signal of m/z = 20 is plotted for both the raw signal and for the curve with the baseline being subtracted. The data comes from one of the measurements from the dataset presented further in figure 53.

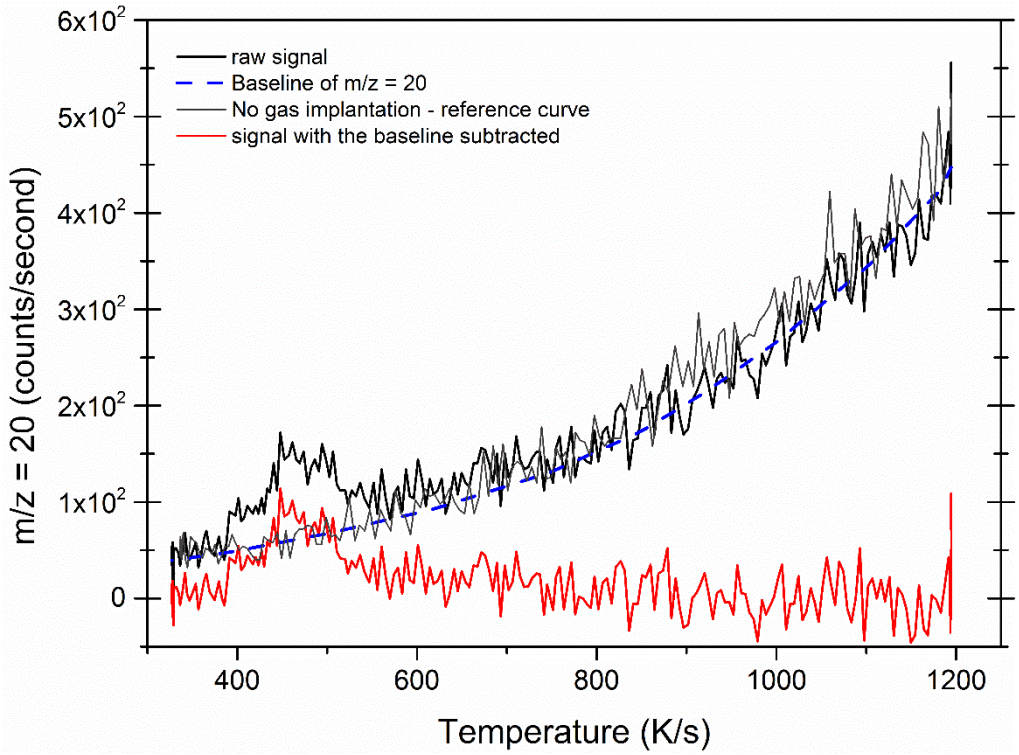


***Figure 52 – The method used for the subtraction of the baseline from the m/z = 20 signal. The figure shows a reference signal (grey curve), a raw signal (black curve), the baseline (dashed blue curve) that is constructed for the raw signal by taking into account the shape of the reference curve, and the final result for the signal after the baseline is subtracted (red curve)***

The uprising trend observed for the signal obtained for a sequential implantation is similar with the one of a reference curve for m/z = 20 (obtained without any ion implantation - a reference curve is plotted in gray in the above figure). Therefore, this increasing trend comes solely from the increase of the background. This increase of the background leads to a higher noise to signal ratio, at higher temperature during the TPD. When the baseline subtraction is performed, this higher noise in the signal towards higher temperatures results in a higher noise on the baseline-subtracted curve.

The TPD spectra obtained for the low incident fluence regime are shown in figure 53, for the desorption of deuterated ammonia ($ND_3$). These curves were obtained on sample ALMT#4.

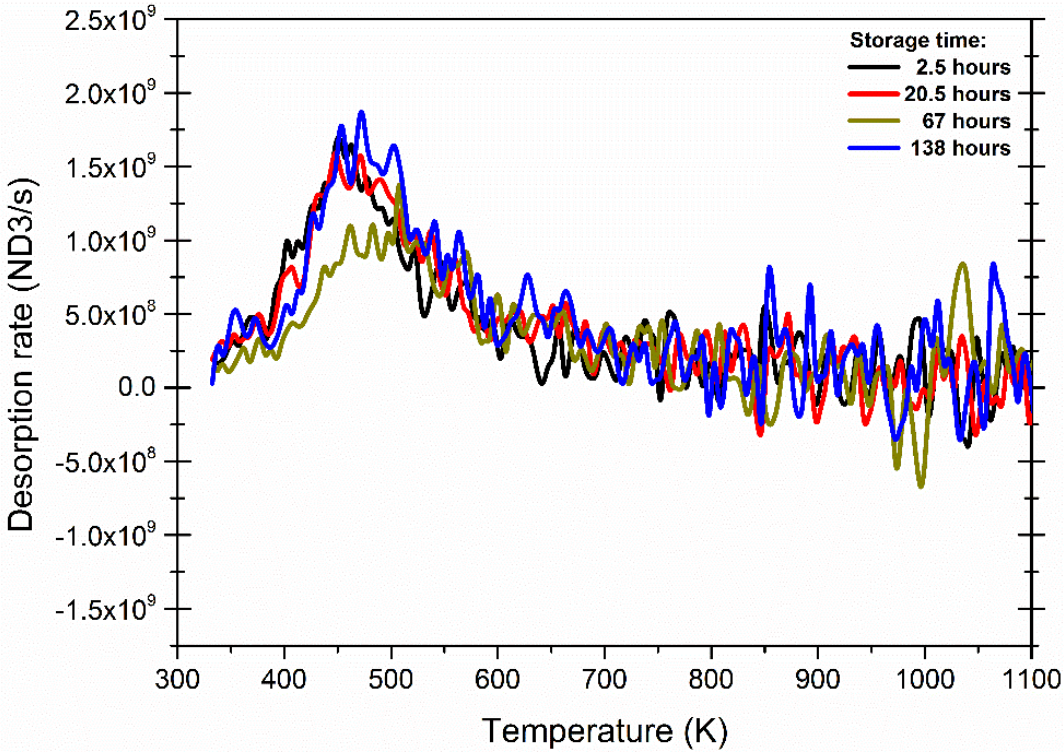


***Figure 53 – TPD spectra of deuterated ammonia ($ND_3$) obtained after different storage times; lower incident fluence regime; Incident fluence: 1.23 × $10^{20}$ N/$m^2$ followed by 2.81× $10^{19}$ D/$m^2$ Sample: ALMT#4***

The curves of ammonia desorption from tungsten are characterized by a single peak of desorption which has a position and width similar to the peak of desorption of deuterium. From the intensity of the peaks for the four storage times tested it is noticed that they look similar, except for the one at 67 hours storage time. The same issue was noticed for the spectra of nitrogen released as $N_2$ obtained in the same set of measurements (the nitrogen desorption and the smaller intensity for the spectra at 68 hours are discussed in Chapter 4). Just like there, if we consider that there was a problem with the data obtained for the storage time = 67 hours, we see that the amount of desorbed ammonia does not change with the storage time.

The curves, for the ammonia desorption after the sequential implantation of nitrogen and deuterium in the higher regime of incident fluence, are shown in figure 54. These results were obtained on sample ALMT#5. Since there were less individual measurements performed for each storage time, the curves are characterized by a lower signal to noise ratio. The number of individual measurements was limited because of the long durations of implantation needed in order to reach the desired fluences, especially for the nitrogen implantation.

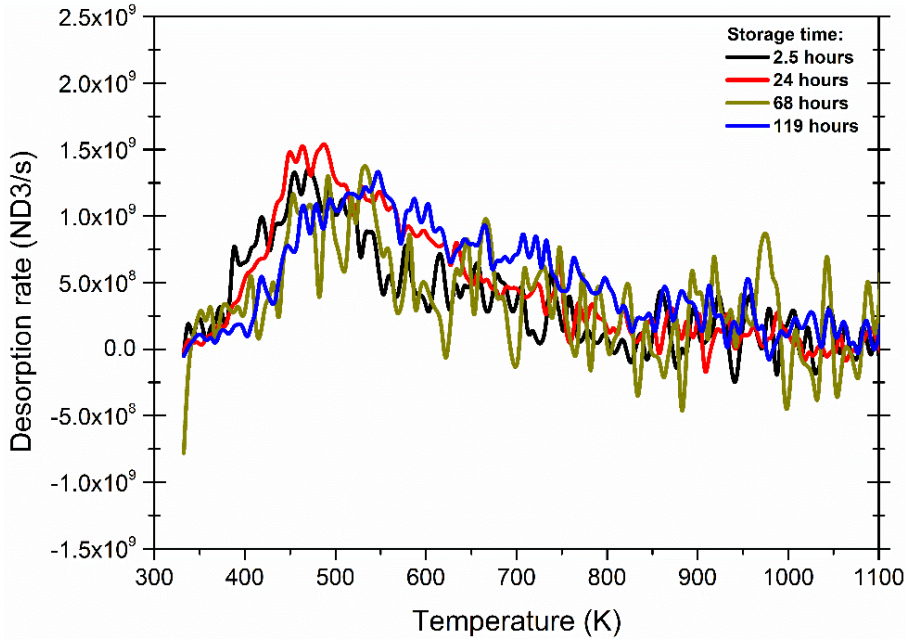


***Figure 54 – TPD spectra of deuterated ammonia ($ND_3$) obtained after different storage times; higher incident fluence regime; Incident fluence: 4.5 × $10^{20}$ N/$m^2$ followed by 1.23 × $10^{20}$ D/$m^2$; Sample: ALMT#5***

The spectra look similar to those of the low incident fluence regime. In this case as well, the intensity of the desorption peak seems to remain constant when storage time is increased. An average of the curves is performed for each regime of incident fluence, and the two desorption spectra that are obtained are shown in figure 55.

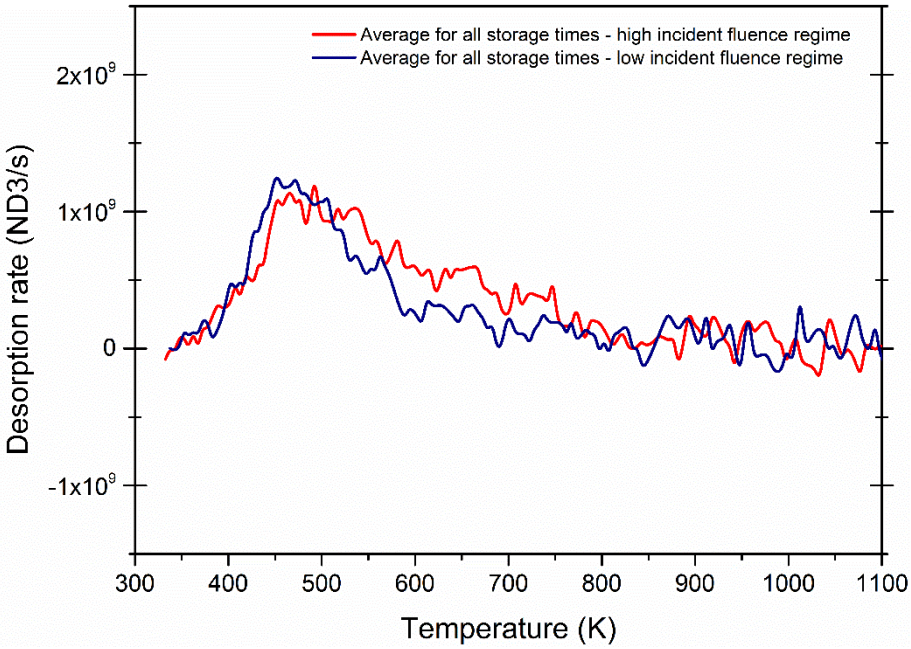


***Figure 55 – Averaged spectra of deuterated ammonia ($ND_3$) for the two regimes of incident fluence; lower incident fluence regime: 1.23 × $10^{20}$ N/$m^2$ followed by 2.81× $10^{19}$ D/$m^2$ – ALMT#4; higher regime of incident fluence: 4.5 × $10^{20}$ N/$m^2$ followed by 1.23 × $10^{20}$ D/$m^2$ – ALMT#5***

The two curves look very similar, with the one obtained for the higher fluences appearing to show a slightly higher retention (the difference is noticed on the temperature interval 500 – 800 K). In order to decide whether this difference is significant, the two curves are zoomed on the 500 – 800 K temperature interval, and the standard deviation of the mean of the desorption rate in each temperature bin (5 K intervals) is indicated:

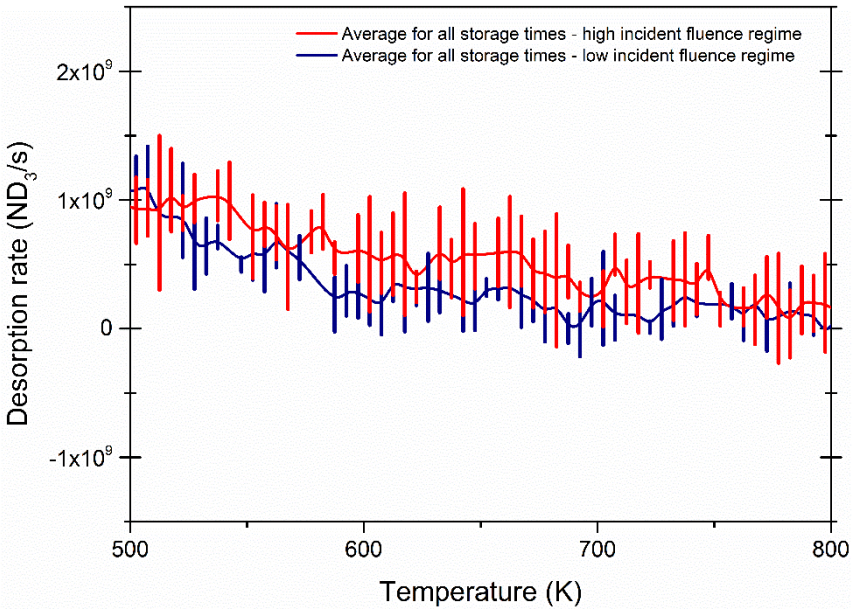


***Figure 56 - Zoom on the TPD spectra presented in the previous figure (figure 52)***

With the standard deviation bars superimposed to the plotted curves, it can be readily deduced that the apparent difference between the two curves is not significant. Therefore, the amounts of ammonia being produced for the two regimes of incident fluence tested are concluded to be very similar. This can be verified another way, by integration of these spectra and comparing the total number of $ND_3$ molecules for the two regimes of incident fluence.

The integrated values are shown in figure 57 as ammonia retention vs. the storage time (solid points). The two regimes of incident fluence are plotted on the same graph for comparison. Similar to the TPD spectra, the points obtained for each regime of incident fluence were averaged and are plotted as dotted lines in figure 57. Since more replicate measurements were performed for the low incident fluence regime, the corresponding data points are described with better statistics as compared to the high incident fluence regime.

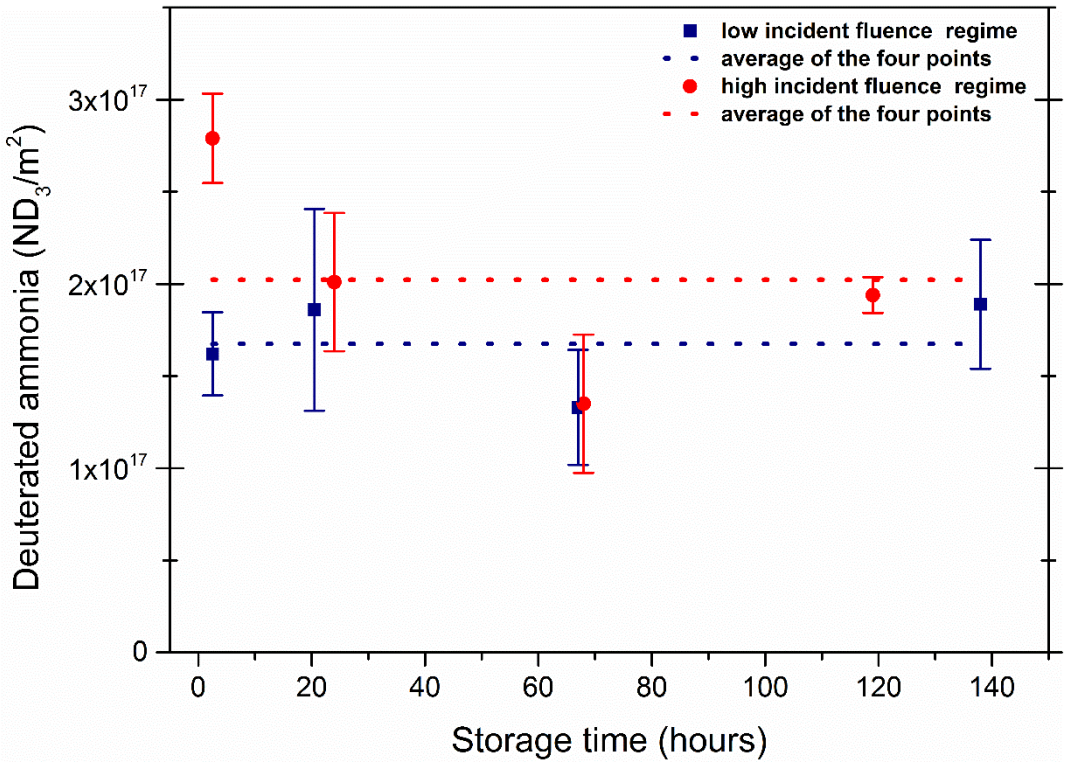


***Figure 57 – Amounts of detected ammonia after different storage time intervals; low incident fluence regime: 1.23 × $10^{20}$ N/$m^2$ followed by 2.81× $10^{19}$ D/$m^2$ – ALMT#4; high incident fluence regime: 4.5 × $10^{20}$ N/$m^2$ followed by 1.23 × $10^{20}$ D/$m^2$ – ALMT#5***

For the case of the lower incident fluence, it is clear that the amount of produced ammonia is constant for all the values of the storage time. In the case of the high incident fluence regime, the points show a scattering similar to the one noticed for nitrogen retention (shown in Chapter 4) and they are situated slightly above the ones obtained for the low incident fluence regime. An average value is also provided as the red dotted line, but the point for the shorter storage time (2.5 hours) shows a higher value. Nevertheless, taking into account the vertical bars, which in this case represent the standard deviation of the mean, it is suggested that the amount of produced ammonia for the two regimes of incident fluence varies very slightly. In order to rigorously conclude on this observation, improved statistics would be necessary but is not available for the present thesis. However, these observations suggest that ammonia production might suffer saturation when the incident fluence of the implanted deuterium is increased. This hypothesis is investigated in the next section.

### 5.4.3 The effect of the incident deuterium fluence on ammonia production

In order to investigate how the amounts of formed ammonia depend on the incident deuterium fluence, sequential implantations of nitrogen and deuterium were performed as follows: the incident fluence of nitrogen was kept constant at 4.5 × $10^{20}$ N/$m^2$, while only the

incident fluence of deuterium was varied. This configuration was chosen in order to have a close to saturation amount of implanted nitrogen, which will serve as a source for ammonia production, and which will be constant for each of the measurements. For deuterium, the incident fluence was varied from 2.81 × $10^{19}$ D/$m^2$ up to 4.5 × $10^{20}$ D/$m^2$. The amounts of produced ammonia, in this configuration, are presented below. Each point is an average of two or three individual measurements, except the highest fluence which represents a single measurement. These results were obtained on sample ALMT#5.

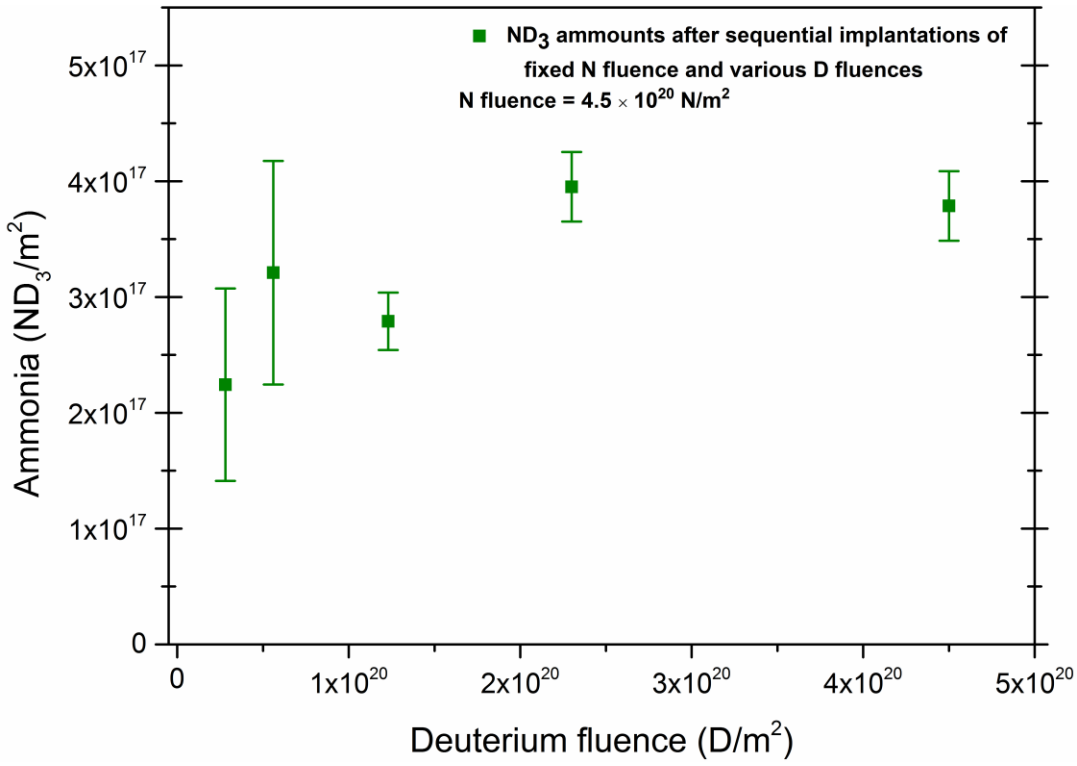


***Figure 58 – Ammonia produced amounts as a function of the incident fluence of deuterium; nitrogen incident fluence is fixed at 4.5 × $10^{20}$ N/$m^2$; Sample ALMT#5***

The amount of produced ammonia quickly saturates when the incident fluence of deuterium is increased. It is observed that saturation is already reached for conditions identical to the ones of the higher regime of incident fluence discussed previously (third point in this figure).

### 5.4.4 Ammonia formation process

From all the obtained results it is possible to reason on the physical process that leads to the formation of ammonia. The starting point for this is the similarity between the peaks of desorption for ammonia and deuterium. These two peaks have similar positions in temperature and similar widths. A second observation that can be used is the fact that the amount of detected ammonia remains constant with the storage time. The only case where this

is not a sure fact is for the minimum storage time data for the higher regime of incident fluence. To illustrate the similarities between the peaks, the spectra for deuterium release as $HD+D_2$ and for the deuterium released as ammonia ($ND_3$) are plotted on the same graph in figure 59. Both curves of desorption correspond to a storage time of 2.5 hours and are obtained on sample ALMT#4 for the low regime of incident fluence.

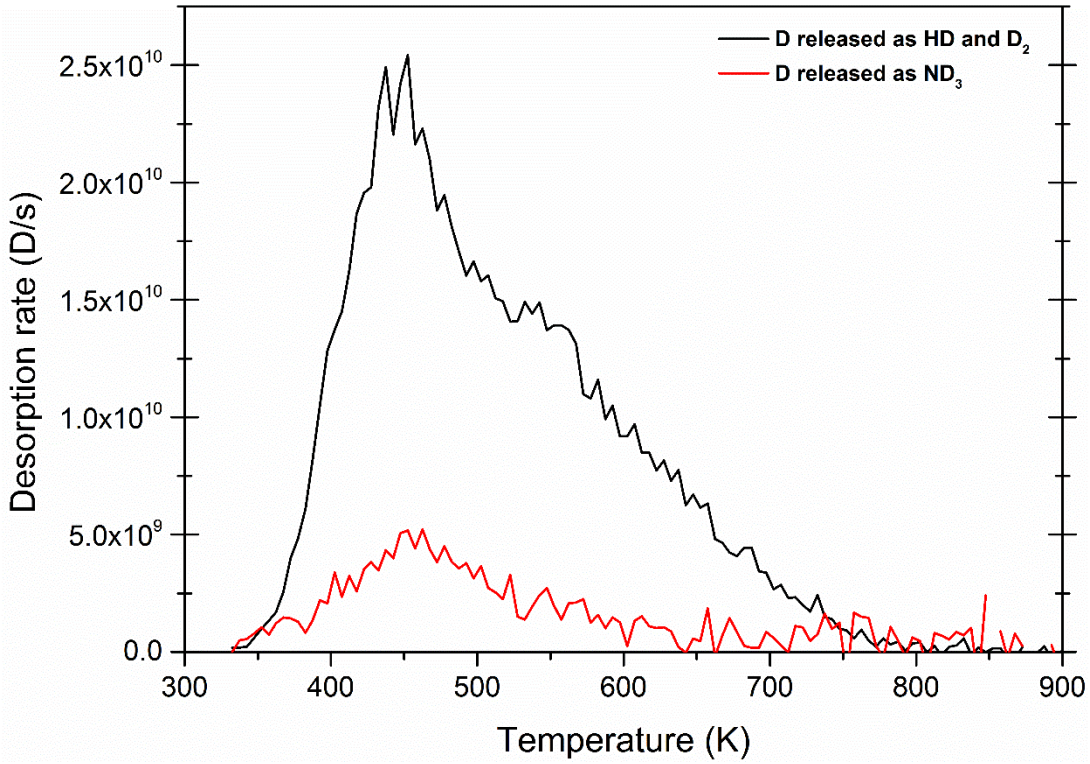


***Figure 59 – Comparison between the curve of desorption for $ND_3$ and the curve of desorption for D (released as HD and $D_2$); Incident fluence: $1.23 \times 10^{20} N/m^2$ followed by $2.81 \times 10^{19}$ $D/m^2$ Sample: ALMT#4***

It is noticed that the peak of ammonia has the same position, and similar shape and width as compared to the peak of desorption for deuterium. This observation suggests a connection between the formation of ammonia and the release of deuterium from the bulk. As it was shown in Chapter 4, the position of the peak for nitrogen desorption is situated at a higher temperature than the one for deuterium and ammonia. This raises the question from where does come the nitrogen that contributes to ammonia formation. In order to answer this question, a new experiment was designed, as follows:

- nitrogen was implanted first for sufficiently high incident fluence to reach saturation;
- in the second step deuterium was implanted for an incident fluence sufficiently high to lead to ammonia saturation as well;

- an incomplete TPD was performed up to a fixed temperature (800 K) below the temperature at which nitrogen would start to desorb. During this step, ammonia and deuterium are desorbed;
- with nitrogen still in the sample, a new implantation of deuterium was performed followed by an incomplete TPD ramp up to the same temperature as above. This step was performed twice;
- in the final step, a new deuterium implantation was performed followed by a complete TPD ramp, desorbing all nitrogen from the sample.

This type of experiment was performed for two combinations of incident fluence. The amount of ammonia that was detected in this manner, for each time a TPD ramp was performed (incomplete or complete) is shown in figure 60. For the determination of the error bars, the highest value of the standard deviation from the mean, obtained for the high regime of incident fluence in section 5.4.2 was used. Additionally, the error induced by the baseline subtraction step was included by taking into account the typical variation of the retained amounts, obtained for a single measurement, when the integration procedure is repeated more than once (the procedure is presented in Chapter 2, section 2.4).

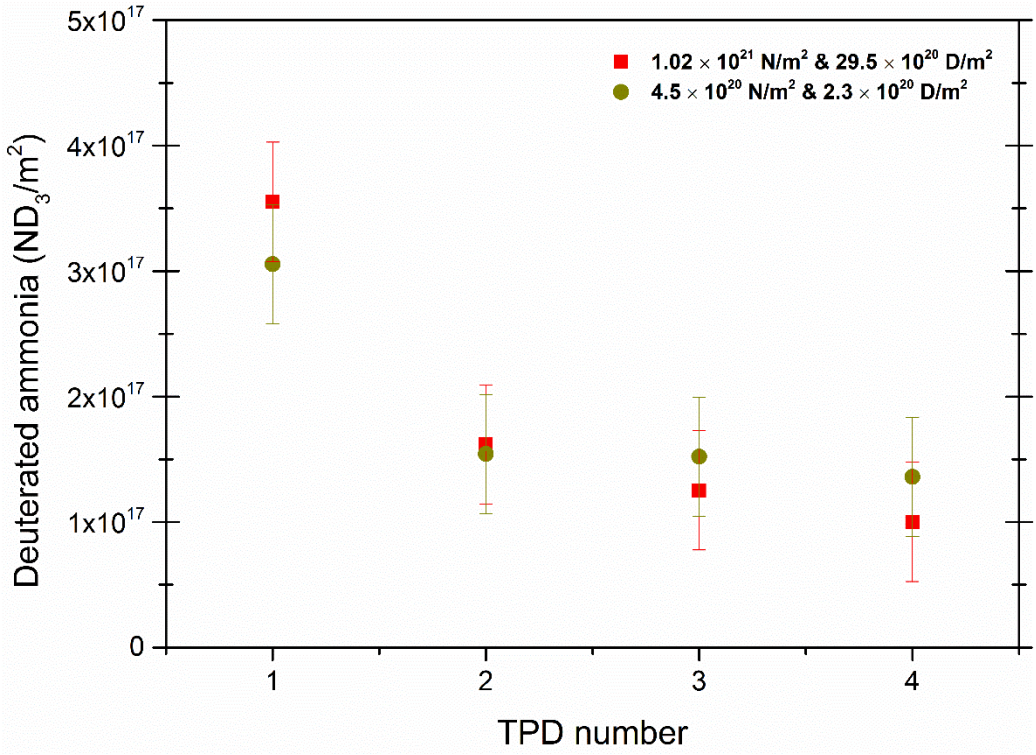


***Figure 60 – Investigation of the available nitrogen depletion to form ammonia; Sample: ALMT#5***

It is observed that, even though no extra nitrogen is implanted, for every new deuterium implantation a certain amount of ammonia is produced. The noticed trend consists in a decrease of this amount when more implantation-TPD cycles are performed. When error bars are taken into consideration, the amounts of ammonia produced during the two experiments are very similar and they also decrease in a similar manner. This decrease, noticed for both experiments, points towards a fast depletion of the available nitrogen for the formation of ammonia when the sample is heated up to 800 K.

### 5.4.5 Analysis and interpretation

Performing sequential implantations of nitrogen and deuterium in tungsten has as a main goal the investigation of ammonia production. The amount of produced ammonia is quantified and then, the evolution of this amount is followed as a function of different parameters.

With the signal of m/z = 20 being correlated to $ND_3$ in Table 3, and with the calibration procedure presented in the section 2.3.4, it is possible to determine the amount of produced ammonia and to follow how this amount evolves with the storage time in UHV and with the incident fluence. From these results it is further possible to determine how much of the trapped nitrogen and deuterium will be released in the form of $ND_3$. The evolution of all the trapped nitrogen atoms is monitored by taking into account the release as $N_2$ and as $ND_3$, and similarly, the evolution of all the trapped deuterium atoms is followed by taking into account the release as HD, $D_2$ and $ND_3$.

From the results available it is also desired to hypothesize on the mechanisms at the origin of ammonia production and ammonia release during TPD.

Following the exposure of the polycrystalline tungsten sample to the sequential implantation of nitrogen and deuterium, the number of produced ammonia molecules is comprised between $1 \times 10^{17}$ and $3 \times 10^{17}$ $ND_3/m^2$. For the case of the low incident fluence regime the amount of detected ammonia is constant for all values of the storage time, and its average value is found to be around $1.7 \times 10^{17}$ $ND_3/m^2$. At higher incident fluences, from the available measurements it is not clear whether there is a significant decrease between the value recorded at 2.5 hours storage time and the following data points. The ammonia amounts detected for the data obtained at longer storage time decreases by only 28% compared to the amount detected for a 2.5 hours storage time. Since statistics are poor for this set of measurements, and since the analysis on the TPD spectra suggested that the amount of ammonia detected is similar independently of the storage time, it should be safe enough to

consider that the amount of ammonia produced in the case of the high regime of incident fluence also remains constant with the storage time, similar to the low regime of incident fluence. More measurements are needed in order to clarify if there is an evolution of ammonia amounts with the storage time and also how significant is the difference between the amounts detected for each regime of incident fluence.

In figure 60 it was shown that the number of nitrogen atoms that act as a source for ammonia production (about $8 \times 10^{17}$ N/m$^2$) gets depleted rapidly after only a small number of deuterium implantation-TPD cycles. However, the number of nitrogen atoms that are still present in the sample during each of these implantation-TPD cycles is at least a 40 times higher than the number of nitrogen atoms desorbed as ammonia, since nitrogen was implanted up to saturation ($3.55 \pm 0.99 \times 10^{19}$ N/m$^2$) and the TPD temperature ramps are stopped before the desorption of nitrogen occurs. This observation suggests that the source of ammonia production is well accounted by the nitrogen atoms found on the topmost layer of the sample surface. This idea is consistent with the rather constant amount of produced ammonia, observed in figure 57 in section 5.4.2 and with the observation of the ammonia saturation noticed in figure 58.

The fact that the detected ammonia remains constant for the longer storage times indicates that the nitrogen atoms from the surface, i.e. the source for ammonia formation, does not decrease nor get depleted during storage at ambient temperature. This is consistent with the absence of storage time dependency of nitrogen retention as shown in Chapter 4. However, in Chapter 3 it was shown that deuterium suffers a dynamic release from the sample, and a certain number of deuterium atoms will be desorbed in the first few tens of hours (the short term retention). The orders of magnitude for the short term deuterium retention and the detected ammonia amounts are very similar, meaning that they incorporate similar numbers of deuterium atoms. Still, the dynamic release of deuterium atoms does not decrease the detected amounts of ammonia, meaning that it does not engage a significant number of the close-to-surface nitrogen atoms which were suggested as the source (reservoir) for ammonia formation. Therefore, the following hypothesis is proposed: ammonia formation takes place only during the TPD ramp, it consumes the nitrogen from/close to the surface, and it is a process activated at a temperature slightly higher than the ambient temperature. This higher temperature also leads to the activation of the release from the bulk process of trapped deuterium atoms (released from grain boundaries – the long term deuterium retention, as explained in Chapter 3).

To conclude on the quantity of nitrogen and deuterium is released in the form of ammonia, the composition of the ammonia molecule ($ND_3$) has to be taken into account, meaning that for a detected molecule one nitrogen atom and three deuterium atoms will be counted.

It is found that for the low incident fluence regime, where nitrogen is not saturated in the implanted zone, around 15 to 30 % of the total deuterium is released in the form of $ND_3$. This percentage is smaller for shorter storage time and it increases when the storage time is increased. But this change is solely the result of the dynamic release of deuterium (it is the HD + $D_2$ component that is decreasing while the detected $ND_3$ remains constant). From the total number of nitrogen atoms that are trapped in the sample, the atoms released as $ND_3$ account for a percentage between 1.5 and 2 %.

For the higher regime of incident fluence, where nitrogen is closer to saturation in the implantation zone (90% of saturation), the deuterium atoms released in the form of $ND_3$ account for 8 to 10 % of the total number of retained deuterium atoms. This smaller percentage is the result of a more significant increase for the HD + $D_2$ component, while the $ND_3$ remains roughly the same. From the total number of the retained nitrogen atoms, less than 1% is released as $ND_3$.

The percentages of deuterium atoms and nitrogen atoms released as $ND_3$ (presented in the two previous paragraphs) are plotted in figure 61 for the various storage times tested:

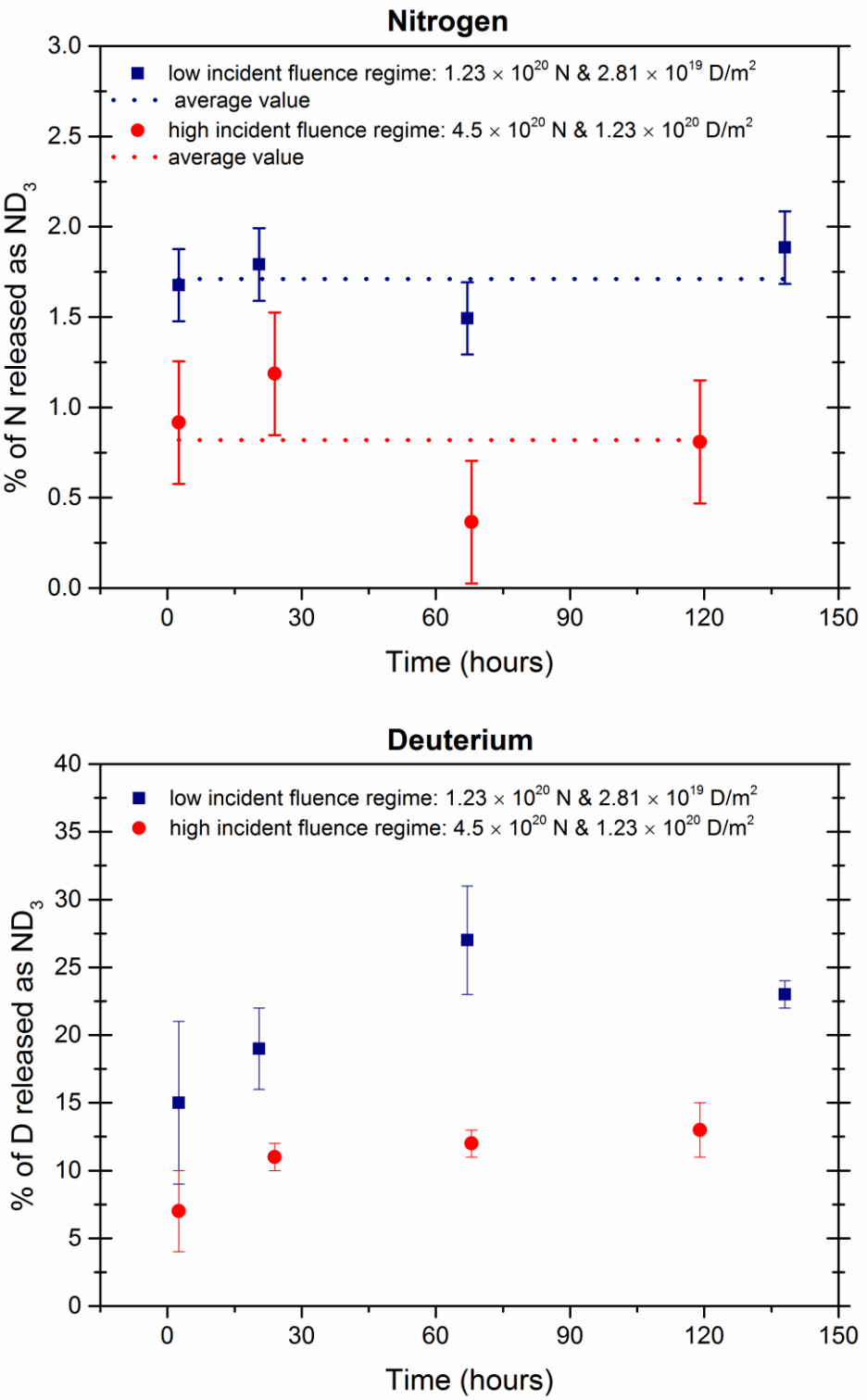


***Figure 61 – The percentage of atoms (nitrogen and deuterium) that get released as deuterated ammonia ($ND_3$) as a function of the storage time; both regimes of fluence shown; low incident fluence regime results are obtained on sample ALMT#4; high incident fluence regime results are obtained on sample ALMT#5***

Similarly, it will be shown how the percentages of nitrogen and deuterium atoms released as $ND_3$ will vary with the fluence. For this case, the experiment presented in section 5.4.3 will be used; therefore this dependency will be discussed only for the variation of deuterium incident fluence.

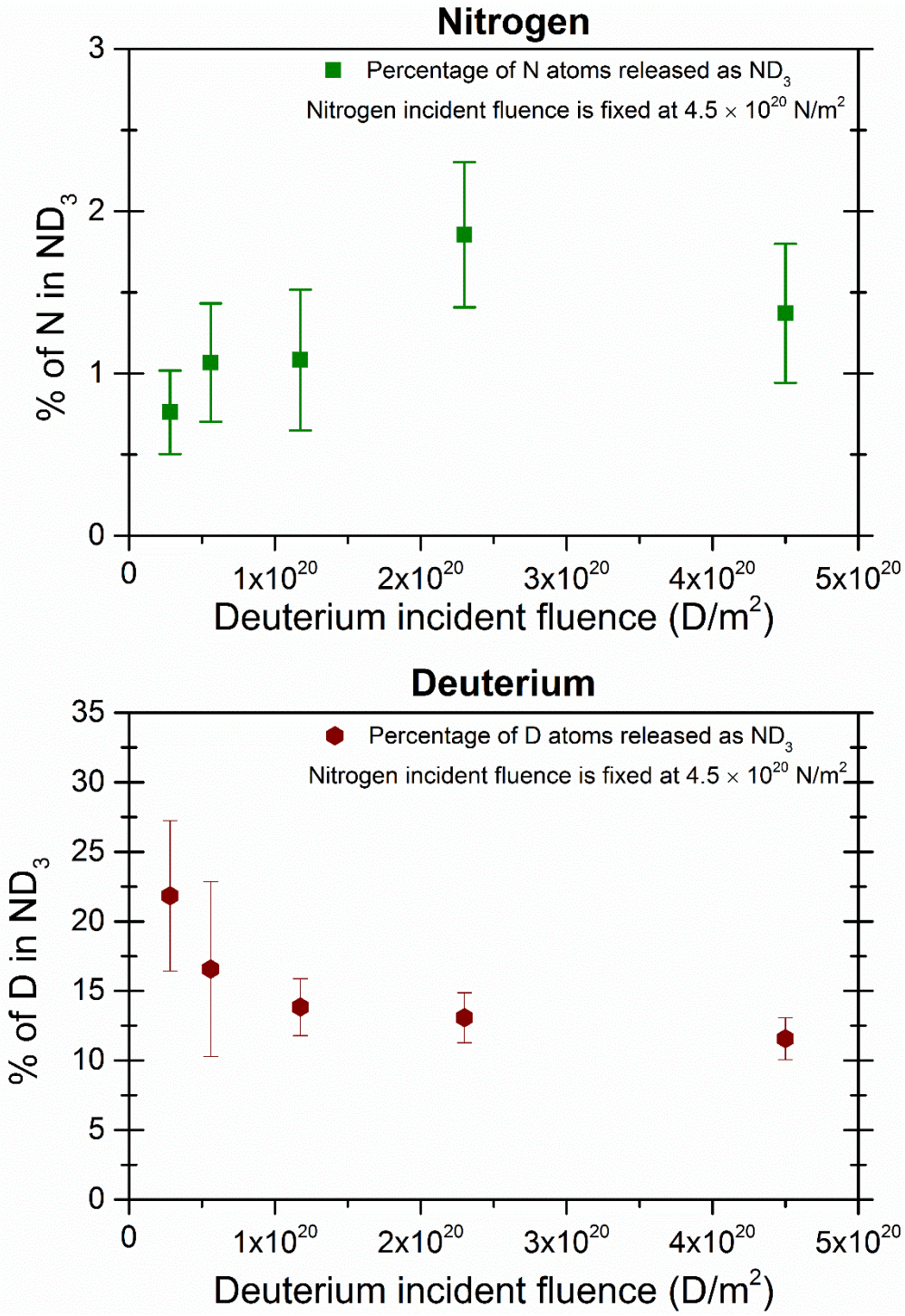


***Figure 62 – The percentage of atoms (nitrogen and deuterium) that get released as deuterated ammonia (ND3) as a function of the incident fluence of deuterium; the incident fluence of nitrogen is fixed at 4.5 × $10^{20}$ N/m$^2$; results obtained on sample ALMT#5***

The percentage of nitrogen varies in good agreement with the values shown in the previous figure, from around 1% at lower fluence and increasing to not more than 2% at higher fluences. The percentage of deuterium released as $ND_3$ is higher for smaller incident fluences and decreases when the fluence is increased. This is consistent with the saturation of ammonia

for these values of fluence, meaning that the $ND_3$ component is constant but the HD + $D_2$ component is increasing with the incident fluence.

As average values, the total number of detected $ND_3$ molecules is found to be between $1.5 \times 10^{17}$ and $2.6 \times 10^{17}$ $ND_3/m^2$ for the two regimes of incident fluence. From figure 58 it can be seen that, for high nitrogen fluence and lower deuterium fluence, that ammonia is not yet saturated. Therefore, a close to saturation nitrogen coverage is not a sufficient condition for the saturation of ammonia production. It could be that the deuterium fluence also needs to be high enough for the ammonia saturation to be achieved. But, when the typical retention of deuterium (counted as HD and $D_2$) is compared to the amount of produced ammonia, it is observed that the HD+$D_2$ component is at least a few times higher than the $ND_3$ component. In this configuration, there would be enough atoms in the bulk available for the formation of ammonia all the way to saturation (i.e. engaging most of the available nitrogen atoms from the surface). This could show that during implantation some of the deuterium atoms will already attach to nitrogen atoms forming $ND_x$ products, and this number will depend of course on the incident fluence. Then, during TPD, the atoms released from the bulk will contribute to form a complete $ND_3$ molecule that will be desorbed. When the deuterium fluence is low (discussion is for figure 58), less $ND_x$ compounds are available and therefore less ammonia is formed. This reasoning is consistent with the lack of ammonia production when nitrogen implantation is followed by deuterium leaking ($N_2^+$ followed by $D_2$), where deuterium sticking is observed but no ammonia is formed: either no $ND_x$ were formed during/due to deuterium leaking, or the number of "sticked" deuterium atoms is too small to form complete $ND_3$ molecules.

To summarize, the formation of ammonia was investigated for two regimes of incident fluence. Even though these two regimes are described in this chapter as low vs. high regime, in fact both incident fluence regimes are relatively small compared to the particle loads expected in ITER [87]. It was deduced nevertheless, that the production of ammonia is limited by the number of nitrogen atoms found on the topmost layer of the sample, i.e. the nitrogen surface coverage. Therefore the total amount of ammonia formed inside a given reactor depends less on the fluences and more on the available tungsten surface area onto which the nitrogen can be stored as a reservoir for ammonia production. The results obtained in this chapter offer a valuable insight on how ammonia is produced and on its behavior related to different parameters. As a perspective to this chapter, the amount of produced ammonia needs

to be investigated for the other materials used as a first wall inside the ITER vacuum vessel, i.e. beryllium and 316L stainless steel.

# Chapter 6

# Conclusions and perspectives

This thesis presented the results of gas/surface experiments focused on the interaction of nitrogen and deuterium ions with tungsten solids. The experimental set-up used ion beams with low flux densities and probed their interactions with tungsten at low incident fluences, as compared to the literature. The outcomes of the individual interactions were followed by measuring gas retention, meaning the number of atoms remaining trapped inside the metal sample, and gas release with the Temperature Programmed Desorption (TPD) technique. Synergetic interactions originating from sequential implantation of nitrogen and deuterium were additionally studied and allowed to evidencing and quantifying the production of deuterated ammonia products.

The experiments were presented in three steps, by investigating first the gas/surface interaction for the case of individual implantation, for deuterium in tungsten in Chapter 3, and for nitrogen in tungsten in Chapter 4, and then moving on to the sequential implantation of both species, in Chapter 5.

The main questions that received an answer from these experiments are:

1. How significant is deuterium retention in tungsten, what are the trapping mechanisms for deuterium retention, and what happens with the retained deuterium for the short and long term storage time?
2. How significant is nitrogen retention in tungsten, what are the trapping mechanisms for nitrogen retention, what happens with the trapped nitrogen atoms for the short and the long term storage time, and lastly, does nitrogen bombardment affect the surface reactivity in a significant manner?
3. What changes are introduced when the two species are sequentially implanted in tungsten? How do retention values change for both species, are there any new types of trapping mechanisms that appear for any of the species, is there any change in the evolution of retention with the storage time for the two species?

4. Is there any ammonia production for the sequential implantation case? In the affirmative, how significant is this amount, how does it changes when species incident fluence is varied, how does it evolve with the storage time and how does ammonia form?

The answers to these questions will be presented in the following section and provide useful insight for the phenomena that will take place in the divertor area of ITER. Possible directions for the continuation of this work will also be suggested in the perspectives section.

### 6.1 Conclusions

For the study of **deuterium retention in tungsten presented in Chapter 3**, an extensive number of parameters were investigated. The implantations were performed in both polycrystalline and single crystal tungsten samples, at various implantation temperatures, and with a special focus on the evolution of the retained atoms with the storage time. The retention was shown to be of two types: a short term retention described by an exponential decay with a time constant of roughly half a day at room temperature; a long term retention which is described by a constant amount of trapped atoms that does not change (i.e. the retained atoms do not desorb at 300 K) for storage times as long as 330 hours at room temperature. The dependency of retention with incident fluence was shown to follow a squared root law, consistent with a diffusion limited retention, and no saturation was observed.

An extensive analysis was performed in order to determine the trapping mechanisms for deuterium in tungsten and their contribution for the two types of retention (short and long term). It was shown that the decaying behavior specific to the short term retention is related to the diffusion of deuterium atoms through the native oxide layer found on the surface of the sample. The long term retention was shown to be related to the trapping in vacancies and the oxide layer for the single crystal tungsten, while for the polycrystalline tungsten samples, the most significant contribution (for the long term retention) is related to trapping in grain boundaries.

The study of **nitrogen retention in tungsten presented in Chapter 4** was focused on the interaction of nitrogen with polycrystalline tungsten samples, for implantations performed at ambient temperature.

The number of retained atoms (retention) was shown to have a quick increase as the incident fluence is increased, but only up to a certain value, after which retention starts to

saturate. The regime of saturation was determined to be completely achieved for an incident fluence of around $7.5 \times 10^{20}$ N/m$^2$ and corresponding to a nitrogen retention of $3.55 \pm 0.99 \times 10^{19}$ N/m$^2$.

The trapping mechanism for nitrogen retention in tungsten, which was known from the literature to be the formation of tungsten nitride WN, was found to be consistent with the experimental results obtained in this thesis. Therefore, the reasons for reaching saturation are the small implantation depth combined with the low diffusivity of nitrogen in tungsten, and the fact that nitrogen remains trapped only as tungsten nitride WN. The retained amounts of nitrogen were found to remain constant for all durations of storage tested (up to 140 hours) .

The surface changes induced by the nitrogen bombardment were also evidenced, and the way they affect the deuterium sticking on the sample was quantified. These changes were followed in the perspective of detecting ammonia and determining the way ammonia is formed.

In **Chapter 5,** the study of **the sequential implantation of nitrogen and deuterium in tungsten** allowed to obtain results that can be relevant for the divertor area of ITER.

Implantations were performed only in polycrystalline tungsten samples, at ambient temperatures, with the focus being set on the evolution of retention for the various released products (deuterium, nitrogen, and deuterated ammonia).

The retention of nitrogen and deuterium following sequential implantation was investigated and compared with the values obtained for the individual implantation cases. No loss/erosion of the implanted nitrogen was observed in the investigated fluence range. In contrast, the retention of deuterium was higher for the sequential implantation case as a result of the near surface chemical modifications. Nevertheless, from the analysis of deuterium retention as a function of the storage time, it is found that the trapping mechanisms responsible for deuterium retention do not change. The same exponential decay is observed for the short term retention and, similarly, a constant number of deuterium atoms remain trapped on the long term. These observations remained valid even when the incident fluence of nitrogen was increased in such a way that nitrogen would be close to saturation.

As one of the main goals of the chapter, it was proven that the implantation of nitrogen and deuterium leads to the production of deuterated ammonia from the tungsten surface. The amounts of formed ammonia were investigated in relation with the saturation level of nitrogen in tungsten, by using two regimes of fluence: a regime of low nitrogen incident fluence (about 1/3 of saturation) and a regime of high incident fluence (about 90 % of saturation). Despite

the increase of the nitrogen incident fluence, the amount of produced ammonia did not show a significant change. It was hypothesized that ammonia gets formed solely at the tungsten surface and thus depends on the number of nitrogen atoms found close to the topmost layer of the tungsten surface. This hypothesis was validated in a series of experiments where the depletion of the available nitrogen for ammonia formation was found to be much faster than the evolution of the quantity of nitrogen available throughout the surface and bulk. This result makes our study performed at "unrealistic fluences" to be fully relevant for "realistic" ITER conditions.

The duration of storage was observed not to affect in a significant way the ammonia production. This result is consistent with what was learned about the evolution of trapped nitrogen and deuterium atoms with the storage time, for a polycrystalline sample. Firstly, the nitrogen atoms will not be desorbed from the sample at ambient temperature, meaning that the nitrogen surface coverage remains available over time for ammonia production. Secondly, the source of deuterium atoms that will be available for ammonia formation are the atoms that are trapped in grain boundaries. This surprising result was rationalized by stressing that it is not specifically an effect of grain boundaries. Instead, I interpret this results as a manifestation of the thermally activated mechanism for the creation of a $ND_3$ molecules from $ND_x$ precursors on the tungsten surface.

### 6.2 Perspectives

The experiments presented in this thesis were performed in the context of the construction of ITER and DEMO. Even though the fluences and flux densities used here are far below those that are expected in the divertor area of ITER, these results should be useful for extrapolation by keeping into account the research published on similar topics but in conditions closer to what is expected in ITER. The best applicability of the results presented in this thesis is related to the development of wall models, which aim to simulate the interaction of plasma with plasma facing materials. It was already mentioned in Chapter 3 that the observation presented here were successfully used for constructing a Macroscopic Rate Equations model of tungsten plasma facing materials, as presented in our latest joint article published in 2017 [18].

There are still many parameters that could be investigated for each of the studies presented in the three chapters with experimental results (3, 4 and 5): the implantation temperature for the nitrogen implantation and for the sequential implantations; the use of single crystal tungsten samples with other surface termination; switching the order of the

sequential implantation as well as trying to perform simultaneous implantations of nitrogen and deuterium.

The most intriguing perspectives are related to the results presented in Chapter 3, where the native oxide layer was shown to play an important role in deuterium retention. Further studies on this topic could be performed by using techniques/methods which were not available for this thesis, allowing a fine control of the sample structural quality and chemical composition. More to the point, the results and interpretation described in Chapter 3 could be verified by controlling two parameters: the thickness of the oxide layer from the surface of the tungsten and the density of vacancies in a single crystal sample. With these two possibilities at hand, experiments could be envisaged in order to clearly attribute the two type of retention (short and long term) to their exact trapping mechanisms.

# Bibliography


[1] “Worldometer.info.” [Online]. Available: http://worldometer.info/. [Accessed: 11-Aug-2017].

[2] A. . Fallis, “The 2015 revision, Key findings and advance tables,” 9, 2015.

[3] “International Energy Outlook 2016-World energy demand and economc outlook - Energy Information Administration.” [Online]. Available: https://www.eia.gov/outlooks/ieo/world.php. [Accessed: 11-Aug-2017].

[4] “Climate change evidence: How do we know?,” *Climate Change: Vital Signs of the Planet*. [Online]. Available: https://climate.nasa.gov/evidence. [Accessed: 11-Aug-2017].

[5] M. Carlowicz, “World of Change: Global Temperatures : Feature Articles,” 09-Dec-2010. [Online]. Available: https://earthobservatory.nasa.gov/Features/WorldOfChange/decadaltemp.php. [Accessed: 11-Aug-2017].

[6] “Fifth Assessment Report - Climate Change 2013.” [Online]. Available: http://www.ipcc.ch/report/ar5/wg1/. [Accessed: 11-Aug-2017].

[7] Anonymous, “2050 low-carbon economy,” *Climate Action - European Commission*, 23-Nov-2016. [Online]. Available: https://ec.europa.eu/clima/policies/strategies/2050_en. [Accessed: 11-Aug-2017].

[8] “Hans Bethe - Facts.” [Online]. Available: http://www.nobelprize.org/nobel_prizes/physics/laureates/1967/bethe-facts.html. [Accessed: 11-Aug-2017].

[9] M. Kikuchi, K. Lackner, and M.-Q. Tran, *Fusion physics*. Vienna: International Atomic Energy Agency, 2012.

[10] H. Takatsu, “ITER project and fusion technology,” *Nucl. Fusion*, vol. 51, no. 9, p. 094002, Sep. 2011.

[11] “ITER - the way to new energy,” *ITER*. [Online]. Available: http://www.iter.org. [Accessed: 11-Sep-2017].

[12] J. Roth *et al.*, “Recent analysis of key plasma wall interactions issues for ITER,” *J. Nucl. Mater.*, vol. 390–391, pp. 1–9, Jun. 2009.

[13] K. Dobes, P. Naderer, N. Lachaud, C. Eisenmenger-Sittner, and F. Aumayr, “Sputtering of tungsten by $N^+$ and $N_2^+$ ions: investigations of molecular effects,” *Phys. Scr.*, vol. T145, p. 014017, Dec. 2011.

[14] N. Fernandez, Y. Ferro, and D. Kato, “Hydrogen diffusion and vacancies formation in tungsten: Density Functional Theory calculations and statistical models,” *Acta Mater.*, vol. 94, pp. 307–318, Aug. 2015.

[15] W. Xiao and W. T. Geng, “Role of grain boundary and dislocation loop in H blistering in W: A density functional theory assessment,” *J. Nucl. Mater.*, vol. 430, no. 1–3, pp. 132–136, Nov. 2012.

[16] R. Bisson *et al.*, “Dynamic fuel retention in tokamak wall materials: An in situ laboratory study of deuterium release from polycrystalline tungsten at room temperature,” *J. Nucl. Mater.*, vol. 467, pp. 432–438, Dec. 2015.

[17] R. Frauenfelder, “Solution and Diffusion of Hydrogen in Tungsten,” *J. Vac. Sci. Technol.*, vol. 6, no. 3, pp. 388–397, May 1969.

[18] E. A. Hodille *et al.*, “Retention and release of hydrogen isotopes in tungsten plasma-facing components: the role of grain boundaries and the native oxide layer from a joint experiment-simulation integrated approach,” *Nucl. Fusion*, vol. 57, no. 7, p. 076019, Jul. 2017.

[19] K. Heinola, T. Ahlgren, K. Nordlund, and J. Keinonen, “Hydrogen interaction with point defects in tungsten,” *Phys. Rev. B*, vol. 82, no. 9, Sep. 2010.
[20] Y.-W. You *et al.*, “Dissolving, trapping and detrapping mechanisms of hydrogen in bcc and fcc transition metals,” *AIP Adv.*, vol. 3, no. 1, p. 012118, Jan. 2013.
[21] X.-S. Kong *et al.*, “The role of impurity oxygen in hydrogen bubble nucleation in tungsten,” *J. Nucl. Mater.*, vol. 433, no. 1–3, pp. 357–363, Feb. 2013.
[22] E. Hodille, “Study and modeling of the deuterium trapping in ITER relevant materials,” UNIVERSITE D’AIX-MARSEILLE, 2016.
[23] M. Poon, A. A. Haasz, and J. W. Davis, “Modelling deuterium release during thermal desorption of D+-irradiated tungsten,” *J. Nucl. Mater.*, vol. 374, no. 3, pp. 390–402, Mar. 2008.
[24] O. V. Ogorodnikova, J. Roth, and M. Mayer, “Deuterium retention in tungsten in dependence of the surface conditions,” *J. Nucl. Mater.*, vol. 313, pp. 469–477, 2003.
[25] H. Eleveld and A. van Veen, “Deuterium interaction with impurities in tungsten studied with TDS,” *Fusion React. Mater. Part A*, vol. 191, pp. 433–438, Sep. 1992.
[26] W. . Shu, E. Wakai, and T. Yamanishi, “Blister bursting and deuterium bursting release from tungsten exposed to high fluences of high flux and low energy deuterium plasma,” *Nucl. Fusion*, vol. 47, no. 3, pp. 201–209, Mar. 2007.
[27] V. K. Alimov *et al.*, “Temperature dependence of surface topography and deuterium retention in tungsten exposed to low-energy, high-flux D plasma,” *J. Nucl. Mater.*, vol. 417, no. 1–3, pp. 572–575, Oct. 2011.
[28] L. Buzi *et al.*, “Influence of particle flux density and temperature on surface modifications of tungsten and deuterium retention,” *J. Nucl. Mater.*, vol. 455, no. 1–3, pp. 316–319, Dec. 2014.
[29] G. De Temmerman *et al.*, “High heat flux capabilities of the Magnum-PSI linear plasma device,” *Fusion Eng. Des.*, vol. 88, no. 6–8, pp. 483–487, Oct. 2013.
[30] T. Watanabe, T. Kaneko, N. Matsunami, N. Ohno, S. Kajita, and T. Kuwabara, “In-situ measurement of deuterium retention in W under plasma exposure,” *J. Nucl. Mater.*, vol. 463, pp. 1049–1052, Aug. 2015.
[31] J. Keinonen, J. Räisänen, and A. Anttila, “Diffusion of nitrogen in ion-implanted chromium and tungsten,” *Appl. Phys. Mater. Sci. Process.*, vol. 35, no. 4, pp. 227–232, 1984.
[32] K. Schmid *et al.*, “Interaction of nitrogen plasmas with tungsten,” *Nucl. Fusion*, vol. 50, no. 2, p. 025006, Feb. 2010.
[33] M. Rubel, V. Philipps, L. Marot, P. Petersson, A. Pospieszczyk, and B. Schweer, “Nitrogen and neon retention in plasma-facing materials,” *J. Nucl. Mater.*, vol. 415, no. 1, pp. S223–S226, Aug. 2011.
[34] G. Meisl, K. Schmid, O. Encke, T. Höschen, L. Gao, and C. Linsmeier, “Implantation and erosion of nitrogen in tungsten,” *New J. Phys.*, vol. 16, no. 9, p. 093018, Sep. 2014.
[35] L. R. Clavenna and L. D. Schmidt, “Interaction of N2 with (100) W,” *Surf. Sci.*, vol. 22, no. 2, pp. 365–391, 1970.
[36] R. Neu *et al.*, “Overview on plasma operation with a full tungsten wall in ASDEX Upgrade,” *J. Nucl. Mater.*, vol. 438, pp. S34–S41, Jul. 2013.
[37] O. V. Ogorodnikova *et al.*, “Effect of nitrogen seeding into deuterium plasma on deuterium retention in tungsten,” *Phys. Scr.*, vol. T145, p. 014034, Dec. 2011.
[38] L. Gao, W. Jacob, P. Wang, U. Von Toussaint, and A. Manhard, “Influence of nitrogen pre-implantation on deuterium retention in tungsten,” *Phys. Scr.*, vol. 2014, no. T159, p. 014023, 2014.

[39] D. Neuwirth, V. Rohde, T. Schwarz-Selinger, and ASDEX Upgrade Team, "Formation of ammonia during nitrogen-seeded discharges at ASDEX Upgrade," *Plasma Phys. Control. Fusion*, vol. 54, no. 8, p. 085008, Aug. 2012.
[40] L. Laguardia *et al.*, "Ammonia formation and W coatings interaction with deuterium/nitrogen plasmas in the linear device GyM," *J. Nucl. Mater.*, vol. 463, pp. 680–683, Aug. 2015.
[41] L. Gao, W. Jacob, T. Schwarz-Selinger, and A. Manhard, "Deuterium implantation into tungsten nitride: Negligible diffusion at 300K," *J. Nucl. Mater.*, vol. 451, no. 1–3, pp. 352–355, Aug. 2014.
[42] V. Tiron, I. Velicu, C. Porosnicu, I. Burducea, P. Dinca, and P. Malinský, "Tungsten Nitride Coatings Obtained by HiPIMS as Plasma Facing Materials for Fusion Applications," *Appl. Surf. Sci.*, Apr. 2017.
[43] K. Sugiyama, K. Schmid, and W. Jacob, "Sputtering of iron, chromium and tungsten by energetic deuterium ion bombardment," *Nucl. Mater. Energy*, vol. 8, pp. 1–7, Aug. 2016.
[44] R. D. Bringans, H. Höchst, and H. R. Shanks, "Hydrogen on WO3(001)," *Surf. Sci.*, vol. 111, no. 1, pp. 80–86, 1981.
[45] E. Salje, A. F. Carley, and M. W. Roberts, "The effect of reduction and temperature on the electronic core levels of tungsten and molybdenum in WO3 and WxMo1−xO3—A photoelectron spectroscopic study," *J. Solid State Chem.*, vol. 29, no. 2, pp. 237–251, 1979.
[46] *W Tungsten Metal, Chemical Reactions With Nonmetals Nitrogen to Arsenic*. Springer Verlag, 2013.
[47] L. Laguardia *et al.*, "Influence of He and Ar injection on ammonia production in N 2 /D 2 plasma in the medium flux G y M device," *Nucl. Mater. Energy*, Jun. 2017.
[48] E. Carrasco, M. Jiménez-Redondo, I. Tanarro, and V. J. Herrero, "Chemistry in low-pressure cold plasmas: ions of astrophysical interest," *Plasma Phys. Control. Fusion*, vol. 54, no. 12, p. 124019, Dec. 2012.
[49] A. de Castro, D. Alegre, and F. L. Tabarés, "Ammonia formation in N2/H2 plasmas on ITER-relevant plasma facing materials: Surface temperature and N2 plasma content effects," *J. Nucl. Mater.*, vol. 463, pp. 676–679, Aug. 2015.
[50] H. Kiyooka and O. Matsumoto, "Reaction scheme of ammonia synthesis in the ECR plasmas," *Plasma Chem. Plasma Process.*, vol. 16, no. 4, pp. 547–562, 1996.
[51] K. Sugiyama, K. Akazawa, M. Oshima, H. Miura, T. Matsuda, and O. Nomura, "Ammonia synthesis by means of plasma over MgO catalyst," *Plasma Chem. Plasma Process.*, vol. 6, no. 2, pp. 179–193, Jun. 1986.
[52] P. A. Redhead, "Thermal desorption of gases," *Vacuum*, vol. 12, no. 4, pp. 203–211, 1962.
[53] K. Schmid, V. Rieger, and A. Manhard, "Comparison of hydrogen retention in W and W/Ta alloys," *J. Nucl. Mater.*, vol. 426, no. 1–3, pp. 247–253, Jul. 2012.
[54] D. A. King, "Thermal desorption from metal surfaces: A review," *Surf. Sci.*, vol. 47, no. 1, pp. 384–402, 1975.
[55] A. Založnik, P. Pelicon, Z. Rupnik, I. Čadež, and S. Markelj, "In situ hydrogen isotope detection by ion beam methods ERDA and NRA," *Nucl. Instrum. Methods Phys. Res. Sect. B Beam Interact. Mater. At.*, vol. 371, pp. 167–173, Mar. 2016.
[56] H. C. Straub, P. Renault, B. G. Lindsay, K. A. Smith, and R. F. Stebbings, "Absolute partial cross sections for electron-impact ionization of H 2, N 2, and O 2 from threshold to 1000 eV," *Phys. Rev. A*, vol. 54, no. 3, p. 2146, 1996.
[57] Y. Itikawa, "Cross Sections for Electron Collisions with Nitrogen Molecules," *J. Phys. Chem. Ref. Data*, vol. 35, no. 1, p. 31, 2006.

[58] R. Rejoub, B. G. Lindsay, and R. F. Stebbings, “Electron-impact ionization of NH[sub 3] and ND[sub 3],” *J. Chem. Phys.*, vol. 115, no. 11, p. 5053, 2001.
[59] K. Ikeda, “ITER on the road to fusion energy,” *Nucl. Fusion*, vol. 50, no. 1, p. 014002, Jan. 2010.
[60] “ITER Technical Basis 2002 ITER EDA (Documentation Series No 24) (Vienna IAEA).pdf.” .
[61] M. Keilhacker *et al.*, “High fusion performance from deuterium-tritium plasmas in JET,” *Nucl. Fusion*, vol. 39, no. 2, p. 209, 1999.
[62] T. Shimada, Y. Ueda, and M. Nishikawa, “Mechanism of blister formation on tungsten surface,” *Fusion Eng. Des.*, vol. 66–68, pp. 247–251, Sep. 2003.
[63] R. A. Pitts *et al.*, “Physics basis and design of the ITER plasma-facing components,” *J. Nucl. Mater.*, vol. 415, no. 1, pp. S957–S964, Aug. 2011.
[64] M. Balden *et al.*, “Surface morphology and deuterium retention of tungsten after low- and high-flux deuterium plasma exposure,” *Nucl. Fusion*, vol. 54, no. 8, p. 083014, 2014.
[65] O. V. Ogorodnikova, “Ion-driven deuterium retention in high-Z metals,” *J. Nucl. Mater.*, vol. 390–391, pp. 651–654, Jun. 2009.
[66] M. Poon, R. G. Macaulay-Newcombe, J. W. Davis, and A. A. Haasz, “Flux dependence of deuterium retention in single crystal tungsten,” *J. Nucl. Mater.*, vol. 307, pp. 723–728, 2002.
[67] M. Oya *et al.*, “Deuterium retention in Toughened, Fine-Grained Recrystallized Tungsten,” *J. Nucl. Mater.*, vol. 438, pp. S1052–S1054, Jul. 2013.
[68] Y. Zayachuk, M. H. J. ’t Hoen, P. A. Zeijlmans van Emmichoven, I. Uytdenhouwen, and G. van Oost, “Deuterium retention in tungsten and tungsten–tantalum alloys exposed to high-flux deuterium plasmas,” *Nucl. Fusion*, vol. 52, no. 10, p. 103021, Oct. 2012.
[69] M. H. J. ‘t Hoen, D. Dellasega, A. Pezzoli, M. Passoni, A. W. Kleyn, and P. A. Zeijlmans van Emmichoven, “Deuterium retention and surface modifications of nanocrystalline tungsten films exposed to high-flux plasma,” *J. Nucl. Mater.*, vol. 463, pp. 989–992, Aug. 2015.
[70] V. K. Alimov *et al.*, “Surface morphology and deuterium retention in tungsten and tungsten–rhenium alloy exposed to low-energy, high flux D plasma,” *J. Nucl. Mater.*, vol. 454, no. 1–3, pp. 136–141, Nov. 2014.
[71] C. H. Bennett, “Demons, engines and the second law,” *Sci. Am.*, vol. 257, no. 5, pp. 108–116, 1987.
[72] R. Neu *et al.*, “Tungsten as plasma-facing material in ASDEX Upgrade,” *Fusion Eng. Des.*, vol. 65, no. 3, pp. 367–374, Apr. 2003.
[73] J. P. Coad *et al.*, “Testing of tungsten coatings in JET for the ITER-like wall,” *J. Nucl. Mater.*, vol. 390–391, pp. 992–995, Jun. 2009.
[74] M. Missirlian *et al.*, “The WEST project: Current status of the ITER-like tungsten divertor,” *Fusion Eng. Des.*, vol. 89, no. 7–8, pp. 1048–1053, Oct. 2014.
[75] T. Loarer, “Fuel retention in tokamaks,” *J. Nucl. Mater.*, vol. 390–391, pp. 20–28, Jun. 2009.
[76] T. Loarer *et al.*, “Comparison of long term fuel retention in JET between carbon and the ITER-Like Wall,” *J. Nucl. Mater.*, vol. 438, pp. S108–S113, Jul. 2013.
[77] H. T. Lee *et al.*, “Deuterium retention in tungsten exposed to mixed D+N plasma at divertor relevant fluxes in Magnum-PSI,” *J. Nucl. Mater.*, vol. 463, pp. 974–978, Aug. 2015.
[78] A. Kallenbach *et al.*, “Plasma surface interactions in impurity seeded plasmas,” *J. Nucl. Mater.*, vol. 415, no. 1, pp. S19–S26, Aug. 2011.
[79] O. Gruber *et al.*, “Compatibility of ITER scenarios with full tungsten wall in ASDEX Upgrade,” *Nucl. Fusion*, vol. 49, no. 11, p. 115014, Nov. 2009.

[80] D. A. King and M. G. Wells, “Reaction mechanism in chemisorption kinetics: nitrogen on the ${$100$}$ plane of tungsten,” in *Proceedings of the Royal Society of London A: Mathematical, Physical and Engineering Sciences*, 1974, vol. 339, pp. 245–269.
[81] G. Ehrlich, “The Interaction of Nitrogen with a Tungsten Surface,” *J. Phys. Chem.*, vol. 60, no. 10, pp. 1388–1400, Oct. 1956.
[82] Agency for Toxic Substances and Disease Registry, “Toxicological Profile for Ammonia,” *Fed. Regist.*, no. September, p. 269, 2004.
[83] M. Appl, “Ammonia,” *Ullmanns Encycl. Ind. Chem.*, 2006.
[84] H. Liu, “Ammonia synthesis catalyst 100 years: Practice, enlightenment and challenge,” *Chin. J. Catal.*, vol. 35, no. 10, pp. 1619–1640, Oct. 2014.
[85] M. Dremel *et al.*, “The new build to print design of the ITER Torus Cryopump,” *Fusion Eng. Des.*, vol. 88, no. 6–8, pp. 760–763, Oct. 2013.
[86] J. F. Ziegler, M. D. Ziegler, and J. P. Biersack, “SRIM – The stopping and range of ions in matter (2010),” *Nucl. Instrum. Methods Phys. Res. Sect. B Beam Interact. Mater. At.*, vol. 268, no. 11–12, pp. 1818–1823, Jun. 2010.
[87] M. Merola *et al.*, “ITER plasma-facing components,” *Fusion Eng. Des.*, vol. 85, no. 10–12, pp. 2312–2322, Dec. 2010.

**Résumé du manuscrit en français**

Le travail présenté dans cette thèse est lié à l'utilisation de la fusion nucléaire comme source d'énergie propre. La fusion nucléaire a d'abord été expliquée par Hans Bethe qui a prouvé que l'énergie des étoiles provient de l'interaction de noyaux plus légers qui conduit à la création de noyaux plus lourds. Aujourd'hui, la fusion sur Terre est réalisée en utilisant des dispositifs basés sur le confinement magnétique appelé tokamaks où la réaction de fusion entre les deux isotopes de l'hydrogène (H), du deutérium (D) et du tritium (T) est employée. La réaction est décrite par l'équation:

$$ {}_1^2D + {}_1^3T \rightarrow {}_2^4He(3.5MeV) + \mathrm{n}^0(14.1MeV) $$

Le plus grand tokamak et le premier à produire de l'énergie nette, à savoir ITER, est un projet scientifique qui implique la collaboration entre 35 nations, et qui vise à tester la faisabilité de la fusion nucléaire en tant que source d'énergie propre. L'objectif est de construire le premier dispositif de fusion nucléaire qui produira de l'énergie nette à partir de la fusion.

Les objectifs d'ITER, tels que présentés sur le site officiel, sont:

a. produire 500 MW d'énergie à partir d'une entrée de 50 MW, entraînant un retour d'énergie Q = 10;
b. fournir un passage des technologies qui sont maintenant utilisées dans les dispositifs de fusion plus petits à celles attendues dans les futures centrales électriques basées sur la fusion; les conditions de plasma dans ITER seront similaires à celles dans les futures centrales électriques;
c. réaliser une réaction de plasma soutenue de deutérium et de tritium à l'aide du chauffage interne;
d. tester l'élevage du tritium dans un environnement de fusion réel; l'élevage devrait être utilisé comme source de tritium pour les futures centrales électriques;
e. démontrer que les dispositifs de fusion constituent un moyen sûr de produire de l'énergie.

Notons, qu'ITER a essentiellement un but de recherche scientifique et ne vise pas à fournir de l'électricité de manière commerciale. La prochaine étape après ITER serait la construction de DEMO (Demonstration Power Station), dont la conception devrait être achevée d'ici 2020. En tant que référence pour la conception de DEMO, il est prévu que DEMO devrait fournir au moins 2 GW d'énergie de fusion en continu et qu'il devrait produire 25 fois plus de puissance

que l'entrée. Le but de DEMO est de faire la transition d'ITER en tant que projet scientifique à de futures centrales électriques commerciales.

Parmi les nombreux défis rencontrés pour la conception et la construction d'ITER, dans le présent travail, le problème abordé est représenté par l'interaction du plasma avec les matériaux de la cuve à vide du réacteur. Dans la conception finale d'ITER, les matériaux de revêtement au plasma seront en béryllium pour la première paroi (blanket) et la zone de divertor sera en tungstène.

Dans cette configuration, plusieurs préoccupations ont été soulevées concernant le bon fonctionnement du réacteur. Premièrement, les particules de plasma peuvent être piégées à l'intérieur du matériau face au plasma. Cela signifie que les atomes de deutérium et de tritium iront de l'état de plasma à être piégés à l'intérieur du matériau de tungstène. Dans la communauté de la fusion, le piégeage du combustible de fusion à l'intérieur des matériaux de revêtement du plasma du réacteur est défini comme la rétention du combustible. La rétention du deutérium et du tritium peut conduire à leur proportion déséquilibrée en tant que combustible de fusion, ce qui peut avoir comme conséquence l'échec de la réaction de fusion. Suite à la question de la rétention, il y a aussi les préoccupations liées à l'utilisation du tritium. Comme il s'agit d'un isotope radioactif, son utilisation doit respecter le règlement sur la sûreté nucléaire. En ce moment, la loi en France fixe la limite à 700 g de tritium à l'intérieur de la machine à tout moment. En outre, du point de vue pratique, le tritium n'est pas abondant sur terre et est donc cher. Tout tritium retenu doit être récupéré pour être réutilisé.

Une deuxième préoccupation majeure est représentée par la production éventuelle d'ammoniac due à la présence d'isotopes d'azote et d'hydrogène, qui pourraient être libérés de la surface sous forme d'ammoniac deutéré et/ou tritié. Puisque la molécule d'ammoniac incorpore trois isotopes d'hydrogène, la formation d'ammoniac pourrait également affecter l'équilibre gazeux à l'intérieur du réacteur. De plus, la formation d'ammoniac tritié serait un autre moyen de perdre le tritium. Ce qui peut arriver avec l'ammoniac formé, c'est qu'il est pompé à partir du récipient à vide principal et atteint le stade de cryo-pompes où il va se condenser aux parois. Non seulement il est nécessaire de trouver un moyen d'éliminer cet ammoniac condensé afin de récupérer le tritium incorporé, mais l'ammoniac est corrosif et dangereux en soi. La corrosivité peut conduire à la détérioration du système de pompage tandis que la dangerosité conduit à la nécessité d'avoir des quantités d'ammoniac bien connues et contrôlées.

Dans ce travail, des interactions gaz/surface sont étudiées pour des échantillons de tungstène caractérisés par des défauts naturels pouvant être des types suivants : lacunes uniques, joints de grains, dislocations et fine couche d'oxyde de tungstène d'une épaisseur de quelques nanomètres. Afin d'étudier l'interaction de la surface du tungstène avec l'azote et le deutérium, l'interaction de surface du plasma est simplifiée expérimentalement en exposant les échantillons aux faisceaux d'ions moléculaires ($N_2^+$ et $D_2^+$) et à la pression résiduelle des espèces neutres ($N_2$ et $D_2$).

Les effets synergiques du bombardement de l'azote et du deutérium sur le tungstène ont été étudiés dans un environnement de laboratoire, dans un appareil entièrement in situ fournissant des conditions de vide ultra-élevé (UHV). L'exposition d'échantillons de tungstène aux espèces gazeuses susmentionnées a été effectuée sous la forme de faisceaux d'ions moléculaires. Les techniques de diagnostic ont consisté en l'utilisation d'un spectromètre de masse qui a détecté les particules désorbées d'un échantillon, lorsque l'échantillon a été chauffé. D'autres techniques de diagnostic ont été appliquées, consistant à quantifier le nombre de particules trouvées à l'intérieur de l'échantillon et dans l'imagerie des échantillons. La principale technique utilisée pour caractériser les échantillons après leur exposition à l'implantation d'ions moléculaires est la «désorption à température programmée» (TPD). De plus, les échantillons ont été caractérisés par AFM, SEM, NRA et AES.

L'appareil expérimental consiste en trois chambres à ultravide (UHV) différentes connectées à une quatrième chambre utilisée pour les expositions au plasma :

a) Une chambre de verrouillage de la charge (pression de base inférieure à $1 \times 10^{-9}$ mbar) également utilisée pour le stockage des échantillons;
b) Une chambre d'implantation / thermo-désorption (impl/TPD), avec une pression de base inférieure à $4 \times 10^{-10}$ mbar;
c) une chambre d'analyse chimique;
d) Une chambre d'exposition au plasma.

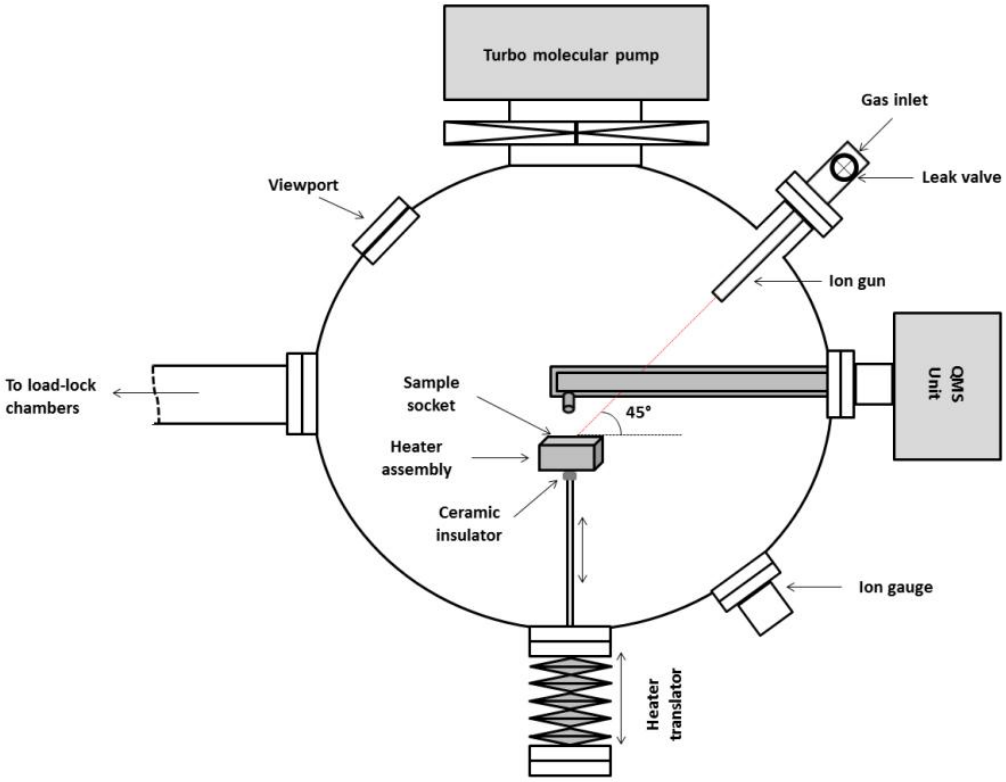


***Schéma de la chambre à vide impl / TPD***

Les expériences ont été présentées en trois étapes, en étudiant d'abord l'interaction gaz/surface pour le cas de l'implantation individuelle, pour le deutérium dans le tungstène au chapitre 3 et pour l'azote dans le tungstène au chapitre 4, puis pour l'implantation séquentielle des deux espèces, au chapitre 5.

Les principales questions qui ont reçu une réponse de ces expériences sont :

1. Quelle est l'importance de la rétention du deutérium dans le tungstène, quels sont les mécanismes de piégeage de la rétention du deutérium, et que se passe-t-il avec le deutérium retenu pour le stockage à court et à long terme ?
2. Quelle est l'importance de la rétention d'azote dans le tungstène, quels sont les mécanismes de piégeage de l'azote, ce qui se passe avec les atomes d'azote piégés à court et à long terme, et enfin, le bombardement azoté affecte-t-il significativement la réactivité superficielle ?
3. Quels changements sont introduits lorsque les deux espèces sont implantées séquentiellement dans du tungstène ? Comment les valeurs de rétention changent-elles pour les deux espèces, y a-t-il de nouveaux types de mécanismes de piégeage

apparaissant pour les espèces, y a-t-il un changement dans l'évolution de la rétention avec le temps de stockage des deux espèces ?

4. Y a-t-il une production d'ammoniaque pour le cas d'implantation séquentielle ? Dans l'affirmative, quelle est l'importance de cette quantité, comment change-t-elle lorsque la fluence de l'espèce varie, comment évolue-t-elle avec le temps de stockage et comment l'ammoniac se forme-t-elle ?

Les réponses à ces questions seront présentées dans la section suivante et fourniront un aperçu utile des phénomènes qui se produiront dans la zone divertor d'ITER. Des orientations possibles pour la poursuite de ce travail seront également suggérées dans la section des perspectives.

Pour l'étude de la rétention du deutérium dans le tungstène présentée au chapitre 3, un grand nombre de paramètres ont été étudiés. Les implantations ont été réalisées à la fois dans des échantillons de tungstène polycristallin et monocristallin, à différentes températures d'implantation, avec un accent particulier sur l'évolution des atomes retenus avec le temps de stockage. La rétention s'est avérée être de deux types: une rétention à court terme décrite par une décroissance exponentielle avec une constante de temps d'environ une demi-journée à température ambiante; une rétention à long terme qui est décrite par une quantité constante d'atomes piégés qui ne change pas (c'est-à-dire que les atomes retenus ne désorbent pas à 300 K) pendant des durées de stockage aussi longues que 330 heures à température ambiante. On a montré que la dépendance de la rétention avec la fluence incidente suit une loi racine au carré, compatible avec une rétention limitée par diffusion, et aucune saturation n'a été observée.

Une analyse approfondie a été réalisée afin de déterminer les mécanismes de piégeage du deutérium dans le tungstène et leur contribution pour les deux types de rétention (à court et à long terme). Il a été montré que le comportement de décroissance spécifique à la rétention à court terme est lié à la diffusion des atomes de deutérium à travers la couche d'oxyde natif trouvée à la surface de l'échantillon. La rétention à long terme est liée au piégeage dans les lacunes et la couche d'oxyde pour le tungstène monocristallin, tandis que pour les échantillons de tungstène polycristallin, la contribution la plus significative (pour la rétention à long terme) est liée au piégeage dans les joints de grains.

L'étude de la rétention d'azote dans le tungstène présentée au chapitre 4 a porté sur l'interaction de l'azote avec des échantillons de tungstène polycristallin, pour des implantations réalisées à température ambiante.

Le nombre d'atomes retenus (rétention) augmente rapidement à mesure que la fluence incidente augmente, mais seulement jusqu'à une certaine valeur, après quoi la rétention commence à se saturer. Le régime de saturation a été déterminé comme étant complètement atteint pour une fluence d'environ $7,5 \times 10^{20}$ N/m$^2$ et correspondant à une rétention d'azote de $3,55 \pm 0,99 \times 10^{19}$ N/m$^2$.

Le mécanisme de piégeage pour la rétention d'azote dans le tungstène, qui était connu dans la littérature comme étant la formation de nitrure de tungstène WN, s'est révélé être en accord avec les résultats expérimentaux obtenus dans cette thèse. Par conséquent, les raisons pour atteindre la saturation sont la faible profondeur d'implantation combinée à la faible diffusivité de l'azote dans le tungstène, et le fait que l'azote reste piégé uniquement sous forme de nitrure de tungstène WN. Les quantités d'azote retenues se sont avérées constantes pour toutes les durées de stockage testées (jusqu'à 140 heures).

Les changements de surface induits par le bombardement d'azote ont également été mis en évidence, et la manière dont ils affectent le collage du deutérium sur l'échantillon a été quantifiée. Ces changements ont été suivis dans la perspective de détecter l'ammoniac et de déterminer la façon dont l'ammoniac est formé.

Au chapitre 5, l'étude de l'implantation séquentielle de l'azote et du deutérium dans le tungstène a permis d'obtenir des résultats pertinents pour la zone de divertor d'ITER.

Les implants ont été réalisés uniquement dans des échantillons de tungstène polycristallin, à température ambiante, en mettant l'accent sur l'évolution de la rétention des différents produits libérés (deutérium, azote et ammoniac deutéré).

La rétention d'azote et de deutérium suite à une implantation séquentielle a été étudiée et comparée aux valeurs obtenues pour les cas individuels d'implantation. Aucune perte/érosion de l'azote implanté n'a été observée dans la plage de fluence étudiée. En revanche, la rétention du deutérium était plus élevée pour le cas de l'implantation séquentielle en raison des modifications chimiques à proximité de la surface. Néanmoins, à partir de l'analyse de la rétention du deutérium en fonction du temps de stockage, on constate que les mécanismes de piégeage responsables de la rétention du deutérium ne changent pas. La même décroissance

exponentielle est observée pour la rétention à court terme et, de même, un nombre constant d'atomes de deutérium restent piégés à long terme. Ces observations sont restées valables même lorsque la fluence incidente de l'azote a été augmentée de telle sorte que l'azote serait proche de la saturation.

Comme l'un des principaux objectifs du chapitre, il a été prouvé que l'implantation d'azote et de deutérium conduit à la production d'ammoniac deutéré à partir de la surface du tungstène. Les quantités d'ammoniac formé ont été étudiées en relation avec le niveau de saturation en azote du tungstène, en utilisant deux régimes de fluence : un régime de faible fluence d'incidence d'azote (environ 1/3 de saturation) et un régime de fluence d'incidence élevée (environ 90 % de saturation). Malgré l'augmentation de la fluence de l'azote, la quantité d'ammoniac produite n'a pas montré de changement significatif. On a émis l'hypothèse que l'ammoniac se forme uniquement à la surface du tungstène et dépend donc du nombre d'atomes d'azote trouvés près de la couche supérieure de la surface du tungstène. Cette hypothèse a été validée dans une série d'expériences où l'épuisement de l'azote disponible pour la formation d'ammoniac s'est avéré être beaucoup plus rapide que l'évolution de la quantité d'azote disponible à la surface et en masse. Ce résultat rend notre étude réalisée à des «fluences irréalistes» pour être pleinement pertinente pour les conditions «réalistes» d'ITER.

Il a été observé que la durée de stockage n'affecte pas de manière significative la production d'ammoniac. Ce résultat est cohérent avec ce qui a été appris sur l'évolution des atomes d'azote et de deutérium piégés avec le temps de stockage, pour un échantillon polycristallin. Premièrement, les atomes d'azote ne seront pas désorbés de l'échantillon à la température ambiante, ce qui signifie que la couverture de surface d'azote reste disponible au fil du temps pour la production d'ammoniac. Deuxièmement, la source d'atomes de deutérium qui seront disponibles pour la formation d'ammoniac sont les atomes qui sont piégés dans les joints de grains. Ce résultat surprenant a été rationalisé en soulignant qu'il ne s'agit pas spécifiquement d'un effet des joints de grains. Au lieu de cela, j'interprète ces résultats comme une manifestation du mécanisme activé thermiquement pour la création d'une molécule ND3 à partir de précurseurs $ND_x$ sur la surface du tungstène.

Les expériences présentées dans cette thèse ont été réalisées dans le cadre de la construction d'ITER et de DEMO. Même si les fluences et les densités de flux utilisées ici sont très inférieures à celles attendues dans la zone divertor d'ITER, ces résultats devraient être utiles pour l'extrapolation en tenant compte des recherches publiées sur des sujets

similaires mais dans des conditions plus proches d'ITER. La meilleure applicabilité des résultats présentés dans cette thèse est liée au développement de modèles de parois, qui visent à simuler l'interaction du plasma avec des matériaux de revêtement plasma. Il a déjà été mentionné au chapitre 3 que l'observation présentée ici a été utilisée avec succès pour la construction d'un modèle d'équations macroscopiques des matériaux de revêtement au plasma de tungstène, tel que présenté dans notre dernier article conjoint publié en 2017.

Il y a encore beaucoup de paramètres qui pourraient être étudiés pour chacune des études présentées dans les trois chapitres avec des résultats expérimentaux (3, 4 et 5) : la température d'implantation pour l'implantation d'azote et pour les implantations séquentielles; l'utilisation d'échantillons de tungstène monocristallin avec d'autres terminaisons de surface; changer l'ordre de l'implantation séquentielle et essayer d'effectuer des implantations simultanées d'azote et de deutérium.

Les perspectives les plus intrigantes sont liées aux résultats présentés au chapitre 3, où la couche d'oxyde natif joue un rôle important dans la rétention du deutérium. D'autres études sur ce sujet pourraient être réalisées en utilisant des techniques/méthodes qui n'étaient pas disponibles pour cette thèse, permettant un contrôle précis de la qualité structurelle de l'échantillon et de sa composition chimique. Plus précisément, les résultats et l'interprétation décrits au chapitre 3 ont pu être vérifiés en contrôlant deux paramètres: l'épaisseur de la couche d'oxyde de la surface du tungstène et la densité des lacunes dans un échantillon monocristallin. Avec ces deux possibilités, des expériences pourraient être envisagées afin d'attribuer clairement les deux types de rétention (court et long terme) à leurs mécanismes de piégeage précis.

## Résumé:

Le projet expérimental international ITER vise à tester la faisabilité de la fusion nucléaire en tant que source d'énergie. Le banc d'essai sera un réacteur tokamak où le deutérium et le tritium seront fusionnés et des ions d'hélium et des neutrons énergétiques seront produits. Une partie de l'énergie produite sera déposée dans la zone divertor du tokamak. Afin de préserver le divertor en tungstène d'ITER, il est envisagé d'injecter de l'azote au niveau du divertor afin de rayonner plus uniformément la charge d'énergie. Ce mode opérationnel soulève plusieurs questions. Tout d'abord, comment la rétention du combustible de fusion (deutérium et tritium) dans les premières parois de tokamak sera-t-elle affectée? En particulier, est-ce que l'azote implanté agira comme une barrière à la désorption pour le tritium? Deuxièmement, à quelle production d'ammoniac peut-on s'attendre due aux processus réactifs sur les matériaux des premières parois? En effet, une production efficace d'ammoniac tritiée à partir des composants face au plasma tokamak affecterait la conception des systèmes de pompage et de recyclage du tritium.

Pour aborder ces problèmes, dans la présente thèse, des expériences consistant à bombarder des échantillons de tungstène avec des faisceaux d'ions ont été effectuées dans un dispositif ultra-vide. La désorption programmée par température a été utilisée *in situ* comme principale technique d'analyse.

Cette thèse présente une étude approfondie de l'interaction du tungstène avec le deutérium et l'azote, avec l'examen de plusieurs facteurs clés: la rétention de l'azote et du deutérium en fonction de la fluence; l'évolution dynamique de la rétention d'atomes de deutérium après l'implantation; l'influence de l'azote pré-implanté sur la rétention de deutérium; et la détermination quantitative de l'ammoniac produit après une implantation séquentielle d'azote et de deutérium dans le tungstène. Une attention particulière est donnée à l'identification précise des mécanismes de piégeage pour chacune des deux espèces de gaz (azote et deutérium) dans le tungstène.

Cette thèse permet de conclure que l'utilisation d'azote dans la zone du divertor ne devrait pas mener à des changements dramatiques de la rétention du deutérium. Il y aura néanmoins une production d'ammoniaque à la surface de tungstène qui devra être prise en compte afin d'améliorer la durée de vie des systèmes de pompage, et plus important, de recycler le tritium avec succès.

## Abstract

The international experimental project ITER aims to test the feasibility of nuclear fusion as an energy source. The test bed will be a tokamak reactor where deuterium and tritium will be fused and energetic helium ions and neutrons will be released. A part of the produced energy will be exhausted in the divertor area of the tokamak. In order to preserve the tungsten divertor of ITER, it is envisioned to use nitrogen injection above the divertor in order to radiate more evenly the incident power loads. This operational plan raises several issues. Firstly, how the retention of fusion fuel (deuterium and tritium) in the tokamak first walls will be affected? In particular, does the implanted nitrogen act as a desorption barrier for tritium? Secondly, how much production of ammonia can be expected from reactive processes on the first wall materials? Indeed, an efficient production of tritiated ammonia from the tokamak plasma facing components would affect the design of the pumping and tritium recycling systems.

To address these issues in the present thesis, experiments consisting in the bombardment of tungsten samples with ion beams were performed inside an ultra-high vacuum apparatus. *In*-situ Temperature-Programmed Desorption was used as the main analysis technique.

This thesis presents an extensive study of the interaction of tungsten with deuterium and nitrogen, with several key factors being investigated: the nitrogen and deuterium retention as a function of fluence; the dynamic evolution of retained deuterium atoms after implantation; the influence of the pre-implanted nitrogen on deuterium retention; and the amounts of ammonia that are produced on tungsten after sequential implantation of nitrogen and deuterium. A special focus is directed towards identifying the exact trapping mechanisms for each of the two gas species (nitrogen and deuterium) in tungsten.

The thesis concluded that the use of nitrogen in the divertor area should not lead to dramatic changes for the retention of deuterium. There will be, nevertheless, ammonia formation on the tungsten surfaces and these amounts will need to be accounted for, in order to preserve the lifetime of the pumping systems, and more important, in order to successfully recycle tritium.